A NEW ULTRASOUND INTENSITY METER: CHARACTERIZATION AND OPTIMIZATION

by
Gavin N. Manning

B.Sc. Simon Fraser University, 1982

A THESIS SUBMITTED IN PARTIAL FULFILLMENT OF
THE REQUIREMENTS FOR THE DEGREE OF
MASTER OF SCIENCE
in
THE FACULTY OF GRADUATE STUDIES
DEPARTMENT OF PHYSICS

We accept this thesis as conforming
to the required standard

The University of British Columbia
August 15, 1987

In presenting this thesis in partial fulfilment of the requirements for an advanced degree at the University of British Columbia, I agree that the Library shall make it freely available for reference and study. I further agree that permission for extensive copying of this thesis for scholarly purposes may be granted by the head of my department or by his or her representatives. It is understood that copying or publication of this thesis for financial gain shall not be allowed without my written permission.

Department of PHYSICS

The University of British Columbia
1956 Main Mall
Vancouver, Canada
V6T 1Y3

Date 29 Sept 1987

ABSTRACT

The principle of operation of a novel rotating disk ultrasonic intensity meter is studied. Its characteristics are explained by a competition between acoustic radiation pressure and viscous drag on the disk. Acoustic streaming does not play a significant role in the operation of this meter as it is now configured.

Experiments are described which were done to find the optimum dimensions and position for a nylon disk. In this optimum configuration, the rotation rate of the disk is related to the ultrasonic intensity by a power law. This relationship is theoretically predicted and found to hold as the ultrasonic intensity varies by a factor of at least ten.

TABLE OF CONTENTS

LIST OF TABLES

LIST OF FIGURES

ACKNOWLEDGEMENT

I owe thanks to many people who helped to make this research possible. It is my special pleasure to thank:

My supervisor, Dr. Frank Curzon, for his support and encouragement over the past two years.

John Koblanski for devising the meter that this research is based on, and for his help.

Al Cheuck for his technical assistance.

And Jack Bosma for maintaining the best student machine shop I have seen anywhere, and for giving me many useful ideas.

Last, but not least, a special thank–you to Catherine for making returning to school especially worthwhile.

CHAPTER 1–Introduction

1.1 What This Thesis is About, and Why it Matters

In this thesis, we investigate the properties of a novel device for measuring the intensity of an ultrasonic beam with the aim of clarifying its principle of operation, and studying the scaling laws which will be important in its optimization.

Ultrasonic measurements are important in many industrial processes where a common method of measuring the density of a slurry is to measure the attenuation of an ultrasonic beam passing through it . An example of a process requiring such measurements is the making of paper where it is crucial to maintain the proper concentration of pulp fibers in the slurry. Another area where it is important to measure ultrasonic beam intensities is in the calibration of medical ultrasound equipment.

Several types of ultrasonic intensity meters are currently available. These can be divided into three main groups:[Zieniuk and Chivers 1976]

1.) Transducers such as calorimeters where the energy of the beam is measured directly.

2.) Transducers which measure acoustic pressure, velocity, or displacement such as piezoelectric, magnetostrictive, or capacitive transducers.

3.) Transducers which are based on nonlinear effects in the ultrasonic field such as streaming, which is the steady flow of a fluid caused by an ultrasonic field, or radiation pressure, which is the force exerted by an ultrasonic field on an object or interface in a fluid. The commonest example of this type of transducer is the radiation pressure balance commonly used to calibrate medical equipment.

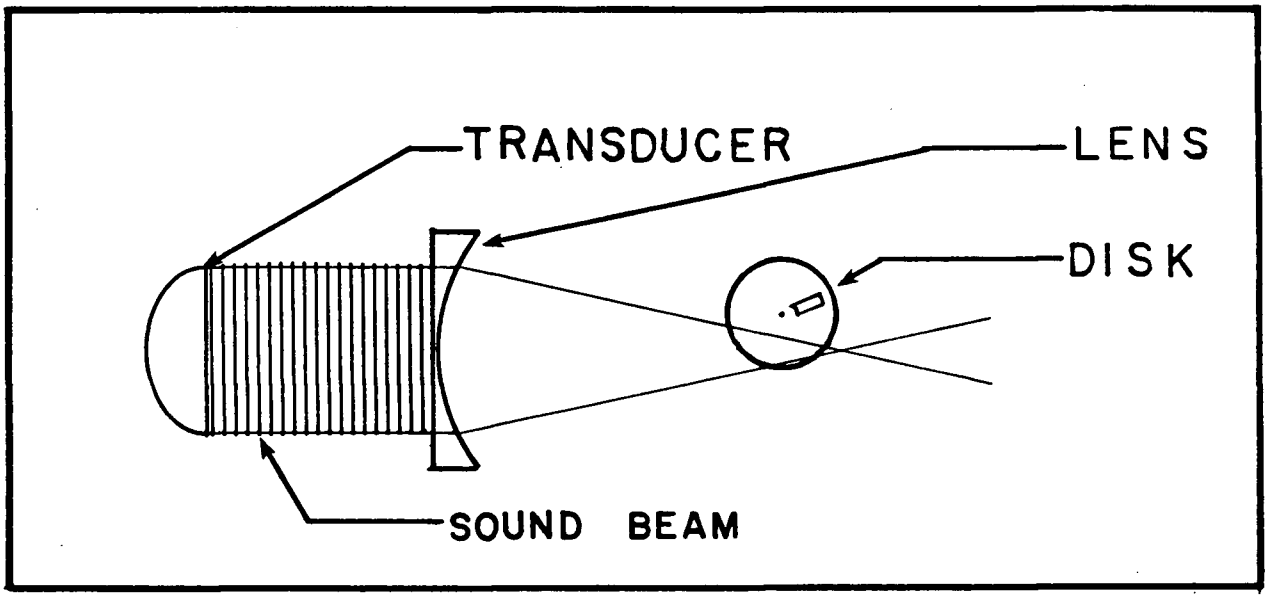

FIGURE 1–The Rotating Disk Intensity Meter

The subject of this thesis is a meter devised by John Koblanski of Ocean Ecology Ltd., Vancouver B.C. This meter falls into the third category above, and consists of a disk mounted on a shaft which is free to rotate on fine bearings, and a lens to focus the ultrasonic beam on the edge of the disk [Koblanski 1983]. The arrangement is shown in Figure 1. When an ultrasonic beam is focussed through the lens, the disk experiences a torque and begins to rotate. There are a great many factors important to the performance of this device: these include the viscosity, speed of sound, and coefficient of sound absorption for

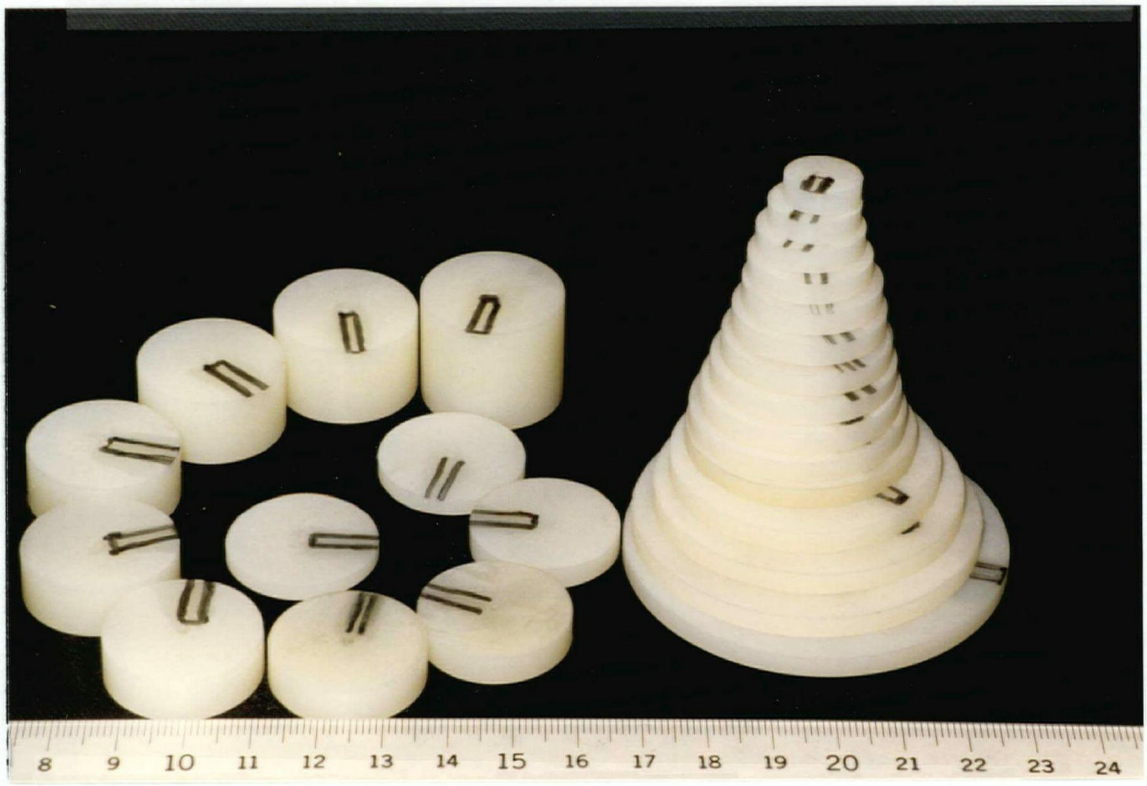

FIGURE 2–Some Disks Used in These Experiments

---

the fluid in which it operates; the materials that the disk and lens are made of, the quality of the bearing surfaces, and several geometric factors such as the shape and focal length of the lens, the diameter and thickness of the disk, the surface condition of the disk, and the positions of the lens and disk relative to each other as well as to the ultrasonic beam. It is the purpose of the research reported in this thesis, first to determine what causes the torque on the disk, whether it is streaming of the fluid, or radiation pressure, and secondly to investigate the effect of varying some of the geometric factors with a view to the optimization of this meter. The effect of varying the disk dimensions and changing the relative position of disk and lens is reported here. Some of the disks used are shown in Figure 2 .

1.2 Thesis Organization

In order to understand this meter, we need to know a little bit about acoustics. In particular we need to understand acoustic radiation pressure, by which an ultrasonic beam directly causes a force on a solid object or interface in the fluid, and acoustic streaming where an ultrasonic beam causes flow in the fluid through which it propagates. The flowing fluid can then impinge on a solid object with a resulting force. These topics compose Chapters 2 and 3 of this thesis.

The torque on our disk arising from its interaction with the ultrasonic field is balanced by viscous drag on the disk. Chapter 4 is therefore devoted to a brief study of the viscous drag on a rotating disk.

Another topic that deserves mention is acoustic cavitation, the creation of cavities in a liquid by an intense ultrasonic field. These cavities interfere with the propagation of sound waves. They can also collapse with enough vigour to damage equipment or grow into bubbles that stick to surfaces and add drag to moving objects. Acoustic cavitation is the subject of Chapter 5.

In Chapter 6 we report on the design of our apparatus, some experiments done to characterize the ultrasonic field, experiments done to clarify which mechanism is responsible for the rotation of our disk, and experiments done to find some scaling laws for this meter. Chapter 7 discusses these experimental results and summarizes the conclusions reached in the course of research for this thesis. In particular, the original contributions made by the author are given in section 7.3.

CHAPTER 2–Radiation Pressure

2.1 What is Radiation Pressure?

The propagation of acoustic waves in a fluid is intrinsically a nonlinear phenomenon. The equations of fluid motion include nonlinear convective terms, and the equation of state for the fluid is also, in general, nonlinear. Although these equations governing the motion of fluids can be linearized, and the resulting 'small amplitude equations' can be used to solve many practical problems where the finite amplitude of the sound waves can be ignored, much interesting physics is missed by this approach. Among the effects that arise because of the nonlinearities present in sound propagation are the formation of shock waves [Beyer 1974], the nonlinear interaction of waves [Ingard and Pridmore-Brown 1956], and two of the topics discussed here, acoustic radiation pressure, and acoustic streaming.

To begin then, we need to take the equations governing fluid flow. Given a fluid through which a harmonic plane acoustic wave is propagating, we can then calculate a value for the time averaged pressure $\langle \mathbf{P} \rangle$ in the beam. This pressure is different from the equilibrium hydrostatic pressure $\mathbf{P}_0$ and it depends on the boundary conditions we impose on the fluid. The different values of $\langle \mathbf{P} \rangle$ we obtain for different boundary conditions correspond to pressures that could be measured in a fluid in different physical circumstances.

2.2 Equations of Fluid Motion

In Eulerian coordinates†, there are three equations that describe all of the allowed motions of a fluid including the propagation of acoustic waves [Temkin 1981]. These are the equation of continuity:

$$\frac{\partial \rho}{\partial t} + \vec{\nabla} \cdot \rho \vec{\mathbf{U}} = 0 \tag{1}$$

The force equation:

$$\rho \frac{\mathrm{D}\vec{\mathbf{U}}}{\mathrm{Dt}} = \rho \vec{\mathbf{F}} - \vec{\nabla} \mathbf{P} \tag{2}$$

and the equation of state:

$$\mathbf{P} = \mathbf{P}(\rho \, , \mathbf{S}) \tag{3}$$

where ρ is the fluid density, $\vec{\mathbf{U}}$ is the fluid velocity, $\vec{\mathbf{F}}$ represents all of the forces acting on elements of the fluid including body forces such as gravity and internal viscous forces, $\mathbf{P}$ is fluid pressure, and $\mathbf{S}$ the entropy of the fluid. D/Dt is the total or material derivative which measures the changes occurring in a fluid element as it moves with the fluid flow ‡.

For investigating the phenomenon of radiation pressure we shall consider soundwaves propagating adiabatically through an ideal nonviscous gas. In this case, the equation of state is given by:

$$\frac{\mathbf{P}}{\mathbf{P}_0} = \left(\frac{\rho}{\rho_0}\right)^{\gamma} \qquad \text{or} \qquad \frac{\mathrm{D}}{\mathrm{Dt}} \left(\mathbf{P} \rho^{\gamma}\right) = 0 \tag{4}$$

---

† See Appendix I for a description of Eulerian and Lagrangian coordinates

‡ The total derivative of a quantity $\mathbf{Q}$ is given by: $\frac{\mathrm{DQ}}{\mathrm{Dt}} = \partial \mathbf{Q}/\partial t + \vec{\mathbf{U}} \cdot \vec{\nabla} \mathbf{Q}$

where γ is the ratio of specific heats C_p/C_v. Assuming (4) for our equation of state is not nearly as restrictive as it might at first seem. Firstly, many real gases behave much like ideal gases over a large range of conditions. Secondly, Equation (4) can be used as an equation of state for almost any isentropic liquid with very little modification [Beyer 1974, p.98–99].

In an isentropic liquid, we know that the pressure $\mathbf{P}$ must be some function of the density ρ. This equation of state can be written as a Taylor series expanded about the point $\rho = \rho_0$ as follows:

$$\mathbf{P} = \mathbf{P}_0 + \mathbf{A}\left(\frac{\rho - \rho_0}{\rho_0}\right) + \frac{\mathbf{B}}{2!}\left(\frac{\rho - \rho_0}{\rho_0}\right)^2 + \cdots \tag{5}$$

where $\mathbf{A}, \mathbf{B}, \mathbf{C}, \ldots$ are constants to be determined for each particular gas. The adiabatic ideal gas equation of state (4) which we would like to use can be expanded by the binomial expansion to yield:

$$\mathbf{P} = \mathbf{P}_0\left(1 + \gamma\left(\frac{\rho - \rho_0}{\rho_0}\right) + \frac{\gamma(\gamma-1)}{2!}\left(\frac{\rho - \rho_0}{\rho_0}\right)^2 + \cdots\right) \tag{6}$$

If we compare (5) and (6) term by term,we obtain the relationships:

$$\mathbf{A} \leftrightarrow \gamma \mathbf{P}_0 \tag{7}$$

and:

$$\mathbf{B} \leftrightarrow \gamma(\gamma - 1)\mathbf{P}_0 \tag{8}$$

hence we can make the direct correspondence:

$$\mathbf{B}/\mathbf{A} \leftrightarrow (\gamma - 1) \tag{9}$$

As long as the third and higher terms of (5) are very small in comparison to the first two terms, we can use (4) to describe liquids as well as gases if we replace γ by the experimentally determined parameter $\left((\mathbf{B/A})+1\right)$. For almost all real liquids at any attainable intensity, the maximum condensation $((\rho-\rho_0)/\rho_0)$ is less than about 10^{-4} [Coppens et.al. 1965] so that even with $\mathbf{C/A}$ given approximately by:[Hagelberg, Holton,Kao 1967]

$$\mathbf{C/A} \approx \frac{3}{2}\left(\frac{\mathbf{B}}{\mathbf{A}}\right)^2 \tag{10}$$

the cubic and higher order terms can be ignored. For water at 20 C and atmospheric pressure, $\mathbf{B/A}$ has been measured to be 5.0 [Beyer 1960].

2.3 Calculating Radiation Pressure in One Dimension

In one dimension, the equations of motion (1) and (2) become:

$$\frac{\partial \rho}{\partial t} + \frac{\partial \rho \mathbf{U}}{\partial x} = 0 \tag{11}$$

and

$$\rho \frac{\partial \mathbf{U}}{\partial t} + \rho \mathbf{U} \frac{\partial \mathbf{U}}{\partial x} = -\frac{\partial \mathbf{P}}{\partial x} \tag{12}$$

Each of these equations has one nonlinear term. In combination with the nonlinear equation of state (4) , these equations form a system of three differential equations which can be solved by the method of successive approximations. In this method, $\rho, \mathbf{U}$, and $\mathbf{P}$ are each expressed as power series in the small parameter ϵ and then substituted into (4) , (11) , and (12). It is convenient to pick:

$$\epsilon = \mathbf{U}_{max}/\mathbf{c}_0 \tag{13}$$

where $\mathbf{U}_{max}$ is the maximum fluid velocity, and c_0 is the speed of sound. This choice for ϵ has the desired property of going to zero for infinitesimal waves. As epsilon is an arbitrary parameter, we must require that the coefficient of each power of ϵ is identically zero so that the solution is independent of the way we pick ϵ. In this way we obtain an infinite hierarchy of systems of ordinary differential equations.The first set is:

$$\rho_0 \frac{\partial \mathbf{U}_1}{\partial t} + \frac{\partial \mathbf{P}_1}{\partial x} = 0 \tag{14}$$

$$\frac{\partial \rho_1}{\partial t} + \rho_0 \frac{\partial \mathbf{U}_1}{\partial x} = 0 \tag{15}$$

$$\frac{\mathrm{D}}{\mathrm{Dt}} \left(\frac{\mathbf{P}_1}{\mathbf{P}_0} - \frac{\gamma \rho_1}{\rho_0} \right) = 0 \tag{16}$$

These first equations can be recognized as the linearized equations of classical acoustics. The second set of equations provides the first nonlinear correction to (14), (15), and (16). These equations are:

$$\rho_0 \frac{\partial \mathbf{U}_2}{\partial t} + \frac{\partial \mathbf{P}_2}{\partial x} = -\rho_1 \frac{\partial \mathbf{U}_1}{\partial t} - \rho_0 \mathbf{U}_1 \frac{\partial \mathbf{U}_1}{\partial t} \tag{17}$$

$$\frac{\partial \rho_2}{\partial t} + \frac{\partial (\rho_0 \mathbf{U}_2)}{\partial x} = -\frac{\partial (\rho_1 \mathbf{U}_1)}{\partial x} \tag{18}$$

$$\frac{\partial}{\partial t} \left\{ \frac{\mathbf{P}_2}{\mathbf{P}_0} - \frac{\gamma \rho_2}{\rho_0} \right\} = \frac{\partial}{\partial t} \left\{ \frac{\gamma \mathbf{P}_1 \rho_1}{\mathbf{P}_0 \rho_0} - \frac{\gamma(\gamma+1)}{2} \frac{{\rho_1}^2}{{\rho_0}^2} \right\} + \mathbf{U}_1 \frac{\partial}{\partial x} \left\{ \frac{\gamma \rho_1}{\rho_0} - \frac{\mathbf{P}_1}{\mathbf{P}_0} \right\} \tag{19}$$

These second order equations are exactly the same as the corresponding first order equations above except that while (14) , (15) , and (16) are homogeneous, these equations each have a forcing term on the RHS which is completely determined once the first order equations are solved. In fact, all of the higher order sets of equations are of this form with different forcing terms on their RHS. When these equations are solved for an initially

harmonic plane wave disturbance, the time-averaged Eulerian pressure can be calculated to be:

$$\langle \mathbf{P} \rangle = \mathbf{P}_0 + \left(\frac{\gamma - 3}{8} \right) \rho_0 c_0^2 \epsilon^2 \tag{20}$$

The detailed calculations can be found in Appendix II. Some authors explain alternative methods for solving (4), (11), and (12) including solution by the method of characteristics [Blackstock 1962], or time averaging the equations of motion [Chu and Apfel 1982]. They obtain the same result for (20).

2.4 Range of Validity for Our Solution

There have been several assumptions made in attaining the result (20) which should be pointed out. Firstly, we have assumed that the sound wave propagates adiabatically through a nonviscous fluid which obeys the ideal gas equation of state. For the assumption of adiabatic behaviour to hold, we require that both the thermal conductivity, κ, of the fluid, and the frequency, ω, of the sound be reasonably small. In air, deviation from adiabatic behaviour is not observed until frequencies on the order of 10^8 Hz are attained [Randall 1951].

The assumption that the fluid is nonviscous is equivalent to requiring that the sound not be significantly attenuated in the region of interest. We can therefore only apply this theory in cases where the absorption length for sound is greater than the scale length of our problem. As we saw above, many real gases and liquids approximately satisfy the ideal gas equation of state (4) under conditions typical for sound propagation. As long as we pick a value of γ appropriate for the fluid in question, this assumption is not too restrictive.

We made other approximations in solving the equations to calculate $\langle \mathbf{P} \rangle$. Foremost among these was the assumption that ϵ is small enough that terms containing ϵ^3 and higher powers of ϵ could be neglected. With ϵ defined in (13) it is clear that this limits our theory to cases where the intensity of the sound beam is low enough that the maximum fluid particle velocity is much less than the speed of sound in the fluid. Another limit on the size of the region of interest, which depends on the intensity of the beam is that the fluid particle velocity must remain a single valued function of position. As this theory now stands, it predicts that the harmonic content of a beam increases as it propagates, and that the resulting steepening of the wavefront will continue until the wave 'breaks' at a distance, $\mathbf{X_{SF}}$, from its source given by: [Beyer 1974, p.104]

$$\mathbf{X_{SF}} = \left(1 + \frac{B}{2A}\right) \frac{\omega \mathbf{U}_{max}}{c_0^2} \tag{21}$$

What really happens is that a shock wave forms before the fluid velocity can become double valued, something that this theory does not include. The distance (21) is commonly referred to as the shock–formation distance, $\mathbf{X_{SF}}$. Our theory is only valid for distances less than $\mathbf{X_{SF}}$. At 1.0MHz , and 1 atmosphere pressure, at an acoustic Mach number $\mathbf{U}_{max}/c_0 = 0.046 \times 10^{-3}$, the shock formation distance in water is 148 cm [Beyer 1974, p.105].

A final tacit assumption which also limits the range of intensities for which this theory is valid is that the fluid remains continuous. If the sound intensity is too large, the pressure will be extremely low in the regions where the fluid is rarefied. In extreme cases, voids can form. This situation is discussed more fully in Chapter 5 on cavitation. To ensure that the fluid remains homogeneous, the sound intensity must be kept below the cavitation threshold for that fluid. In the case that the sound originates from a moving

piston, Blackstock [Blackstock 1962] calculates that the piston velocity must also satisfy:

$$\dot{\mathbf{X}}(t) \geq -\frac{2c_0}{(\gamma - 1)} \tag{22}$$

so that the fluid will remain in contact with the piston.

2.5 Different Types of Radiation Pressure

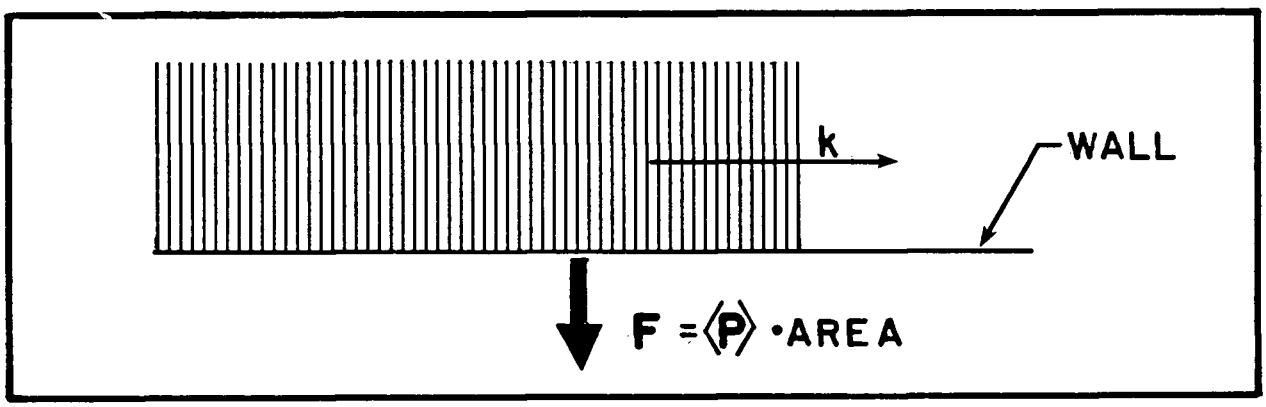

FIGURE 3–Sound Beam Laterally Confined by a Rigid Wall

We have calculated an average pressure, but should be sure that we understand what it means physically. (21) is the average pressure that would be recorded by a microscopic hydrophone fixed in space, and so small as not to affect the motion of the fluid. It is also the pressure that would act on a rigid wall laterally confining the sound beam as shown in Figure 3 . (21) is *not* the pressure that would act on the surface of an object partially blocking the sound beam.

To calculate the radiation pressure on a completely absorbing target which does block the sound beam, it is best to use Lagrangian coordinates. By definition, the surface

of a completely absorbing target exactly follows the motion of the fluid layer immediately next to it. The absorbing target thus feels the Lagrangian pressure on its surface so the radiation pressure on such a target is given by the time averaged Lagrangian pressure $\langle \mathbf{P}^L \rangle$. This quantity can be calculated using one of the same methods used for calculating the average Eulerian pressure $\langle \mathbf{P} \rangle$ but beginning with the fluid equations of motion in Lagrangian coordinates [Blackstock 1962]. The result is:

$$\langle \mathbf{P}^L \rangle = \mathbf{P}_0 + \frac{(\gamma+1)}{8} \rho_0 c_0^2 \epsilon^2 \tag{23}$$

So far, we have considered the one-dimensional case where the sound beam extends infinitely laterally. If the beam is finite, the force on an obstacle in the beam depends on whether fluid is allowed to flow into and out of the region of the beam, or is confined by impermeable walls. When the fluid is confined, the preceeding analysis holds true. It is customary to define the 'Rayleigh pressure', $\mathbf{P}^{\mathbf{Ra}}$ to be:

$$\mathbf{P}^{\mathbf{Ra}} = \langle \mathbf{P}^L \rangle - \mathbf{P}_0 \tag{24}$$

$\mathbf{P}^{\mathbf{Ra}}$ is the net force per unit area acting on a perfectly absorbing target one side of which is exposed to a laterally confined sound beam, and the other to fluid at rest. This situation is shown in Figure 4 .

If the sound beam is not laterally confined and fluid is allowed to flow in a direction perpendicular to the wavevector, the force on an absorbing target will be different from (24). This is because, given the chance, a fluid will flow in such a way as to reduce pressure gradients. For the sake of clarity, assume that there is a sharp boundary between the beam and the surrounding fluid although this is not a necessary condition [Beissner 1982]. As the fluid surrounding the beam is undisturbed, it will be at pressure $\mathbf{P}_0$. We have seen above that the fluid inside the beam is pressing outward as if it were pressurized to the

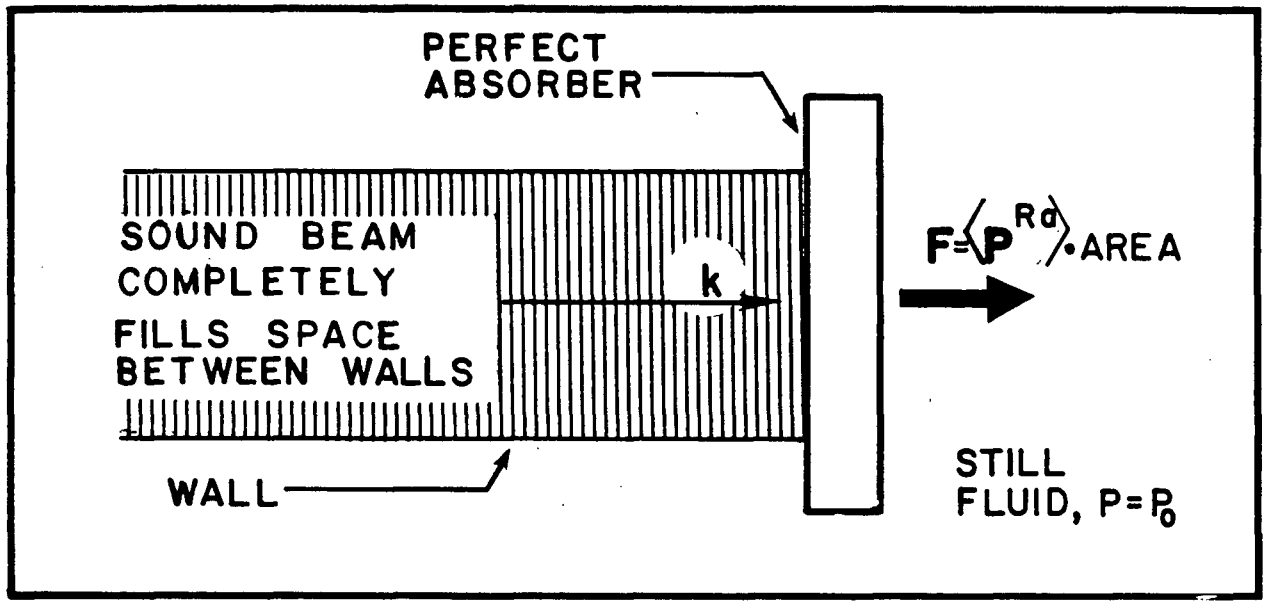

FIGURE 4–The Physical Meaning of Rayleigh Pressure

Eulerian average pressure $\langle \mathbf{P} \rangle$. Fluid will flow into or out of the beam until equilibrium is established at which point the average Eulerian pressure just inside the beam will equal $\mathbf{P}_0$, the pressure just outside the beam. The fluid flow changes the density of fluid in the beam effectively changing the base pressure in the beam from $\mathbf{P}_0$ to $\mathbf{P}'_0$ where $\mathbf{P}'_0$ is given by:

$$\mathbf{P}'_0 = \mathbf{P}_0 - \frac{(\gamma - 3)}{4}\langle \mathbf{E} \rangle \qquad \langle \mathbf{E} \rangle = \rho_0 c_0^2 \epsilon^2 \tag{25}$$

The pressure on the side of a perfectly absorbing target will still be given by (23) if $\mathbf{P}_0$ is replaced by $\mathbf{P}'_0$ to give:

$$\langle \mathbf{P}^L \rangle' = \mathbf{P}'_0 + \frac{(\gamma + 1)}{4}\langle \mathbf{E} \rangle = \mathbf{P}_0 + \langle \mathbf{E} \rangle \tag{26}$$

In analogy with the Rayleigh pressure, the 'Langevin'pressure, $\mathbf{P}^{Lan}$, is defined to be:

$$\mathbf{P}^{Lan} = \langle \mathbf{P}^L \rangle' - \mathbf{P}_0 = \langle \mathbf{E} \rangle \tag{27}$$

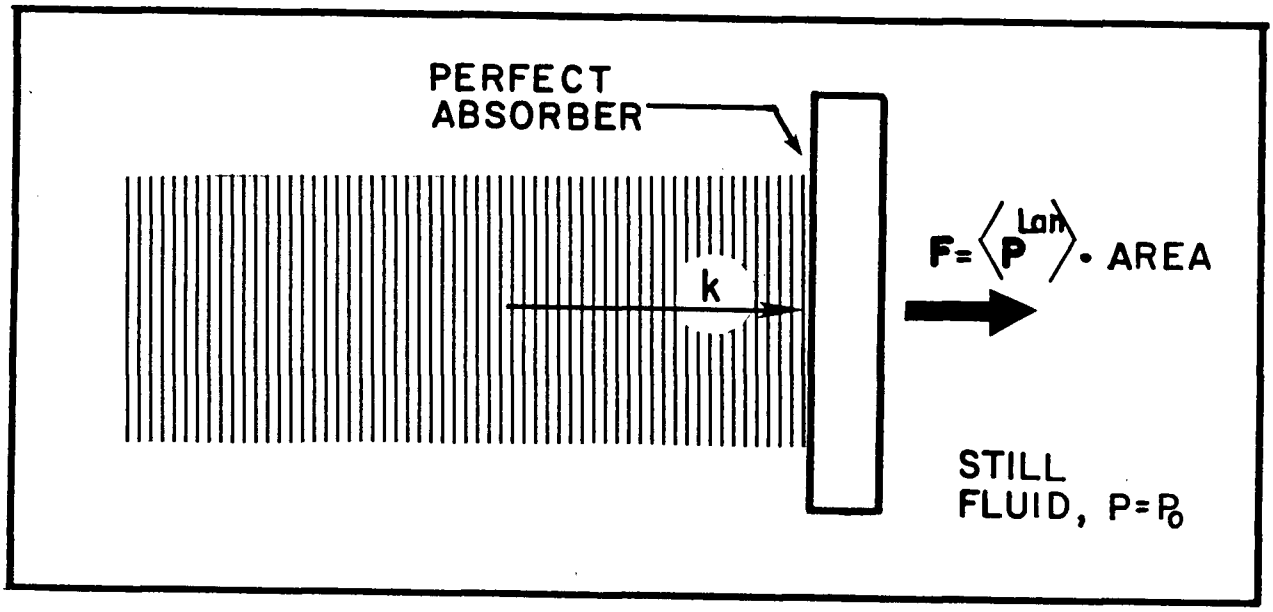

FIGURE 5–The Physical Meaning of Langevin Pressure

Figure 5 shows the physical meaning of the Langevin pressure.

2.6 The Relationship of Radiation Pressure to Momentum Flux

As was mentioned at the beginning of this chapter, radiation pressure is a direct consequence of the conservation of momentum. The momentum density, $\vec{\mathbf{J}}$, at any point in the fluid is clearly given by:

$$\vec{\mathbf{J}} = \rho\vec{\mathbf{U}} = (\rho_0 + \rho_1\epsilon + \rho_2\epsilon^2 + \cdots)(\mathbf{U}_1\epsilon + \mathbf{U}_2\epsilon^2 + \cdots) \tag{28}$$

To second order in ϵ then, $\vec{\mathbf{J}}$ is given by:

$$\vec{\mathbf{J}} \simeq (\rho_0 \mathbf{U}_1)\epsilon + (\rho_0 \mathbf{U}_2 + \rho_1 \mathbf{U}_1)\epsilon^2 \tag{29}$$

Assuming a one dimensional sinusoidal waveform, the first order displacement, ξ, of each fluid element from its equilibrium position can be written in Eulerian coordinates as:

$$\xi = \xi_0 \sin(\omega t - kx) \tag{30}$$

the first order velocity field can then be written:

$$\vec{\mathbf{U}_1} = \dot{\xi} = \omega \xi_0 \cos(\omega t - kx) \tag{31}$$

$\vec{\mathbf{U}_2}$ will consist of two components, one a steady flow representing acoustic streaming, and another oscillating at frequency 2ω. The density at any point in the fluid is given by Beyer to be [Beyer 1974, p.27]:

$$\rho = \frac{\rho_0}{1 + \frac{\partial \xi}{\partial x}} \simeq \rho_0 (1 - \frac{\partial \xi}{\partial x}) = \rho_0 (1 + k\xi_0 \cos(\omega t - kx)) \tag{32}$$

With these results, it is easy to calculate the total momentum carried by the acoustic beam in a block of fluid one wavelength long with unit cross sectional area. Integrating (29) while ignoring the constant streaming term gives:

$$\begin{aligned} \text{Total Momentum} &= \int_0^{\frac{2\pi}{k}} \rho_0 \omega \xi_0 \cos(\omega t - kx)(1 + k\xi_0 \cos(\omega t - kx))\, dx \\ &= \rho_0 \omega \xi_0^2 \int_0^{\frac{2\pi}{k}} \cos^2(\omega t - kx) k\, dx = \rho_0 \omega \xi_0^2 \pi \end{aligned} \tag{33}$$

because:

$$\int_0^{\frac{2\pi}{k}} \cos(kx - \omega t)\, dx = 0 \text{ and } \int_0^{\frac{2\pi}{k}} \cos 2(kx - \omega t)\, dx = 0 \tag{34}$$

The connection to radiation pressure comes through Newtons second law:

$$\vec{\mathbf{F}} = -\frac{d\vec{p}}{dt} \tag{35}$$

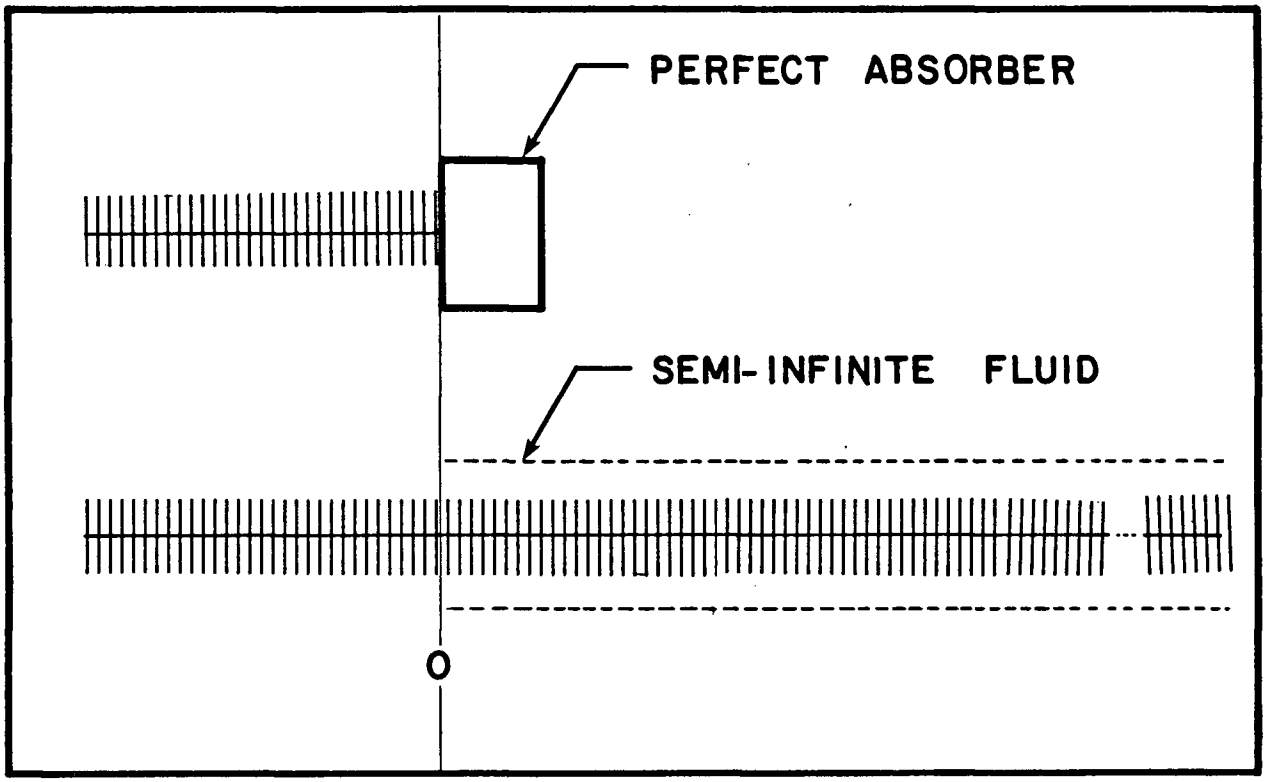

FIGURE 6–A Perfectly Absorbing Target
To the left of $x = 0$ these two situations are identical.

Here, $d\vec{\mathbf{p}}/dt$, is the rate of momentum flow into the target, and, $\vec{\mathbf{F}}$, is the force on the target. To calculate the radiation pressure on a perfectly absorbing target then, it remains to calculate how fast momentum flows from the fluid into the target. One way to see clearly what is happening is to realize that a perfectly absorbing target behaves exactly as a semi–infinite body of fluid into which waves can propagate but are never reflected as shown in Figure 6. With this model for our target, it is clear that after each cycle of the acoustic beam one more wavelength of the fluid in the target has been set into motion hence the amount of momentum that has flowed into each unit area of the target is given by (33). In other words, momentum flows along the acoustic beam with speed c_0 [Stapper 1978]. The radiation pressure on this target is then given by (33) and (35) to be:

$$\mathbf{P}^{Lan} = \frac{1}{\text{Period}} \rho_0 \omega \xi_0^2 \pi = \frac{\rho_0 \omega^2 \xi_0^2}{2} = \frac{\rho_0 \mathbf{U}_{max}^2}{2} = \frac{\rho_0 c_0^2 \epsilon^2}{2} = \langle \mathbf{E} \rangle \tag{36}$$

which is the same result we obtained previously.

2.7 Torque on a Disk due to Radiation Pressure

It is useful to adopt the point of view that radiation pressure arises from conservation of momentum because this can aid us in visualizing the forces which cause torques on the rotating disk in our meter. This approach is especially useful when the wavelength of the sound beam is small compared to the size of the disk so that the propagation of the sound beam near the disk can be described by geometrical acoustics. We can, for example, show that to first approximation, no torque results when a sound beam is reflected from the disk. This situation is shown in Figure 7. $\vec{\mathbf{J}}$ and $\vec{\mathbf{J}}'$ represent the momentum flux in the incident and reflected beams respectively. According to (35), the radiation force will be directed

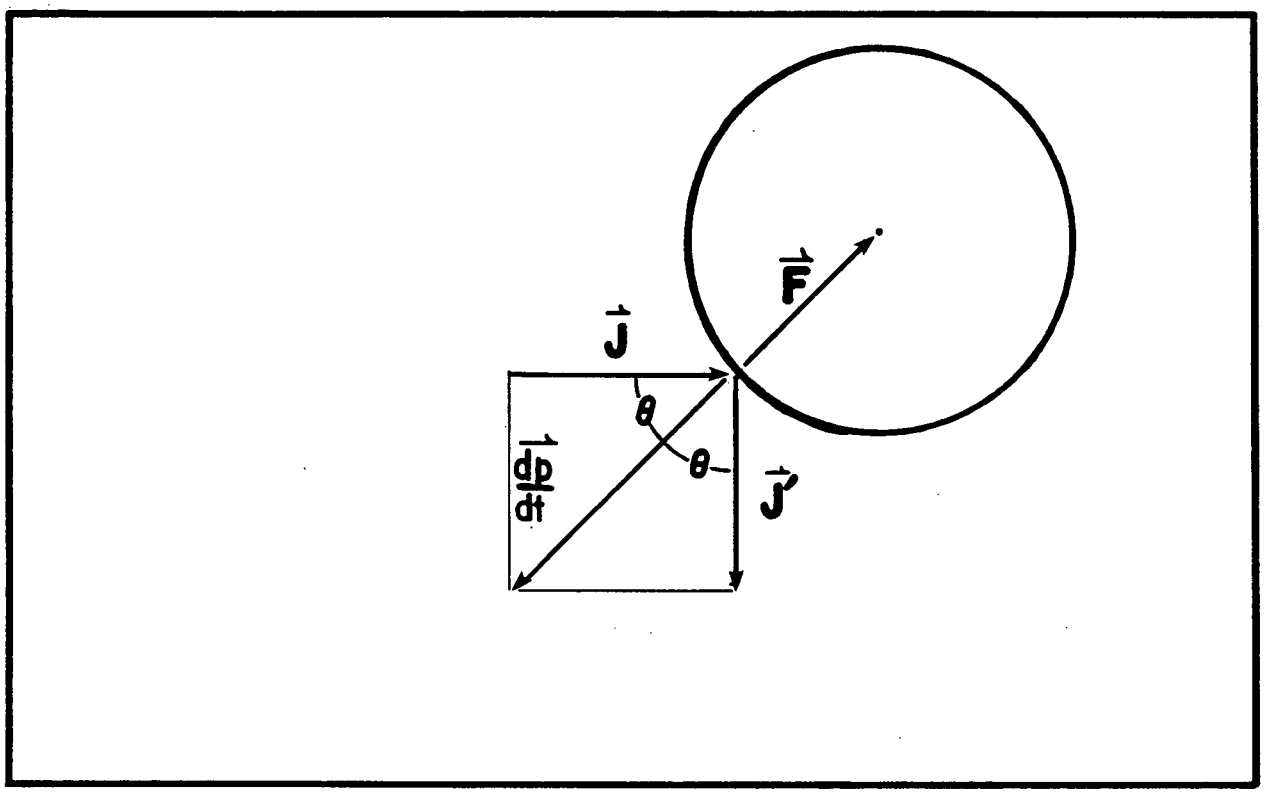

FIGURE 7–Acoustic Forces on a Reflecting Disk

---

opposite to $d\vec{\mathbf{p}}/dt$. It is immediately clear that the radiation force will be directed along a radius of the disk so that there will be no torque resulting on the disk. This analysis has ignored diffraction of the sound beam by the disk as well as any interaction of incident and reflected waves.

Torque will arise if the sound beam is absorbed in the disk as shown in Figure 8. Here, all of the momentum carried by the incident beam is absorbed in the disk causing a force directed opposite to $\Delta\vec{\mathbf{J}}$. This example illustrates why the term 'Radiation Pressure' is a misnomer of sorts. A pressure generally acts along the normal to a surface. We have here a force acting in a direction parallel to the wavevector of the incident acoustic beam. Radiation pressure is really a tensor quantity [Beyer 1978] and must be treated as such when dealing with complicated three dimensional geometries. We have seen that

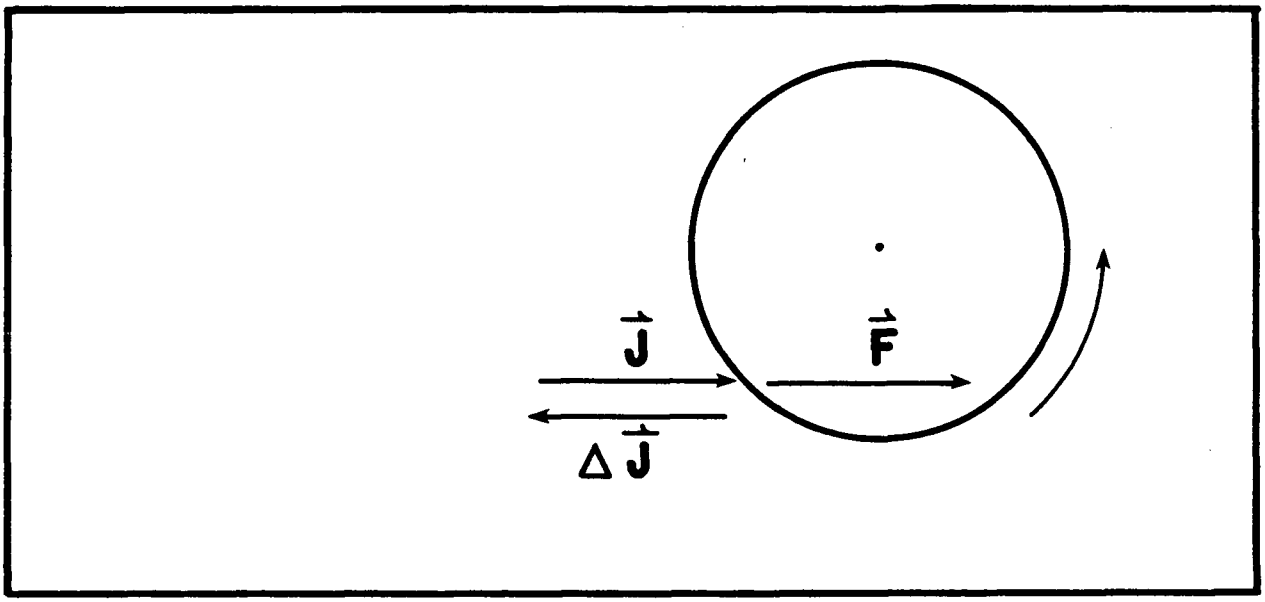

FIGURE 8–Acoustic Forces on a Sound Absorbing Disk

---

for radiation pressure to cause a torque on our disk, some of the acoustic beam must be absorbed in the disk. For this reason it is appropriate at this point to look briefly at the reflection and refraction of an acoustic beam at a liquid–solid interface.

2.8 Reflection and Refraction of Sound at a Liquid–Solid Interface

When an acoustic beam propagating through a liquid impinges at an angle on the plane surface of an elastic solid, several things occur. As shown in Figure 9, some of the wave will be reflected into the liquid, some will be transmitted into the solid as a longitudinal wave, and some will be transmitted into the solid as a transverse shear wave. The angles made by the wavevectors of the refracted beams and the normal to the surface are given by: [Brekhovskikh 1960, eq.[7.9]]

$$\frac{\sin\theta}{c_0} = \frac{\sin\theta_1}{c_1} = \frac{\sin\gamma_1}{b_1} \tag{37}$$

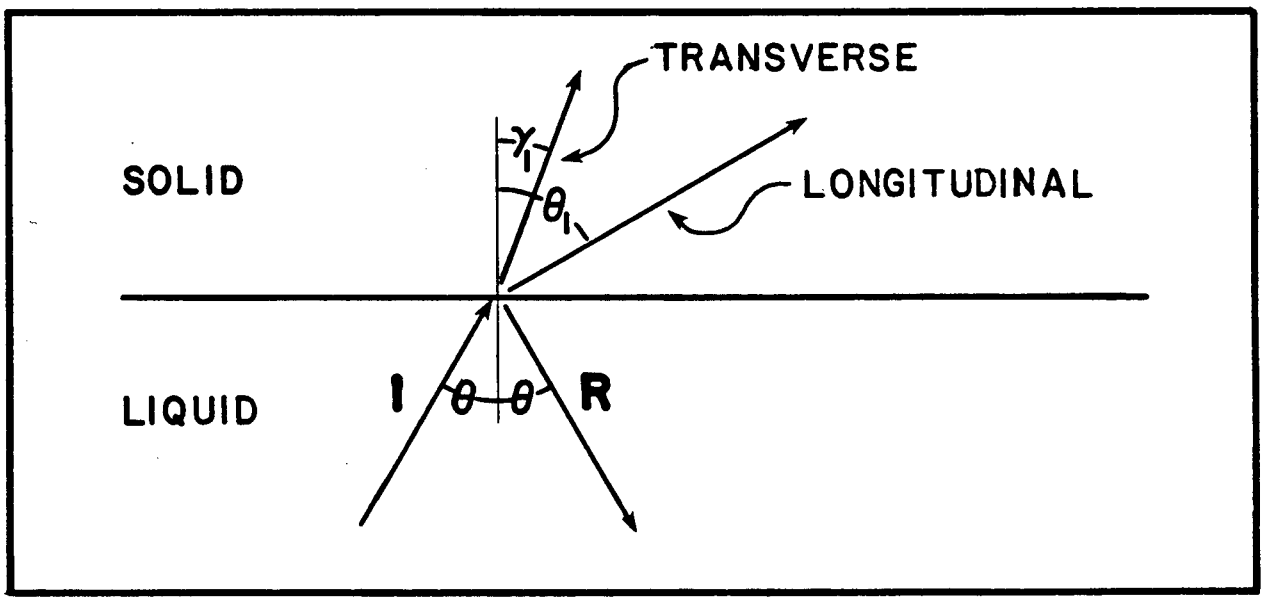

FIGURE 9–Reflection and Refraction of an Acoustic Beam at a Liquid–Solid Interface
Shown here is a Nylon–Water interface with $\theta = 30°$, $\theta_1 = 60°$, and $\gamma_1 = 21°$.

---

where the velocities of longitudinal and transverse waves in the solid are c_1 and b_1 respectively, and the angles θ, θ_1, and γ_1 are as shown in Figure 9. In general, the velocities of longitudinal and transverse waves in the solid differ from each other, and from c_0, the velocity of longitudinal waves in the liquid. Often these three velocities are related by:

$$c_1 > c_0 > b_1 \tag{38}$$

At a Nylon-Water interface for example, $c_1 = 2620\,\text{m/s}$, $b_1 = 1070\,\text{m/s}$, and $c_0 = 1496.7\,\text{m/s}$ [CRC Press 1976, p.E-47]. We can see from (37) that when (38) holds there

will be a certain critical angle, θ_c, beyond which θ_1 is imaginary. When $\theta > \theta_c$ there will be no refracted longitudinal wave in the solid. This critical angle is given by:

$$\theta_c = \sin^{-1} \frac{c_0}{c_1} \tag{39}$$

For a Nylon-Water interface, $\theta_c = 34.8°$. There is no corresponding critical angle for transverse waves in the solid so long as (38) holds.

We have seen that in order to cause a torque, the sound beam must be absorbed in the disk. If we assume that all of the waves transmitted into the disk are completely absorbed, the torque on the disk will be proportional to the intensity of the beam, the transmission coefficient at the boundary of the disk, and the perpendicular distance to the axis of the disk from the plane of the incident beam. By conservation of energy, this transmission coefficient,**T**, is related to the coefficient of reflection, **R**, by:

$$\mathbf{T} = 1 - \mathbf{R} \tag{40}$$

If the wavelength and diameter of the beam are both small compared to the radius of curvature of the disk, the interface can be considered approximately planar. In this case **R** is given by:

$$\mathbf{R} = VV^* \tag{41}$$

where V is the amplitude reflection coefficient from a plane surface, and the asterisk represents complex conjugation. V is given by:[Brekhovskikh 1960, eq.[7.13]]

$$V = \frac{(Z_l \cos^2 2\gamma_1 + Z_t \sin^2 2\gamma_1 - Z)}{(Z_l \cos^2 2\gamma_1 + Z_t \sin^2 2\gamma_1 + Z)} \tag{42}$$

with Z, Z_l, and Z_t given by:

$$Z = \rho_{liquid} c_0 / \cos\theta \qquad Z_t = \rho_{solid} b_1 / \cos\gamma_1 \qquad Z_l = \rho_{solid} c_1 / \cos\theta_1 \tag{43}$$

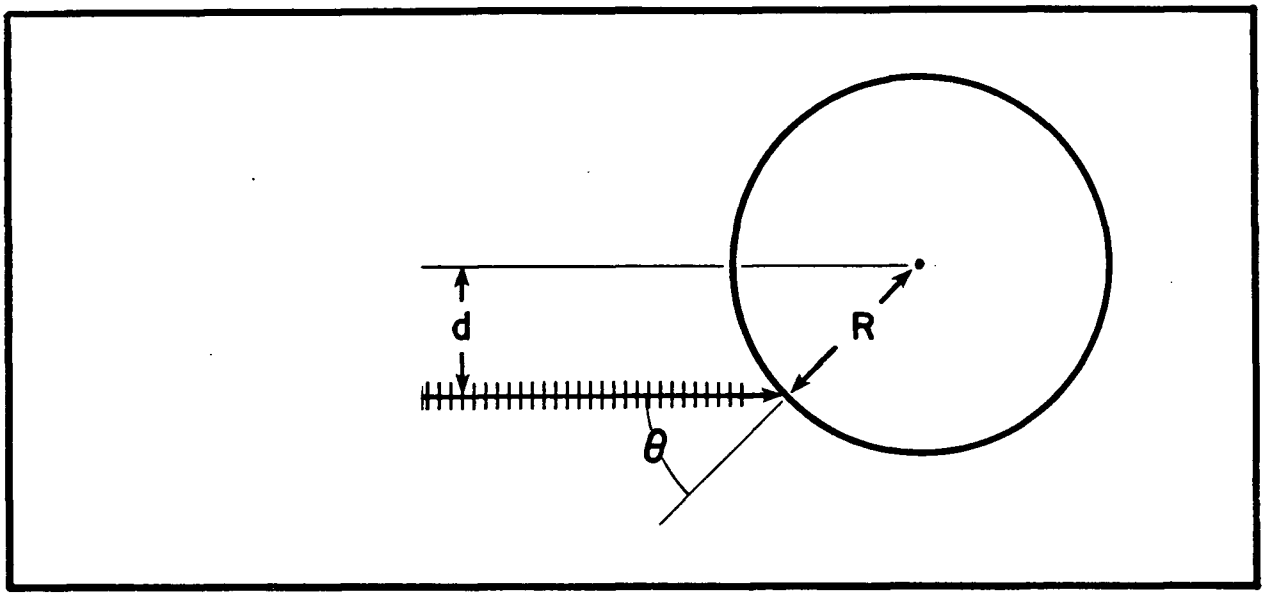

FIGURE 10–How the Angle of Incidence is related to the Impact Parameter, d

---

In summary, the force that causes torque on the disk will be proportional to the amount of the sound beam absorbed in the disk, and will act in the direction of the incident sound beam. The torque on the disk is the product of this force with the perpendicular distance , d, from the line of action of the force to the disk axis as shown in Figure 10. The angle of incidence, θ, is related to d by:

$$\theta = \sin^{-1}(d/R) \tag{44}$$

where R is the radius of the disk. At large angles of incidence, where d approaches R, the magnitude of the amplitude reflection coefficient $\|V(\theta)\|$ approaches unity so very little of

the sound beam is absorbed in the disk and the component of the force on the disk which causes a torque becomes small. If d is very small, the torque will also be reduced. We see that the torque will be maximised when d lies somewhere between 0 and R.

2.9 Summary

In summary, we have four definitions for different kinds of acoustic radiation pressure each valid for a different physical situation. There is the Eulerian average pressure which acts on an impermeable wall laterally confining the beam, and which is the pressure that would be recorded by a microscopic transducer held fixed in the fluid. For the case of one-dimensional travelling waves, this pressure is given by:

$$\langle \mathbf{P} \rangle = \mathbf{P}_0 + \frac{(\gamma - 3)}{4} \langle \mathbf{E} \rangle \tag{45}$$

There is the average Lagrangian pressure which acts on the surface of a perfectly absorbing target blocking the sound beam, and would be recorded by a tiny transducer free to move with the fluid. For one-dimensional plane waves, this pressure is given by:

$$\langle \mathbf{P}^L \rangle = \mathbf{P}_0 + \frac{(\gamma + 1)}{4} \langle \mathbf{E} \rangle \tag{46}$$

Next, there is the Rayleigh pressure which is defined as the net pressure acting on the perfectly absorbing target in the specific situation shown in Figure 4 where the sound beam is laterally confined. The Rayleigh pressure is given by:

$$\mathbf{P}^{Ra} = \frac{(\gamma + 1)}{4} \langle \mathbf{E} \rangle \tag{47}$$

Finally there is the Langevin pressure which is the net pressure acting on a perfectly absorbing target where the sound beam is unconfined as shown in Figure 5. This pressure is given by:

$$\mathbf{P}^{Lan} = \langle \mathbf{E} \rangle \tag{48}$$

The Langevin pressure works out to a force on the target of 62.5 mg per Watt of incident power [Zeniuk and Chivers 1976].

For simplicity, we have limited our investigation of radiation pressure to simple one-dimensional situations where perfectly plane waves, initially harmonic, impinge on perfectly absorbing targets. This approach has allowed us to ignore the tensorial nature of radiation pressure. Where there is a component of fluid particle velocity parallel to the target surface, the radiation pressure can not be calculated by simply integrating the energy density $\langle \mathbf{E} \rangle$ over the target surface [Beissner 1982]. If the target is reflecting, there will be nonlinear interactions between incident and reflected waves which, again, we have not included in our theory [Chu and Apfel 1982].

Radiation pressure will definitely cause a torque on the absorbing disk in our meter as shown in Figure 8, but there is another mechanism which may contribute to the torque on the disk. This mechanism is acoustic streaming and is discussed in the next chapter.

CHAPTER 3–Acoustic Streaming

3.1 What is Acoustic Streaming ?

Acoustic streaming is the steady flow induced in a fluid by the passage of an acoustic wave. Streaming arises as a consequence of conservation of momentum. Associated with a travelling acoustic wave is a flux of momentum proportional to the intensity of the wave.[Morse and Ingard 1968, sec.6.2] If the wave is absorbed in the fluid, each fluid element will feel a force because the wave carries more momentum into it than out. This force will cause the fluid element to accelerate until the acoustic force is balanced by the viscous forces which act to reduce any velocity gradients in the fluid. As no real fluid is completely non absorbing, there will be streaming in our meter. This fluid flow may cause torque when it impinges on the rotating disk. In the last chapter on radiation pressure we did not include absorption or viscosity in our theory. Here, we take these factors into account and consider the resulting streaming.

3.2 Equations of Motion for a Viscous Fluid

The equation of motion for the flow of a viscous fluid is the well known Navier-Stokes equation:[Aris 1962]

$$\rho\left[\frac{\partial\vec{\mathbf{U}}}{\partial t}+\vec{\mathbf{U}}\cdot\nabla\vec{\mathbf{U}}\right]=-\vec{\nabla}\mathbf{P}+\vec{\nabla}\left\{\left[\frac{4}{3}\mu+\mathbf{b}\right]\vec{\nabla}\cdot\vec{\mathbf{U}}\right\}-\mu\vec{\nabla}\times\vec{\nabla}\times\vec{\mathbf{U}} \tag{49}$$

where μ and $\mathbf{b}$ are the coefficients of shear viscosity and bulk viscosity respectively. This equation and the continuity equation (1) govern the allowed motions of a viscous Newtonian fluid.

The Navier-Stokes equation is only valid for Newtonian fluids. That is, fluids which are:

1) Isotropic.

2) Homogeneous

3) Such that the stress tensor $\overleftrightarrow{\sigma}$ is a linear function of the rate of deformation tensor $\overleftrightarrow{\mathbf{V}}$.

4) Such that at equilibrium, the stress is the same as the hydrostatic pressure.

Fortunately, many real fluids approximately fit these requirements. We further assume that for a given frequency of acoustic wave, μ and $\mathbf{b}$ are constants independent of pressure and density variations in the wave. Finally, we need to use a modified equation of state which is generally postulated to be of the form: [Nyborg 1965, p.269]

$$\mathbf{P}_1(\rho)=c_0^2\rho_1+R(\omega)\dot{\rho_1} \tag{50}$$

where $R(\omega)$ is some highly frequency dependent quantity, and ρ_1 is the second term in a power series expansion of ρ. Both $\mathbf{P}_1$ and ρ_1 are assumed to be harmonically varying

quantities. The first term on the RHS of (50) is easily recognized as the first term in a Taylor series expansion for a general function $\mathbf{P}(\rho)$ when we see that:

$$c_0^2 = \left(\frac{\partial \mathbf{P}}{\partial \rho}\right)_{\rho=\rho_0} \quad , \quad \rho_1 \approx \rho_0 \tag{51}$$

The second term on the RHS of (50) takes into account the pressure required to overcome the bulk viscosity of the fluid as it is compressed. This term arises from the motion of the fluid and drops out when the fluid is at equilibrium. The relationship between $R(\omega)$ and the bulk viscosity can be made especially clear if (50) is substituted into the RHS of (49). With some manipulation, $R(\omega)$ appears as a term added to the bulk viscosity **b** [Beyer 1974, p.242].

3.3 Calculation of Acoustic Streaming

To calculate the acoustic streaming, we use the method of successive approximations on equation (49). This equation can be rewritten using the continuity equation (20) as:

$$\begin{aligned} \rho\left[\frac{\partial \vec{\mathbf{U}}}{\partial t} + (\vec{\mathbf{U}}\cdot\vec{\nabla})\vec{\mathbf{U}}\right] &= \frac{\partial(\rho\vec{\mathbf{U}})}{\partial t} - \vec{\mathbf{U}}\frac{\partial \rho}{\partial t} + \rho\vec{\mathbf{U}}\vec{\nabla}\vec{\mathbf{U}} \\ &= \frac{\partial(\rho\vec{\mathbf{U}})}{\partial t} + \vec{\mathbf{U}}\vec{\nabla}\cdot\rho\vec{\mathbf{U}} + \rho\vec{\mathbf{U}}\cdot\vec{\nabla}\vec{\mathbf{U}} \\ &= -\vec{\nabla}\mathbf{P} + (\frac{4}{3}\mu + \mathbf{b})\vec{\nabla}\vec{\nabla}\cdot\vec{\mathbf{U}} - \mu\vec{\nabla}\times\vec{\nabla}\times\vec{\mathbf{U}} \end{aligned} \tag{52}$$

As before, we write $\mathbf{P}$, ρ, and $\vec{\mathbf{U}}$, as series of successively higher approximations:

$$\mathbf{P} = \mathbf{P}_0 + \epsilon\mathbf{P}_1 + \epsilon^2\mathbf{P}_2 + \ldots \tag{53}$$

$$\rho = \rho_0 + \epsilon\rho_1 + \epsilon^2\rho_2 + \ldots \tag{54}$$

$$\vec{\mathbf{U}} = \quad \epsilon\vec{\mathbf{U}}_1 + \epsilon^2\vec{\mathbf{U}}_2 + \ldots \tag{55}$$

These expressions for $\mathbf{P}$, ρ, and $\vec{\mathbf{U}}$, are then substituted into (52) where terms of equal order are collected and assumed to satisfy the resulting equation independently of terms of other orders. Central to obtaining a solution by this technique is the assumption that each term in (53), (54), and (55), is much smaller than the term preceeding it. If this assumption holds, a solution that is arbitrarily close to the exact solution can be found by solving enough of the linear equations which result from this substitution. The faster the terms in the series (53), (54), and (55) die away, the more rapidly the approximate solutions converge to the exact solution. The first three members of this infinite hierarchy of equations are:

$$-\vec{\nabla}\mathbf{P}_0 = 0 \tag{56}$$

$$\rho_0\frac{\partial\vec{\mathbf{U}}_1}{\partial t} = -\vec{\nabla}\mathbf{P}_1 + \left(\frac{4}{3}\mu + \mathbf{b}\right)\vec{\nabla}\vec{\nabla}\cdot\vec{\mathbf{U}}_1 - \mu\vec{\nabla}\times\vec{\nabla}\times\vec{\mathbf{U}}_1 \tag{57}$$

$$\begin{aligned}\frac{\partial(\rho_0\vec{\mathbf{U}}_2 + \rho_1\vec{\mathbf{U}}_1)}{\partial t} + \rho_0\vec{\mathbf{U}}_1\vec{\nabla}\cdot\vec{\mathbf{U}}_1 + \rho_0\vec{\mathbf{U}}_1\cdot\vec{\nabla}\vec{\mathbf{U}}_1 = -\vec{\nabla}\mathbf{P}_2 + \left(\frac{4}{3}\mu + \mathbf{b}\right)\vec{\nabla}\vec{\nabla}\cdot\vec{\mathbf{U}}_2 \\ - \mu\vec{\nabla}\times\vec{\nabla}\times\vec{\mathbf{U}}_2\end{aligned} \tag{58}$$

(56) is trivial, merely asserting that the equilibrium pressure $\mathbf{P}_0$ is a constant. We expect to obtain a solution which combines the high-frequency oscillation of the acoustic wave with a slow steady flow. Anticipating this, we assume that $\mathbf{P}_1$, ρ_1, and $\mathbf{U}_1$, vary harmonically in space and time at the frequency of the acoustic wave, ω. If we further require that the first-order velocity field be irrotational, we obtain the one-dimensional attenuated plane-wave solution:[Nyborg 1965, p.272]

$$\vec{\mathbf{U}}_1 = \mathrm{e}^{-\alpha x}\mathrm{e}^{i(\omega t - kx)} \tag{59}$$

here, α is given by:

$$\alpha = \frac{(\frac{4}{3}\mu + \mathbf{b} + \rho_0 R)k^2}{2\rho_0 c_0} \tag{60}$$

and k is the wave number for the acoustic beam. This solution will not be valid near boundaries in the fluid where a rotational component of $\vec{\mathbf{U}}_1$ is necessary to satisfy the boundary conditions [Tjøtta 1958, p.3].

While the first order equation (56) yields solutions which, as expected, are consistent with the predictions of classical acoustics, solutions to the second-order equation (57) demonstrate two nonlinear effects, streaming, and frequency doubling. As we are only concerned with steady streaming, we lose nothing by time averaging (57) over several cycles. If the time average, $\langle \mathbf{Q} \rangle$, of any quantity, $\mathbf{Q}$, is defined by:

$$\langle \mathbf{Q} \rangle = \frac{1}{T} \int_0^T \mathbf{Q}(t) dt \tag{61}$$

the time average of (57) is given by:

$$\left\langle \frac{\partial(\rho_1 \vec{\mathbf{U}}_1 + \rho_0 \vec{\mathbf{U}}_2)}{\partial t} - \rho_0(\vec{\mathbf{U}}_1 \nabla \cdot \vec{\mathbf{U}}_1 + \vec{\mathbf{U}}_1 \cdot \nabla \vec{\mathbf{U}}_1) \right\rangle = \left\langle \vec{\nabla} \mathbf{P}_2 + (\frac{4}{3}\mu + \mathbf{b}) \nabla \nabla \cdot \vec{\mathbf{U}}_2 - \mu \nabla \times \nabla \times \vec{\mathbf{U}}_2 \right\rangle \tag{62}$$

which reduces to:

$$\frac{\partial}{\partial t} \left\langle \rho_1 \vec{\mathbf{U}}_1 + \rho_0 \vec{\mathbf{U}}_2 \right\rangle - \rho_0 \left\langle \vec{\mathbf{U}}_1 \nabla \cdot \vec{\mathbf{U}}_1 + \vec{\mathbf{U}}_1 \cdot \nabla \vec{\mathbf{U}}_1 \right\rangle = \nabla \left\langle \mathbf{P}_2 \right\rangle + (\frac{4}{3}\mu + \mathbf{b}) \nabla \nabla \cdot \left\langle \vec{\mathbf{U}}_2 \right\rangle - \mu \nabla \times \nabla \times \left\langle \vec{\mathbf{U}}_2 \right\rangle \tag{63}$$

The first term of (63) is identically zero. The second term, which is completely determined once $\vec{\mathbf{U}}_1$ is known, acts like a driving force field [Nyborg 1965, p.271]. The strategy for calculating streaming velocities is thus first to calculate the first order velocity field $\mathbf{U}_1$ from

the geometry of the situation using classical linearized acoustic theory. This expression for $\mathbf{U}_1$ can then be used in (63) to calculate, $\langle \mathbf{U}_2 \rangle$, the streaming velocity.

3.4 Streaming Between two Parallel Walls

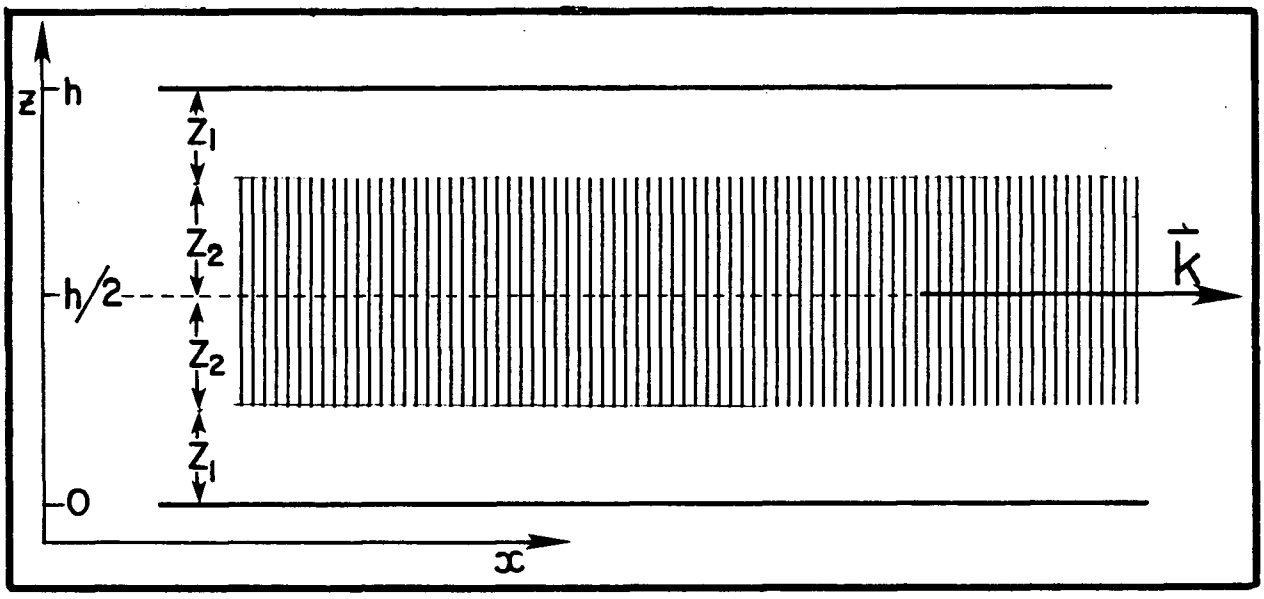

FIGURE 11–Acoustic Streaming Between Two Parallel Walls

One situation for which the streaming velocity is particularly easy to calculate is the streaming in a channel formed between two parallel walls. This configuration is shown in Figure 11. In solving this problem, we assume that the sound beam cuts off sharply on the sides. Inside the beam then, the first order velocity, $\mathbf{U}_1$, is a damped sine wave given by the real part of (60) . Outside the beam, $\mathbf{U}_1$ is zero. With this result, the driving term

in (63) can be calculated to be [Nyborg 1965, p.283]:

$$\vec{\mathbf{F}} = -2\rho_0\left\langle \mathbf{U}_1 \frac{\partial \mathbf{U}_1}{\partial x} \right\rangle \hat{x} = \rho_0 \alpha \mathrm{A}^2 \mathrm{e}^{-2\alpha x} \approx \rho_0 \alpha \mathrm{A}^2 \tag{64}$$

here, A is the amplitude of the incident sound wave. The approximate expression on the RHS of (64) applies if:

$$\alpha x \ll 1 \tag{65}$$

so that the beam intensity is more or less constant in the region of interest. For this one dimensional problem, the streaming equation, (62) reduces to:[Nyborg 1965, p.282]

$$\mu \frac{\partial^2 \mathbf{U}_2}{\partial z^2} - \frac{\partial \mathbf{P}_2}{\partial x} + \mathbf{F}_x = 0 \tag{66}$$

which has the solution:

$$\begin{aligned} \mathbf{U}_2(z) &= \frac{\mathbf{F}_x}{2\mu}(h - 2z_1)z \quad \text{for } 0 < z < z_1 \\ &= \frac{\mathbf{F}_x}{2\mu}(hz - z^2 - z_1^2) \text{ for } z_1 < z < h/2 \end{aligned} \tag{67}$$

Figure 12 shows plots of this solution for several values of z_1. This solution assumes that the channel is open ended in which case the hydrostatic pressure does not vary along its length. In other words, we set:

$$\nabla \mathbf{P}_2 = 0 \tag{68}$$

The streaming velocity is thus seen to be directly proportional to the intensity of the sound beam, and the absorption coefficient, α, and inversely proportional to the coefficient of shear viscosity, μ. (See equation (64) with $\vec{\mathbf{F}} = \mathbf{F}_x = \rho_0 \alpha A^2$: A^2 is proportional to intensity.)

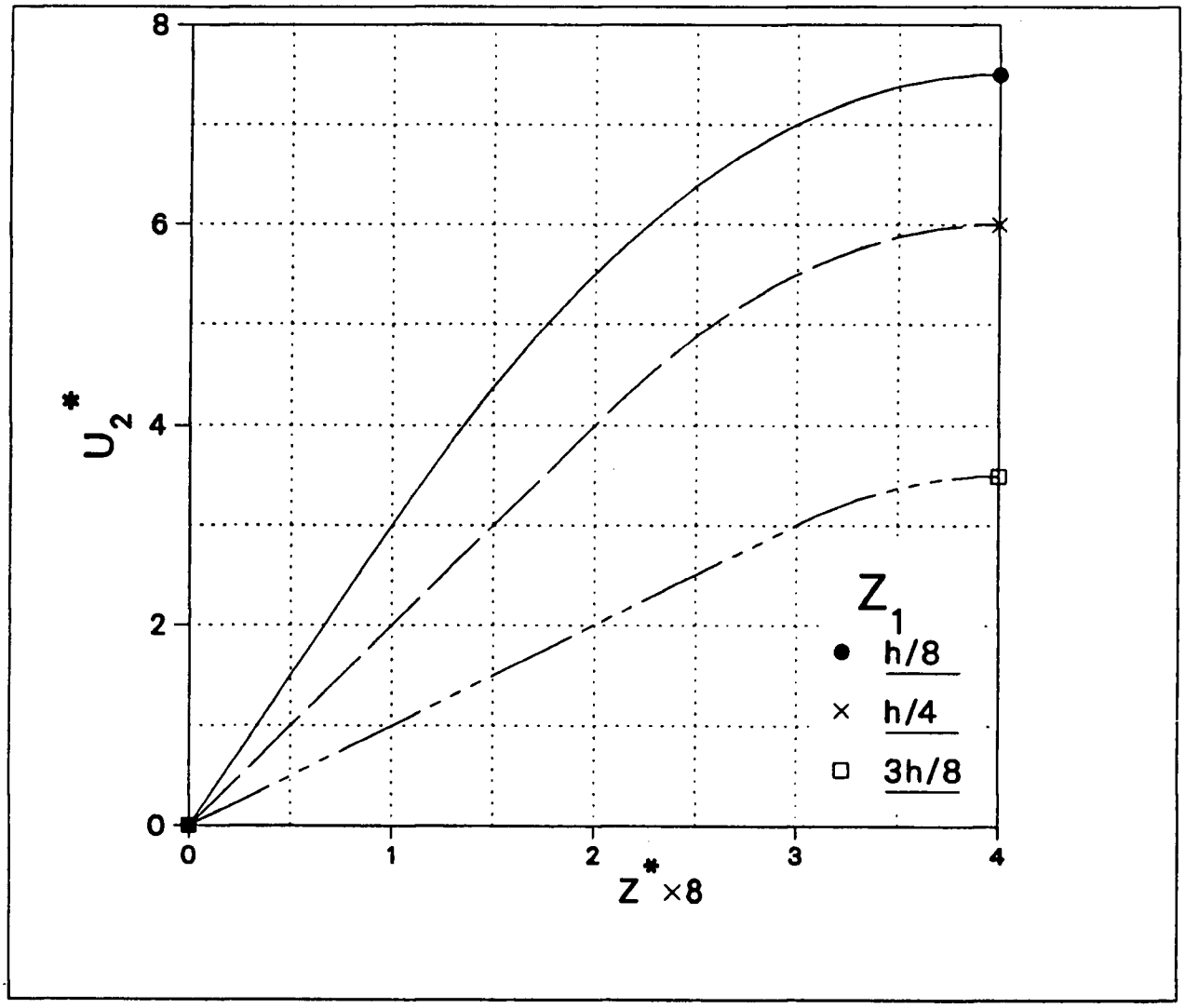

FIGURE 12–Velocity Profiles for Acoustic Streaming Between Two Parallel Walls
These curves are given in terms of the dimensionless parameters $\mathbf{U}_2^* = \mathbf{U}_2 \times (64\mu/h^2\mathbf{F}_x)$ and $Z^* = Z/h$.

Lighthill points out that this treatment is only applicable when the sound intensity is sufficiently low [Lighthill 1978, p.343]. At higher power levels, higher order terms must be taken into account because inertial effects become important to the fluid motion. For the special case of a "Stokeslet" point source dipole radiator in air, this theory breaks down when the radiated power exceeds 10^{-6} W. To a very crude approximation, we can consider the acoustic field near the focus of our sound beam to be similar to that near a Stokeslet source. Given this information, the dimensionless Reynolds number, *Re*, can be used to

predict the intensity for which this theory breaks down in other fluids. The Reynolds number is a measure of the relative importance of inertial forces and viscous forces to the fluid flow. It is given by:

$$Re = \frac{UL}{\mu} = \frac{I\alpha L}{\mu^2} \tag{69}$$

here, U, and L, are a scale velocity, and a scale length respectively. I is the intensity of the sound beam. At the onset of deviation from our model, Re should have the same value in any fluid. Using the values:[CRC Press 1976, pp.E-47,E-49] [Barnes and Beyer 1964]

$$\begin{aligned} \mu_{\text{air}} &= 182.7 \times 10^{-}6 \text{ poise at } 18°\text{C} & \mu_{H_2O} &= 1.053 \times 10^{-2} \text{ poise at } 18°\text{C} \\ \alpha_{\text{air}} &= 314\,\text{dB}/1000' \text{ at } 80\,\text{kHz} & \alpha_{H_2O} &= 25 \times 10^{-17}\nu^2/\text{cm} \\ &= .99763/\text{cm} & &= 1.6 \times 10^{-6}/\text{cm at } 80\text{kHz} \end{aligned} \tag{70}$$

we find this theory valid for radiated power levels of up to several hundred Watts for a Stokeslet source in water.

3.5 Acoustic Streaming Summary

In this chapter, we have seen that when a sound beam is absorbed as it propagates through a fluid, a steady flow of the fluid ensues. This flow arises because an acoustic wave is accompanied by a flux of momentum proportional to its intensity. As the wave is absorbed, this momentum is deposited in the fluid resulting in steady time-averaged motion. For one-dimensional streaming away from boundaries in the fluid, and where the coefficient of sound absorption, α, is small, the streaming velocity is directly proportional to the intensity of the sound field and α, and inversely proportional to the coefficient of shear velocity, μ.

Now that we have described the mechanisms which can cause the torque to rotate the disk in our meter, we need to look at the forces which resist the rotation of the disk. It is the interplay of these drag forces with the driving forces that cause the disk to rotate at a constant speed determined by the intensity of the incident sound beam.

CHAPTER 4–The Drag on a Rotating Disk in a Still Fluid

4.1 The Drag on a Rotating Disk in a Still Fluid

The torque required to rotate a thin disk in an infinite fluid body can be calculated by solving the Navier-Stokes equations in cylindrical coordinates with the appropriate boundary conditions. These calculations can be found in the books by Schlichting [Schlichting 1955, p.78] and Goldstein [Goldstein 1965, pp.110ff] who obtain the result:

$$M = 0.616\pi\rho R^4(\nu\omega^3)^{1/2} \tag{71}$$

Here, M, is the torque acting on the disk, ω is the angular frequency of rotation of the disk, and ν is the kinematic viscosity given by $\nu = \mu/\rho$. This result is derived from an exact solution to the Navier-Stokes equation valid for a disk of infinite radius.

The torque on a finite disk is calculated by assuming that the fluid flows as if the disk were infinite. These velocity components are then used to find the moment acting at each point on the disk surface. The torque needed to rotate the disk is found by integrating the moment over the surface of the disk. Four assumptions are made here, the first two are that perfect cylindrical symmetry is maintained, and that the disk spins in an infinite body of fluid. Neither of these conditions can be achieved in any real experiment but both

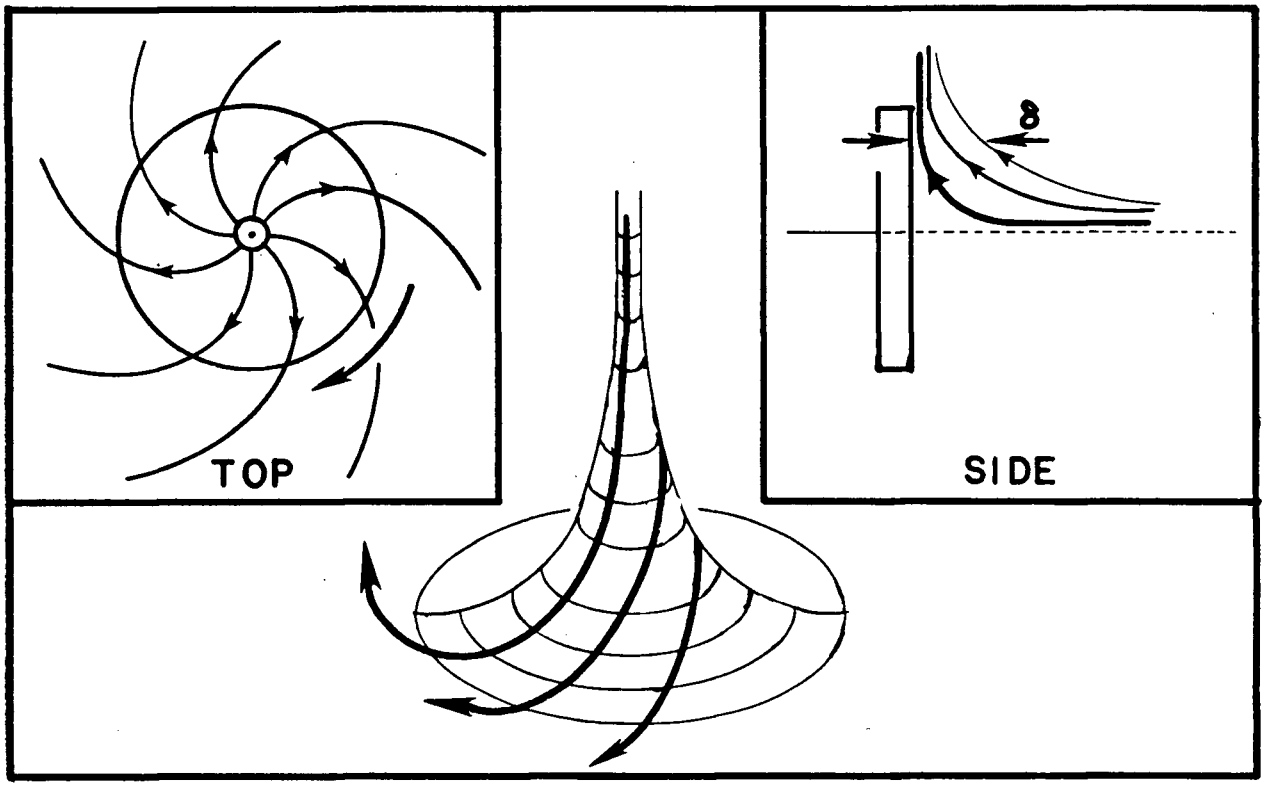

FIGURE 13–Fluid Flow Patterns Near a Rotating Disk

---

may be closely approximated. The third assumption is that the fluid flows in the same way around a disk of radius R as it does near an infinite disk as shown in Figure 13. This assumption is valid so long as the radius of the disk is large compared to the thickness of the fluid layer carried around by the disk as it rotates. The thickness, δ, of this boundary layer is approximately given by [Schlichting 1955, p.76]:

$$\delta \approx \sqrt{\nu/\omega} \tag{72}$$

For water, $\nu = 0.01002\ \mathrm{cm^2 \cdot s^{-1}}$ at 20 C [CRC Press 1976, p.F-49] so for a 2.5 cm diameter disk, this theory would apply for angular frequencies greater than 150 RPM . At this rotation rate, δ is about 1/50 of the radius of the disk. The fourth assumption is that the

fluid flow is laminar. This assumption breaks down at high rotation speeds. For a rotating disk, the flow becomes turbulent when the Reynolds number given by:

$$\mathbf{Re} = R^2\omega/\nu \tag{73}$$

exceeds about 3×10^5 [Schlichting 1955, p.79]. For a 2.5 cm diameter disk in water, this corresponds to a rotation rate of roughly 17,000 RPM.

(71) only gives the torque caused by drag on the flat sides of the disk, a correction must be added to account for the torque on the edge of the disk. For a disk where the thickness is not small compared to the radius, this correction is substantial.

Now we have reviewed the theory behind the forces which cause the disk to rotate, and the viscous drag which resists these forces. Before proceeding to describe the experiments done to test this theory, we should look at a process which can interfere with the propagation of the sound beam in our meter and decrease its performance. This process is acoustic cavitation.

CHAPTER 5–Acoustic Cavitation

5.1 What is Acoustic Cavitation?

In our discussions on streaming, and radiation pressure, we considered only the case of sound waves propagating through a homogeneous fluid. In a liquid, if the acoustic intensity is too great, voids can form under the action of the sound wave. This 'acoustic cavitation' can cause great changes in the behaviour of the liquid, partly by greatly increasing the effective sound absorption coefficient, α. Vigorous cavitation can cause severe damage to solid objects in contact with the cavitating region in a liquid [Erdmann-Jesnitzer et.al. 1973]

Acoustic cavitation is a process by which microbubbles, stabilized by motes of dust, grow, oscillate for some time, and then collapse under the action of an acoustic wave [Flynn 1964]. These bubbles make the liquid nonhomogeneous so that the equations derived above for the propagation of sound waves through homogeneous fluids are no longer strictly valid. These collapsing bubbles effectively concentrate energy from the sound field, collecting it as they grow, and releasing it when they collapse. During collapse, tremendous pressures,

sufficient even to damage hard materials such as stainless steel, can develop inside cavitation bubbles [Hammitt 1980, p.223]. In order to avoid these difficulties, the intensity of the sound field must be kept below the cavitation threshold.

5.2 Types of Cavitation

Cavitation fields can be divided into two classes depending on the behaviour of the cavitation bubbles. If the bubbles form and oscillate for many cycles of the sound beam before they drift away or collapse, the cavitation is called 'stable'. If the bubbles grow to their maximum size and collapse all in one or two cycles of the sound field, the cavitation is termed 'transient'. Most of the physical and chemical effects of cavitation arise from the high temperatures and pressures developed in collapsing bubbles and hence are associated with transient cavitation [Flynn 1964, sec.IV]. The resonantly oscillating bubbles of a stable cavitation field can scatter a sound wave and interfere with its propagation through a liquid. Both types of cavitation are detrimental to the operation of our meter. A cavitation field can display both transient and stable behaviour at the same time. Which type of cavitation dominates depends on the dissolved gas content of the liquid, the atmospheric pressure, and the frequency of the sound field among other factors.

5.3 Cavitation Thresholds

Unless extreme care is taken to make the liquid ultra-pure, cavitation always begins at intensities far lower than necessary to cause stresses that exceed the theoretical tensile strength of the fluid. Cavitation is initiated at nuclei in the liquid which are usually

microbubbles stabilized by motes of dust [Apfel 1970]. The simplest theoretical cavitation threshold, originally due to Blake, considers the equilibrium of small spherical bubbles and calculates the hydrostatic pressure below which these bubbles become unstable and begin to expand explosively. The Blake threshold is the sound intensity at which this pressure is just reached at one point during the cycle. It is given by:[Flynn 1964, p.121]

$$\mathbf{P}_{\mathbf{AC}}^{Blake} = \mathbf{P}_0 - \mathbf{P}_v + \frac{4\sigma}{3\sqrt{3}R_0}\left(1 + (\mathbf{P}_0 - \mathbf{P}_v)\frac{R_0}{2\sigma}\right)^{-1/2} \tag{74}$$

where $\mathbf{P}_{\mathbf{AC}}^{Blake}$ is the pressure amplitude of a sound field at the Blake threshold, $\mathbf{P}_v$ is the vapour pressure of the liquid, σ is the surface tension of the liquid, and R_0 is the equilibrium radius of the tiny spherical bubbles in the liquid which are assumed to serve as cavitation nuclei. From (74) we see that this threshold level is inversely proportional to the size of the nuclei. As there will be a distribution of different sized nuclei in any real liquid, the onset of cavitation will not be sharp, rather, as the intensity of the acoustic field is increased, the intensity of cavitation will increase as progressively smaller nuclei become suitable for initiating cavitation.

There are several mechanisms by which the size spectrum of cavitation nuclei can change with time. Firstly, as a liquid sits, the largest nuclei tend to float to the surface. This has the effect of raising the cavitation threshold. Filtering to remove the larger nuclei has the same effect. The cavitation threshold can be lowered by introducing sediment or by bubbling gas through the liquid. Another process very important in changing the size of cavitation nuclei in a sound field is 'Rectified Diffusion'.

Rectified diffusion is a process by which a sound field pumps dissolved gas from the liquid into a small bubble. If the sound intensity is greater than the threshold for rectified

diffusion the nuclei will grow. This threshold is given by Flynn [Flynn 1964, p.121] to be:

$$\mathbf{P}_{\mathbf{AC}}^{R.D.} = \sqrt{\frac{2}{3}}\mathbf{P}_0\left\{1 + \frac{2\sigma}{R_0\mathbf{P}_0} - \frac{C_\infty}{C_0}\right\}^{1/2} \tag{75}$$

here C_∞ is the concentration of gas molecules dissolved in the liquid far from the bubble, and C_0 is the saturation concentration of the gas at ambient pressure. If the acoustic pressure amplitude exceeds either $\mathbf{P}_{\mathbf{AC}}^{Blake}$ or $\mathbf{P}_{\mathbf{AC}}^{R.D.}$ for the largest nuclei present in the sound field, cavitation will result.

Neither of these thresholds is frequency dependent. Both apply only to bubbles that are much smaller than the resonant size because in deriving (74) and (75), inertial terms in the equation of motion are neglected. The Blake threshold in particular is derived entirely from static equilibrium considerations. At frequencies closer to a bubbles resonant frequency, there is an increased tendency for that bubble to continue in resonant oscillation and not to collapse for many cycles. In other words, as the frequency is increased, the threshold for transient cavitation increases, and cavitation fields take on the characteristics of stable cavitation. In fact, for any bubble field, with any distribution of bubble sizes, it is possible to raise the frequency enough to inhibit transient cavitation. In water, it is very difficult to obtain transient cavitation at frequencies higher than about 3 MHz [Neppiras 1980, p210].

5.4 Cavitation Summary

We have seen that acoustic cavitation can adversely affect the operation of our meter both by interfering with the propagation of the acoustic beam inside it, and by damaging its components. The rotating disk may be less suceptible to cavitation damage

than other types of radiation pressure balances with flat stationary beam absorbers. To avoid cavitation, the intensity of the sound beam must be kept lower than the cavitation threshold for the liquid in the meter. This threshold can be raised by degassing the liquid, and by filtering to remove the dust particles where cavitation arises. The threshold for transient cavitation can be raised by increasing the frequency of the acoustic beam.

CHAPTER 6–Experiments

6.1 Apparatus

The basic requirements for any experiment involving ultrasound are a source of ultrasonic vibrations, and a suitable medium to carry these vibrations to the experiment in the form of ultrasonic acoustic waves. In the early days of acoustic experimentation, sirens and vibrating bars were common sources of ultrasound [Rayleigh 1945, Hueter and Bolt 1955]. Today, it is far more common to use either a piezoelectric or magnetostrictive transducer in combination with an electronic signal generator and amplifier. This combination enables very accurate control of frequency, amplitude, and waveform of the ultrasound. It also can provide a well defined acoustic beam. For the experiments described below, a piezoelectric transducer was used. In addition to this apparatus, equipment is needed to monitor the amplitude, frequency, and waveform of the signal sent to the transducer.

The medium carrying the ultrasound from the transducer to the experiment should have a small coefficient of absorption for ultrasound, preferably, it should also be easily available and non-toxic. For these reasons as well as the fact that the transducer available was designed for use in water, water was used for these experiments. To control cavitation, and the growth of algae, a filtration system is also needed.

After a well characterized sound beam is available, experiments can be done. In this case, we are investigating the behaviour of a meter consisting of a sound absorbing disk free to rotate in the acoustic field of a converging lens placed in the sound beam. We need a disk mounted on some kind of support that allows it to rotate freely, a lens, and supports to hold the lens and disk fixed in the sound beam. We also need equipment to measure the angular frequency of the disk without disturbing its rotation.

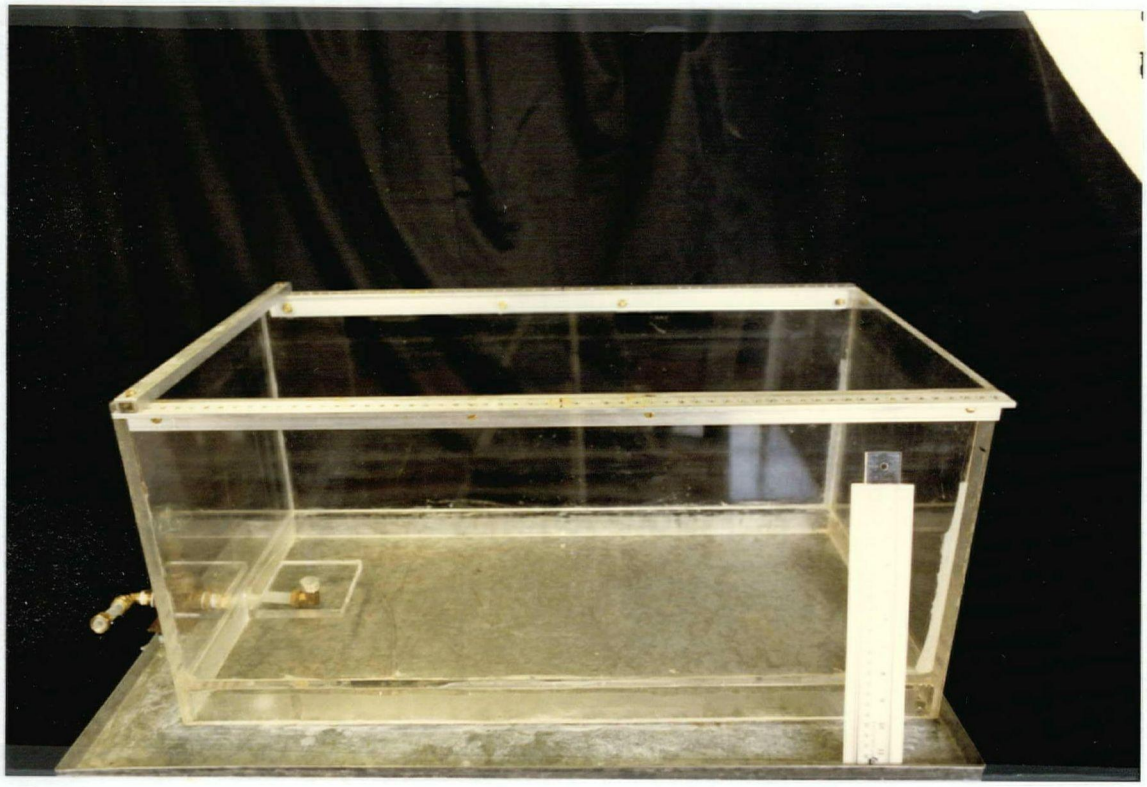

FIGURE 14–The Tank

All of the experiments described here were carried out in a tank of dimensions 76 cm long, by 30 cm deep, by 35 cm wide. These dimensions were chosen to allow flexibility in the design of apparatus to go in the tank, as well as to accomodate a large volume of water to act as a temperature bath and so to avoid large temperature fluctuations when

energy is absorbed from the sound beam. The tank was constructed from sheets of three-eighths inch thick plexiglass glued together with PS–40, a two part acrylic adhesive. Two aluminum rails were mounted along the top sides of the tank. These were drilled and tapped every half inch to provide a flexible way to mount apparatus in the tank. The tank is shown in Figure 14.

The 1.0 MHz ultrasonic beam for this experiment was produced by a transducer designed for medical theraputic use. First a Mettler ME-1017, and later, when this failed, a Mettler transducer designed for use with the Mettler 706 generator was used. These transducers differed only in packaging, electrical and ultrasonic characteristics were identical. Both transducers had a resonant frequency of 1.0 MHz and a radiating area of 10.0 cm^2. The ME-706 transducer has a capacitance of 3.02 nF as measured with a B&K model 830 capacitance meter. This gives an impedance of $\sim 50\,\Omega$ at 1.0 MHz. The transducer was driven by a sine wave signal from a Hewlett-Packard model 3312A function generator amplified by an ENI model 240L RF power amplifier. This amplifier has a gain of 50 dB and will deliver at least 40 W of c.w.power into a $50\,\Omega$ load at frequencies between 20 KHz and 10 MHz. Amplifier output voltage was measured both with a meter built into the amplifier, and a Tektronix model 468 oscilloscope connected to the transducer leads with a $10\times$ probe. The maximum voltage used was 140 V_{p-p} which corresponds to a power of 49 W delivered to a $50\,\Omega$ load. Figure 15 shows the relationship between amplifier output voltage and power delivered to a $50\,\Omega$ load. The frequency of the driving signal was monitored with a DARCY/TSI model 460 frequency counter. In order to have fine control over the frequency, a small power supply was connected to the VCO (Voltage Controlled Oscillator) † input of the function generator. To maintain a stable frequency, both the

† Varying the voltage on the VCO input of the HP3312A function generator between 0 and -2 volts sweeps the oscillator frequency over a 1000:1 range.

HP3312A and the VCO power supply were left on whenever possible. Both were allowed to warm up for at least two hours before an experiment. The electronics for generating the ultrasonic beam are shown in Figure 16.

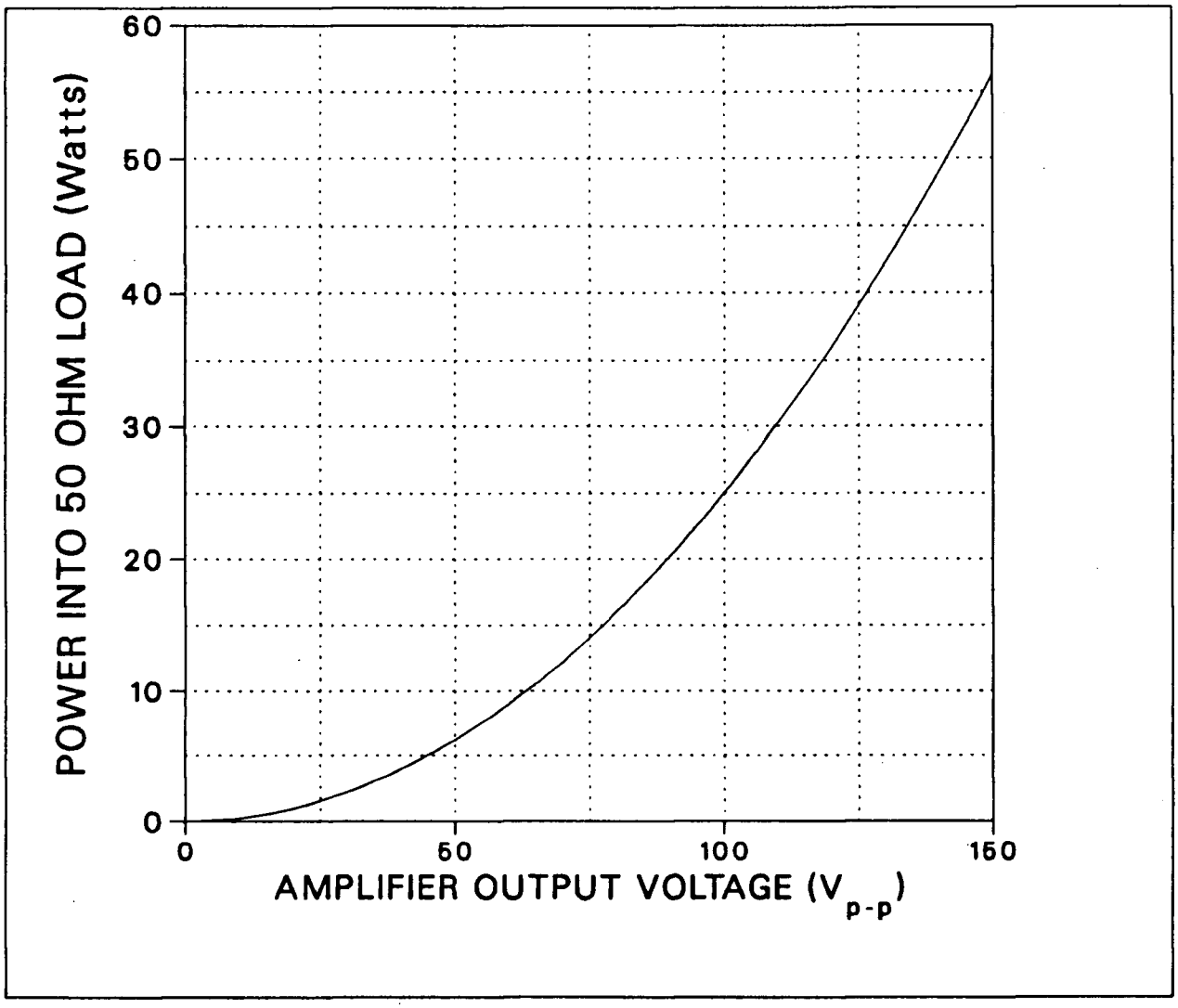

FIGURE 15–Power Delivered to a 50Ω Load vs. Amplifier Output Voltage

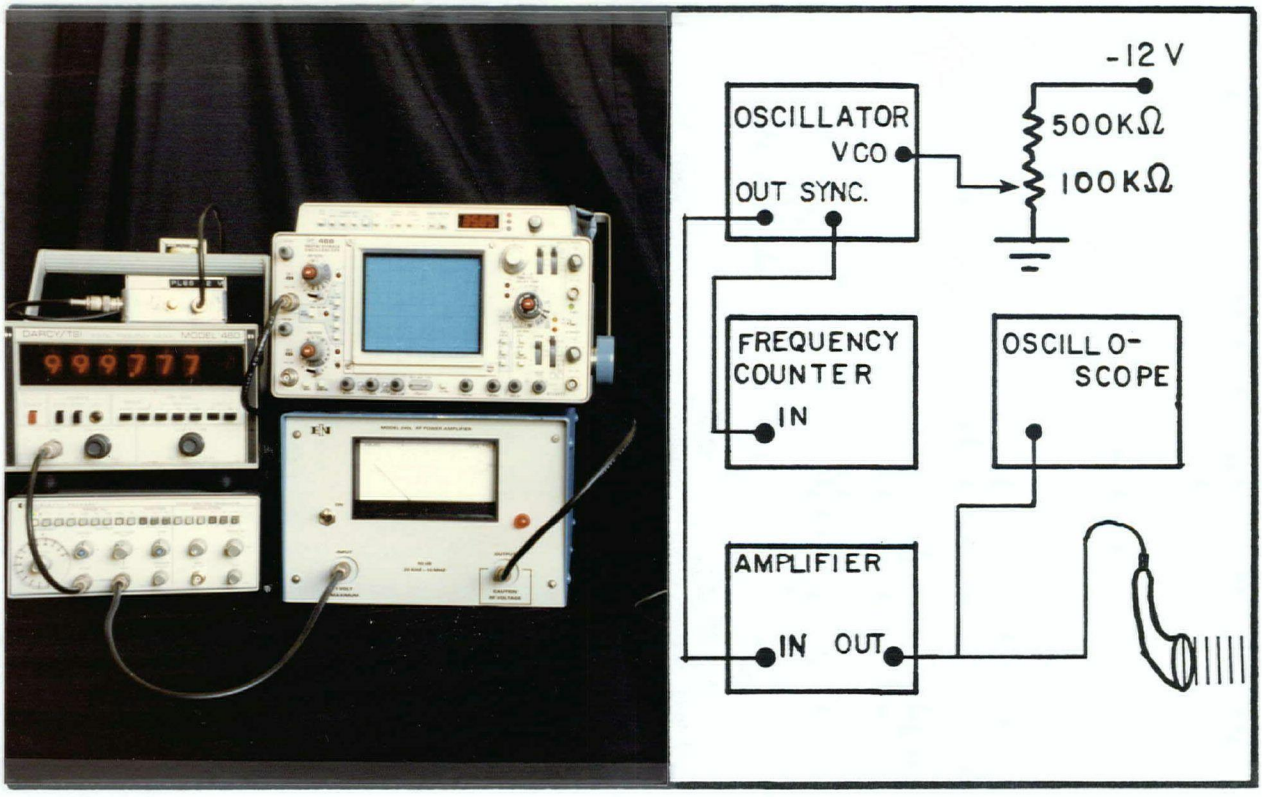

FIGURE 16–The Electronics Used to Generate and Monitor the Acoustic Beam

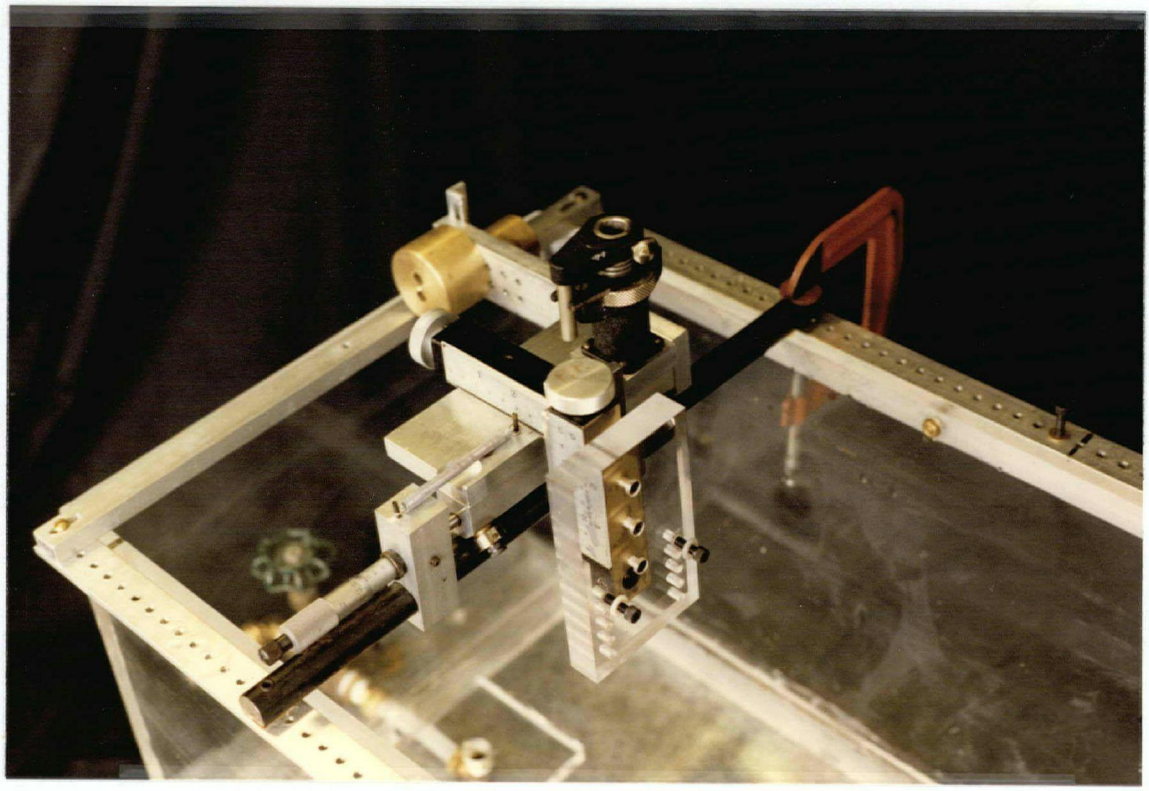

FIGURE 17–The 3–Axis Positioner

The ultrasonic transducer was mounted on a three axis positioner at one end of the tank as shown in Figure 17. The beam was focussed by a plano-concave converging lens which was held flat on the front of the transducer with two small ceramic magnets. The lens could be easily and quickly removed to wipe away the vapour bubbles which grow between it and the transducer. The lens was turned from a section of $2\frac{3}{4}$ inch diameter plexiglass rod and polished until smooth. The concave side has a radius of curvature of 47.7 mm which gives it a focal length of 10.8 cm in water.†

The disks used in these experiments were mounted by press fitting them onto 4 inch long by 1/16 inch hardened stainless steel shafts which were pointed at each end and held horizontally in a support between two friction jewels as shown in Figure 18. To prevent unwanted reflections, and the resulting creation of standing waves in the tank, a beam absorber was placed at the end of the tank. The absorber consists of 150 pink pearl number 100 pencil erasers cut in half and glued to a six inch square piece of plexiglass as shown in Figure 19. The absorber was mounted parallel to and 40 cm in front of the transducer face. The complete tank is shown in Figure 20.

To measure the rate of rotation of the disks, a strip of 0.001 inch thick mylar film was glued to the side of each disk with a very small amount of RTV silicone sealant. The beam from a small HeNe laser was then shone on the side of the disk in such a way that it was reflected by the mylar strip onto one end of an optical fiber once in each rotation. A phototransistor at the other end of the optical fiber converted the light pulses to electrical pulses which were counted electronically. Signals to the counter were gated by a timer

---

† The focal length of a plano-concave lens is given by: $f = \mathrm{R}/(1 - \frac{c_{MED}}{c_{LENS}})$ where R is the radius of curvature of the lens, and c_{LENS}, and c_{MED} are the speed of sound in the lens and in the medium surrounding the lens respectively [Hueter and Bolt 1955, p.265].

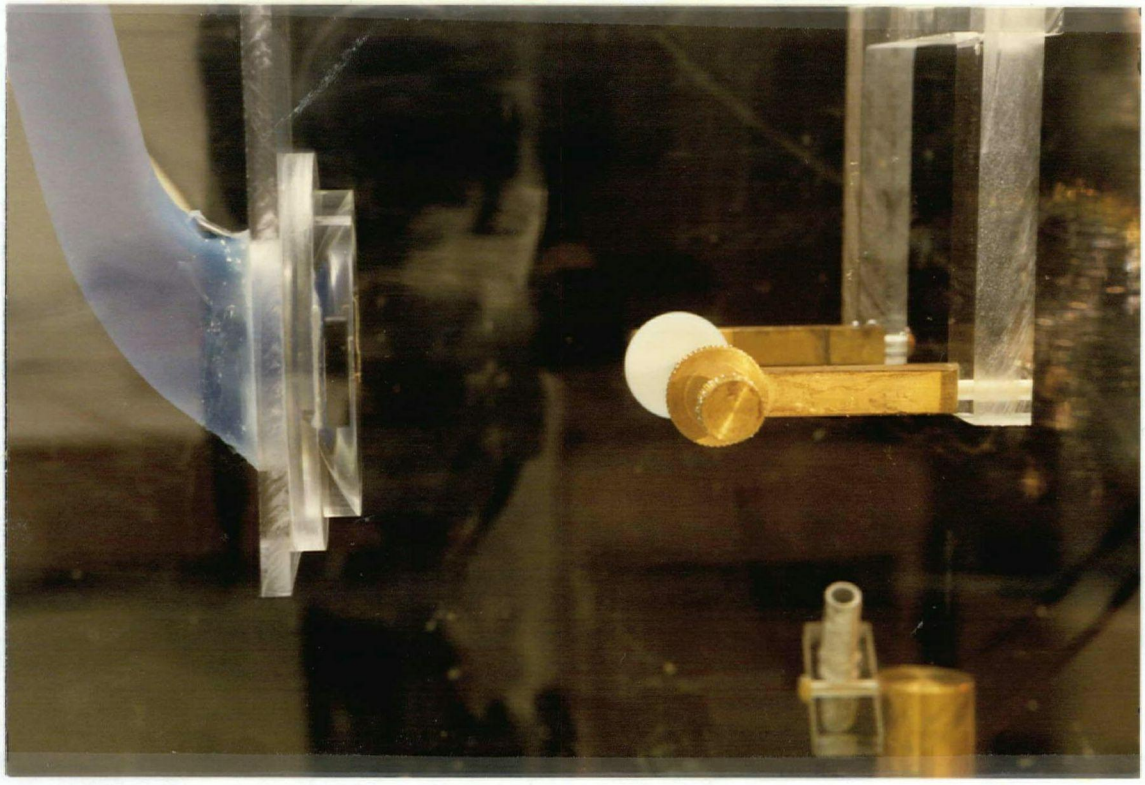

FIGURE 18–A 25 mm Diameter Disk Mounted in the Apparatus
The detector for measuring the rotation rate can be seen on the lower right.

---

clocked at the powerline frequency. This permitted the number of pulses in a convenient time period (usually 30 seconds) to be easily determined. Figure 21 is a diagram of the speed measuring system.

Water in the tank was filtered with a recirculating system consisting of an Eastern/Iwaki model MD–15 magnetic drive pump and two five micron filters in parallel.

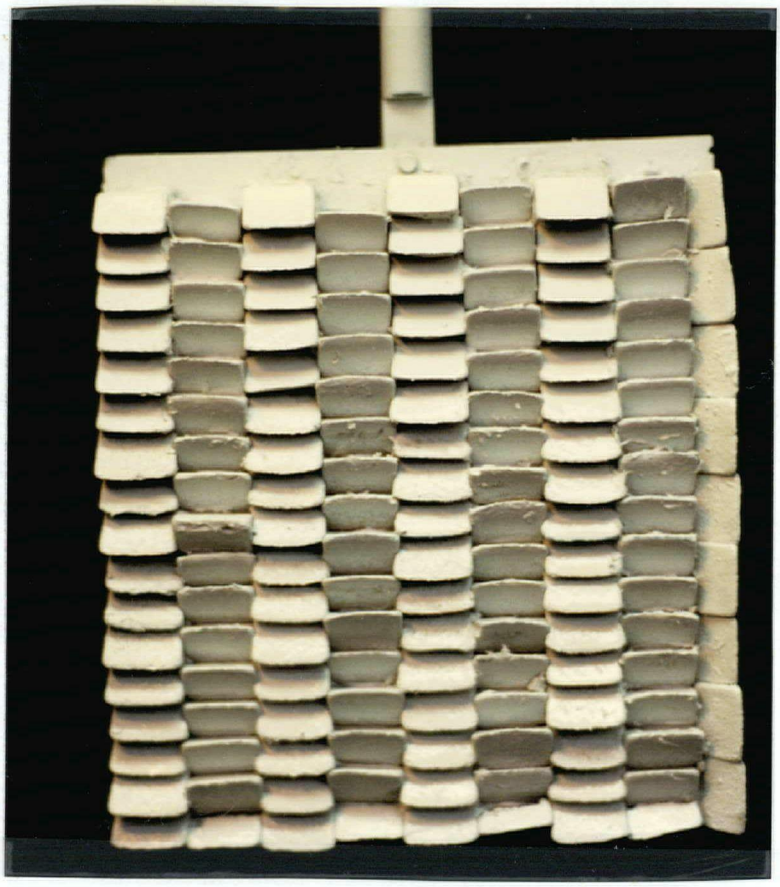

FIGURE 19–The Beam Absorber

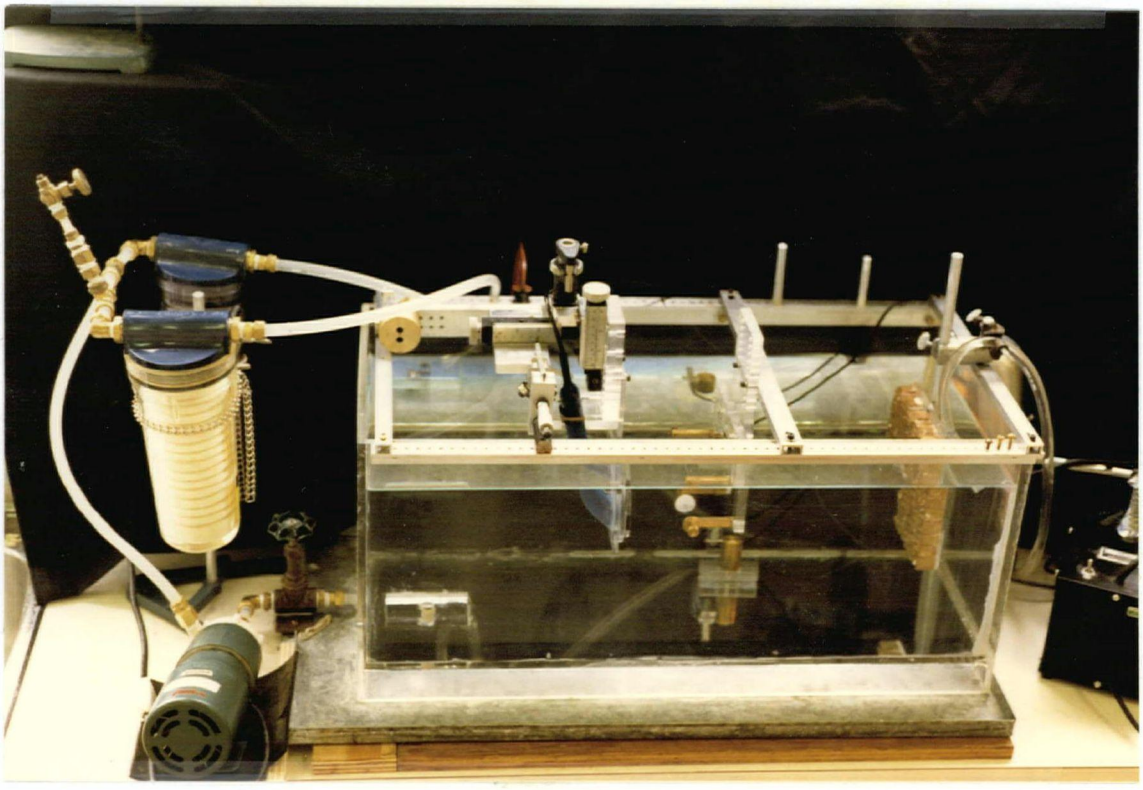

FIGURE 20–The Tank and Assembled Apparatus

From left to right, one can see the filtration system, the three axis positioner with transducer, the disk, and the beam absorber. The detector for measuring the disk rotation rate is at the bottom of the tank below and to the right of the disk.

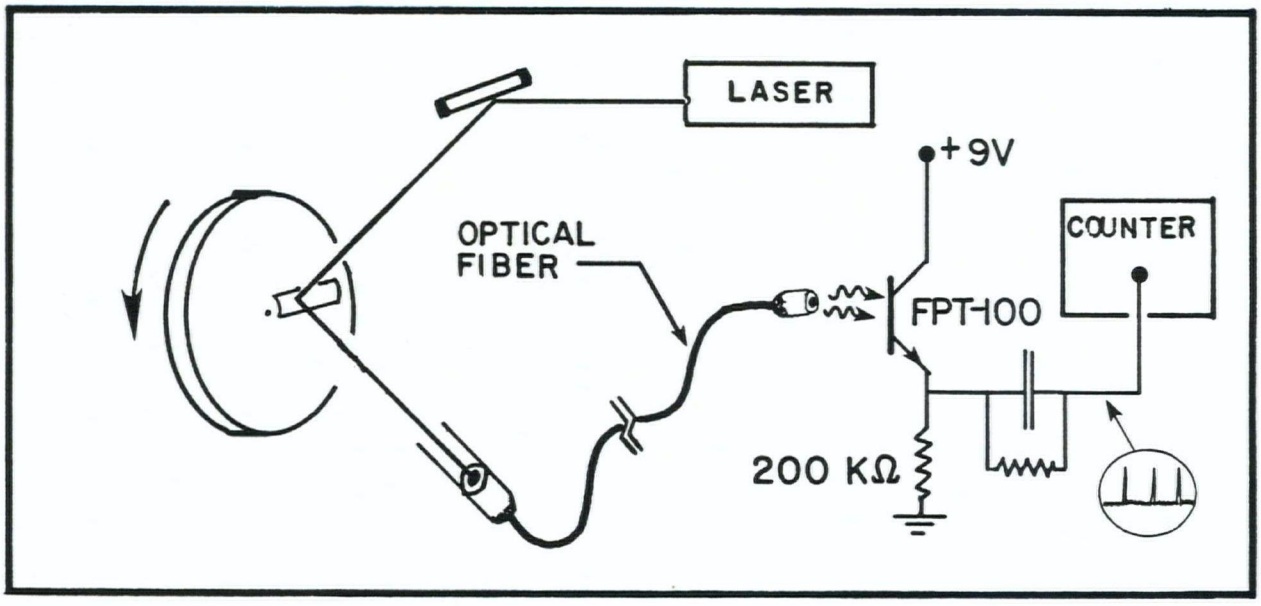

FIGURE 21–The Speed Measuring System

6.2 Beam Characterization

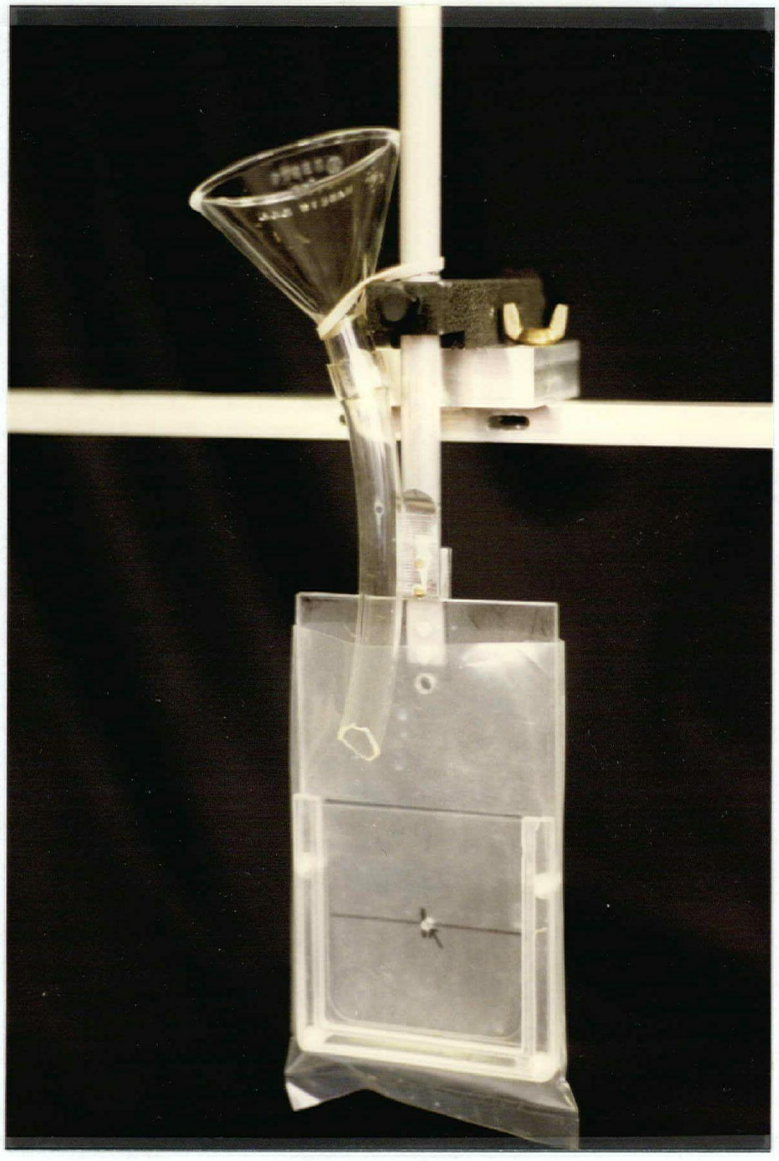

FIGURE 22–Starch Plate Photography System

In order to locate the beam in the tank accurately, and to study its focussing, crude 'photographs' were taken using a starch plate technique. This method, originally developed by Bennett uses the ultrasonically accelerated reaction of starch with Iodine to create a positive image of the beam [Bennett 1952]. Three inch square glass plates were coated with an emulsion made by mixing 10 ml Glide brand laundry starch, 32 ml cornstarch, and 200 ml of distilled water. This mixture was heated over water to 95° C and poured over the glass plates while still hot. The plates were allowed to dry overnight. To make an exposure, the plates were mounted in a plexiglass cassette which could quickly be positioned accurately in the tank perpendicular to the beam. The loaded cassette was then placed in a polyethylene bag and mounted in the tank as shown in Figure 22. Just before the exposure was to be made, 100 ml of developing solution consisting of 1.0 g I_2 crystals, 250 ml methanol, and 750 ml distilled water was diluted 5:95 with distilled water and poured into the polyethylene bag through a funnel. Then the beam was turned on. After an exposure lasting for between two and six minutes, the plate was immediately removed from the cassette, and rinsed under cold water. Figure 23 shows the profile of the beam determined by measuring the spot size on six plates exposed to the beam at half inch intervals near the focal point. Also shown in this figure is the optimum position for a 2.3 cm diameter by 3.9 mm thick nylon disk where it rotates the fastest for a given power input. Figure 24 shows two of the exposed starch plates used to profile the beam.

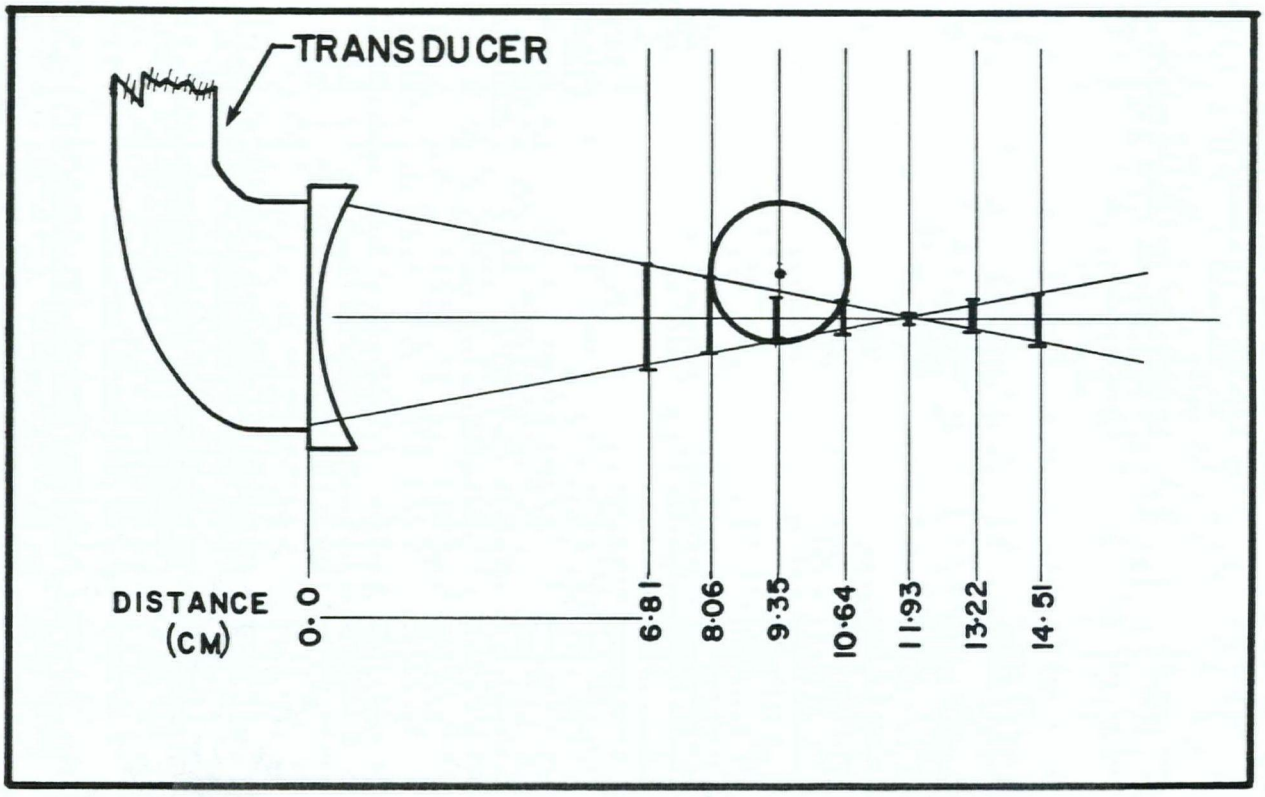

FIGURE 23–Beam Profile Determined from Starch Plate Measurements

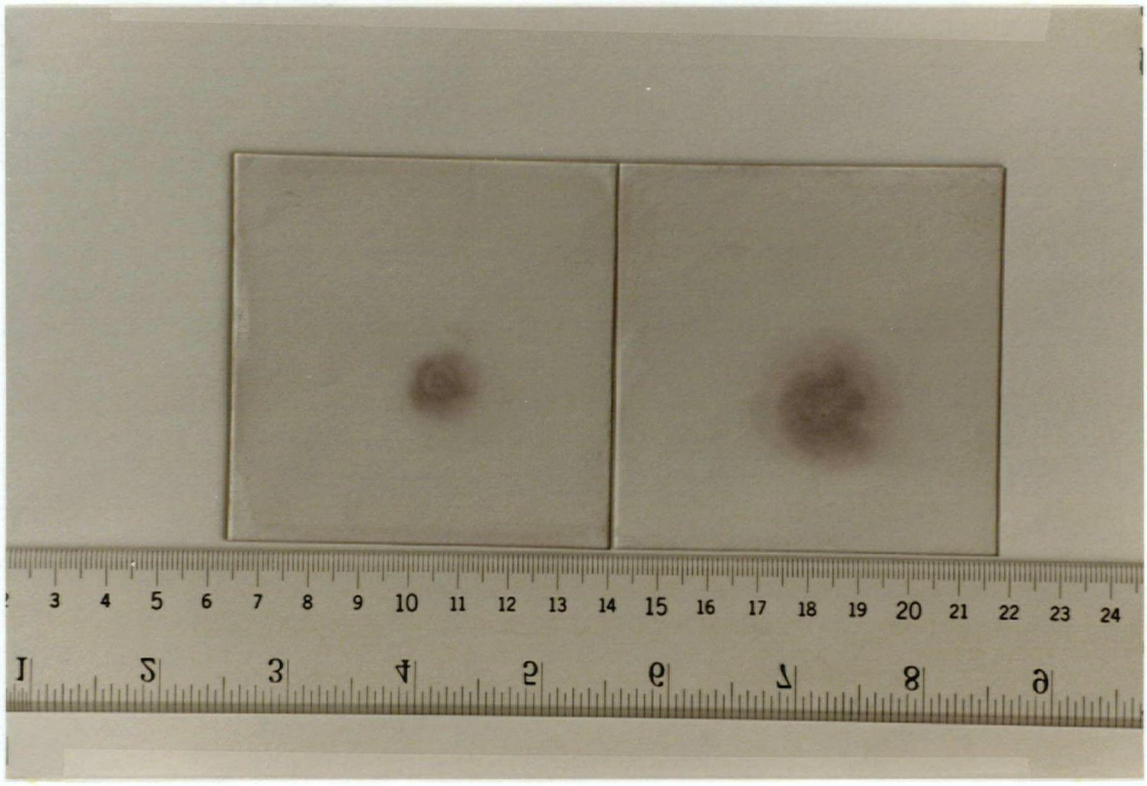

FIGURE 24–Some Exposed Starch Plates

6.3 The Relative Importance of Streaming and Radiation Pressure

To determine the relative importance of streaming and radiation pressure in rotating the disk in our meter, it would be ideal to stop one from acting on the disk without affecting the other. Preventing radiation pressure from acting while allowing streaming would be very difficult because the acoustic wave would have to be removed at the disk yet be unaffected in the fluid surrounding the disk where streaming arises. Preventing streaming, on the other hand, without affecting the radiation pressure on the disk, can be easily accomplished by placing a membrane near the disk that is ideally, perfectly transparent to the acoustic beam yet impermeable to water as shown in Figure 25 [Tjøtta 1958]. Household Saran Wrap very nearly satisfies these criteria. Where such a material is placed in a sound beam, streaming is eliminated but radiation pressure is unaffected.

Two experiments were done, in the first, a sheet of Saran Wrap was stretched over an 11 cm diameter wire hoop and glued in place. This hoop was placed in the beam at several positions between the disk and transducer as shown in Figure 26. There was no significant effect on the rotation of the disk, and the rotation rate was not seen to vary with the position of the hoop. The hoop was then tilted at 45° as shown in Figure 27 so that it could be brought closer to the disk at the point where the beam hit it. There was no noticeable effect on the rotation rate of the disk until the Saran Wrap was brought to within 2 ± 1 mm of its edge.

To eliminate the possibility that disk rotation was affected by streaming initiated in the fluid behind the disk, a second experiment was done. In this experiment, the disk was placed inside a cylinder of Saran Wrap so that the disk and cylinder were concentric. This arrangement is shown in Figure 28. The disk comes to within 2.0 mm of the Saran

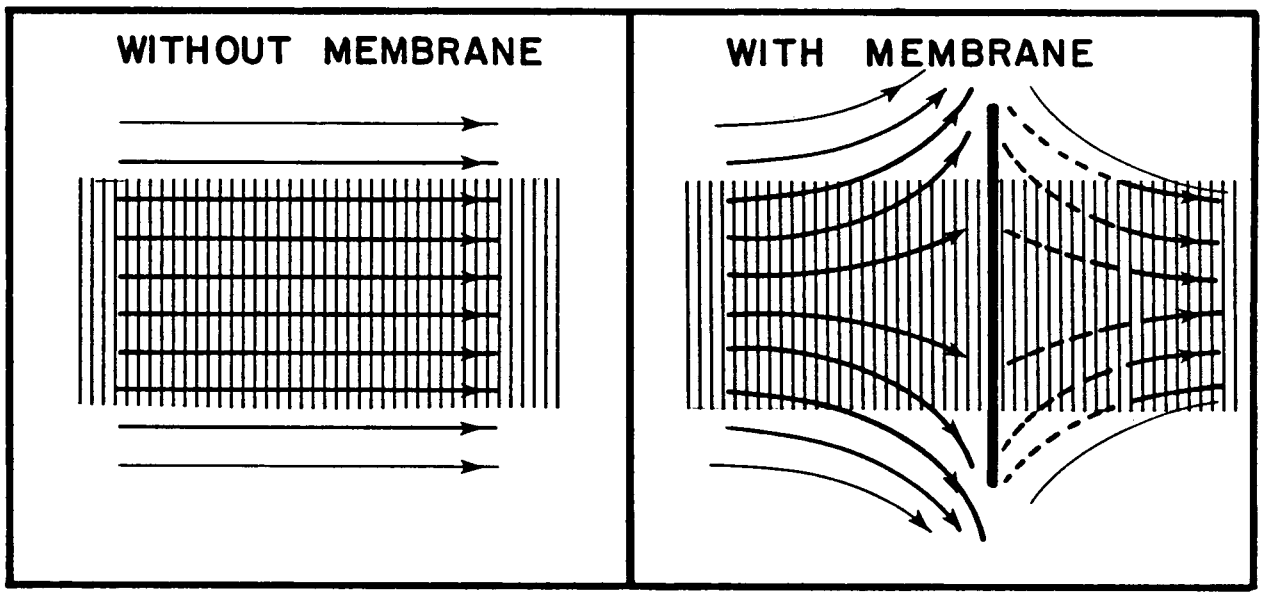

FIGURE 25–Arresting Streaming With an Acoustically Transparent Membrane

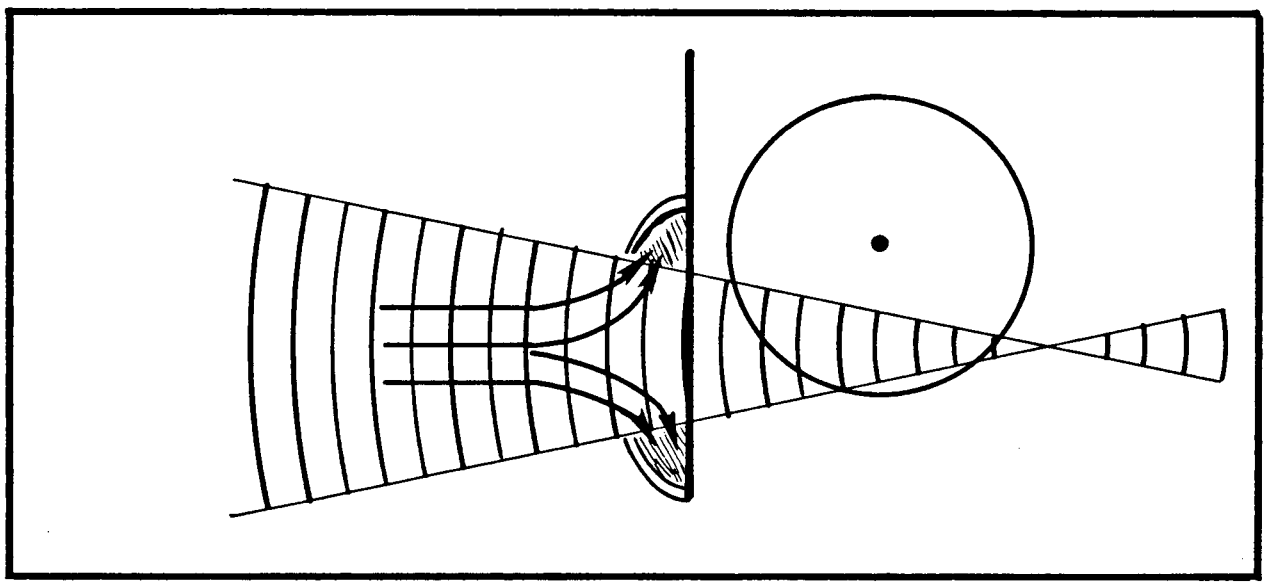

FIGURE 26–Saran Wrap Screen in Place

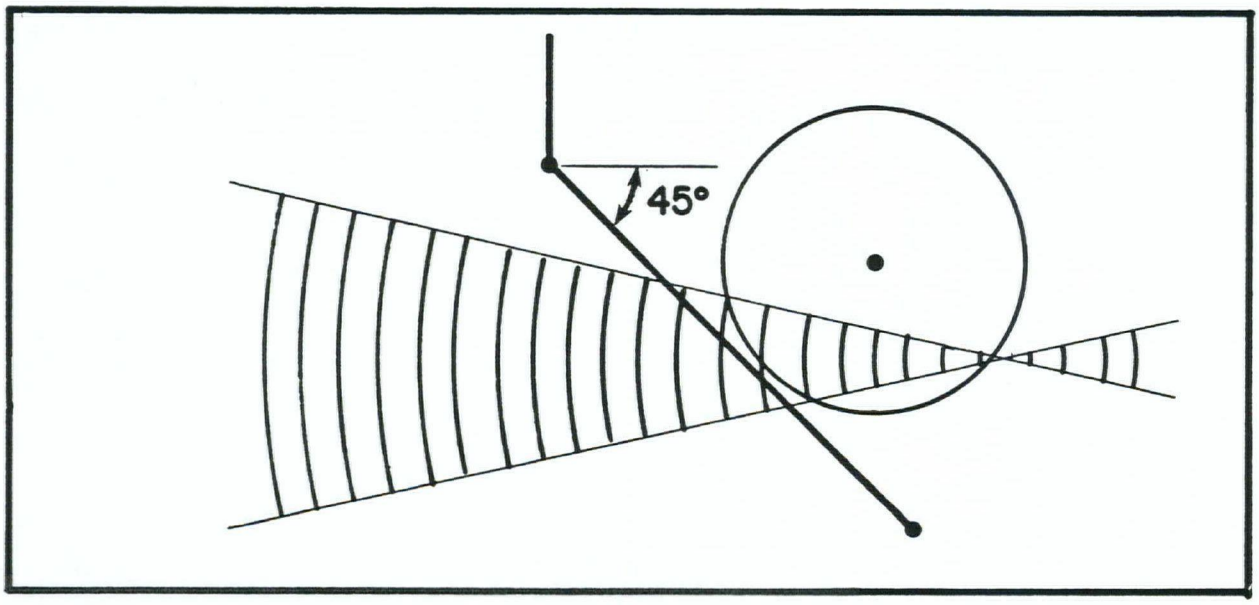

FIGURE 27–The Screen Tilted Near a Disk

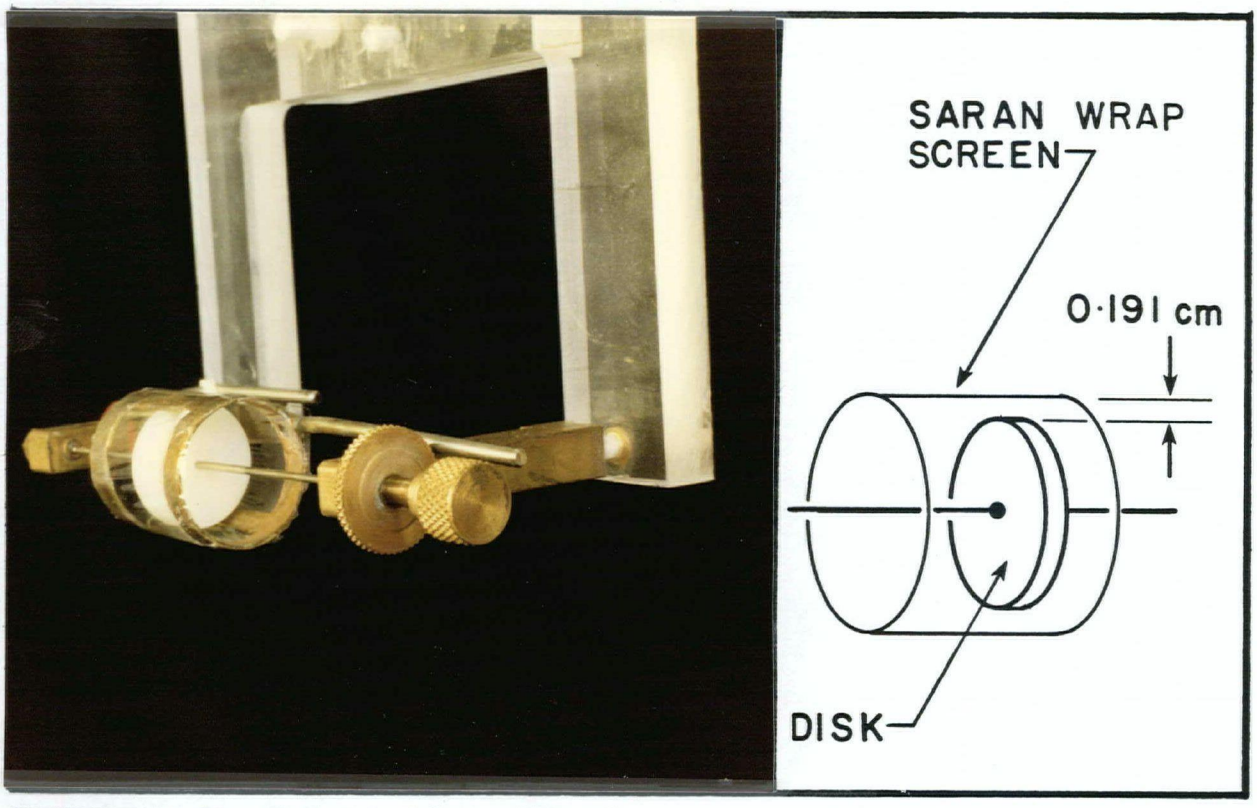

FIGURE 28–The Cylindrical Saran Wrap Screen

Wrap. Figure 29 superimposes two plots of angular velocity vs. beam intensity, one with, and one without the Saran Wrap cylinder. It is clear that neither the general shape of the curve, nor the speed of rotation is greatly altered by the presence of the cylinder.

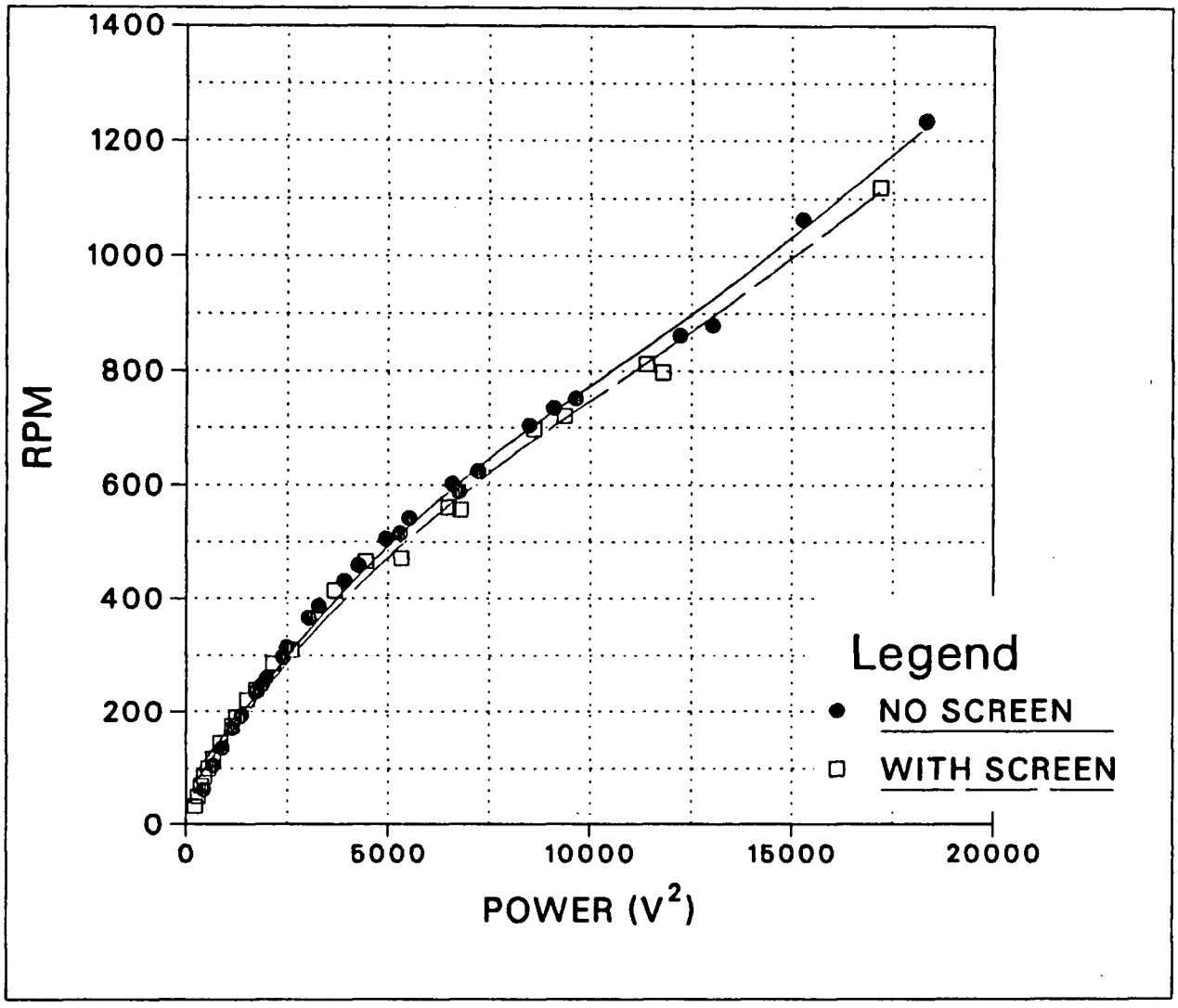

FIGURE 29–RPM vs. Power for PVC Disk, with and without Cylindrical Screen

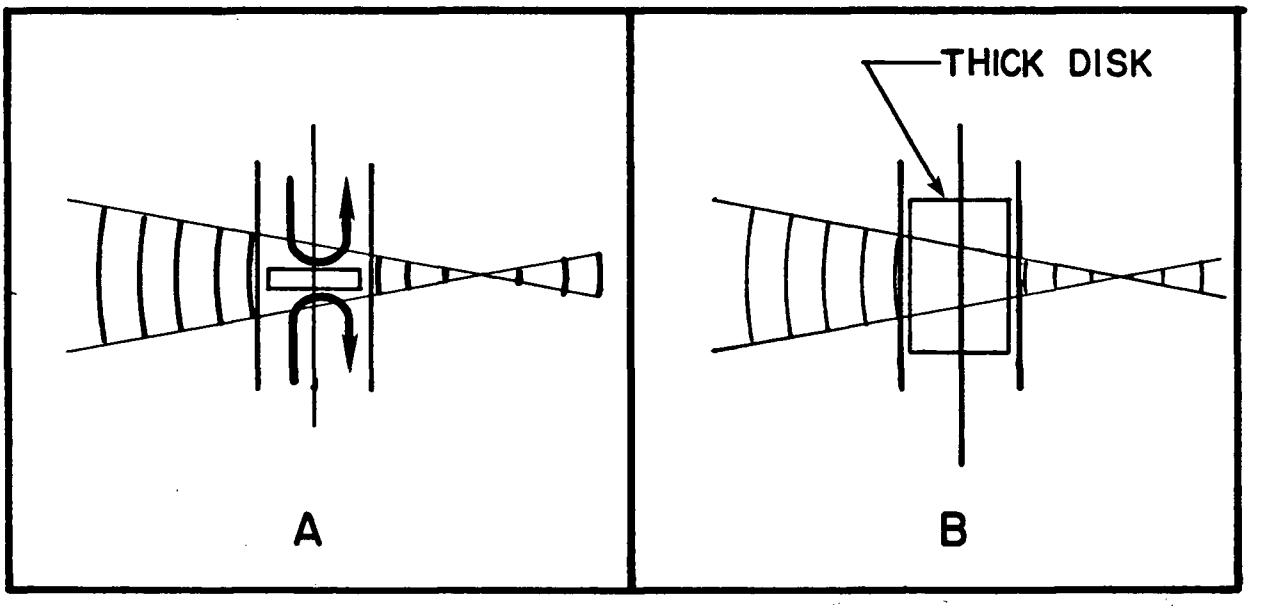

FIGURE 30–Streaming along the Sides of a Disk
A) shows how streaming can occur along the sides of a thin disk inside the screen.
B) shows that this can not happen with a thicker disk.

A final experiment was done to check the unlikely possibility that streaming along the sides of the disk, as shown in Figure 30 could cause a torque. In this experiment a disk 2.03 cm thick was used. As the sound beam is only $\sim$ 1.5 cm in diameter at this point, this type of streaming could not occur. The results of this experiment are shown in Figure 31 This disk rotated approximately 7% faster without the cylinder than it did with the cylinder in place. 281 RPM at 3 W without the cylinder vs. 262 RPM at 3W with the cylinder in place. A large part of this difference must be due to the fact that with this thicker disk, there is a much larger interference between the edge of the disk and the cylinder, and a much larger percentage of the total frictional drag on the disk occurs at its edge. None the less, these results allow us to place an upper limit on the ratio of torque on the disk due to streaming to the torque due to radiation pressure. With the cylinder, it would take $\sim$ 4.6 W to drive this disk at the same speed of 414 RPM that it attains at

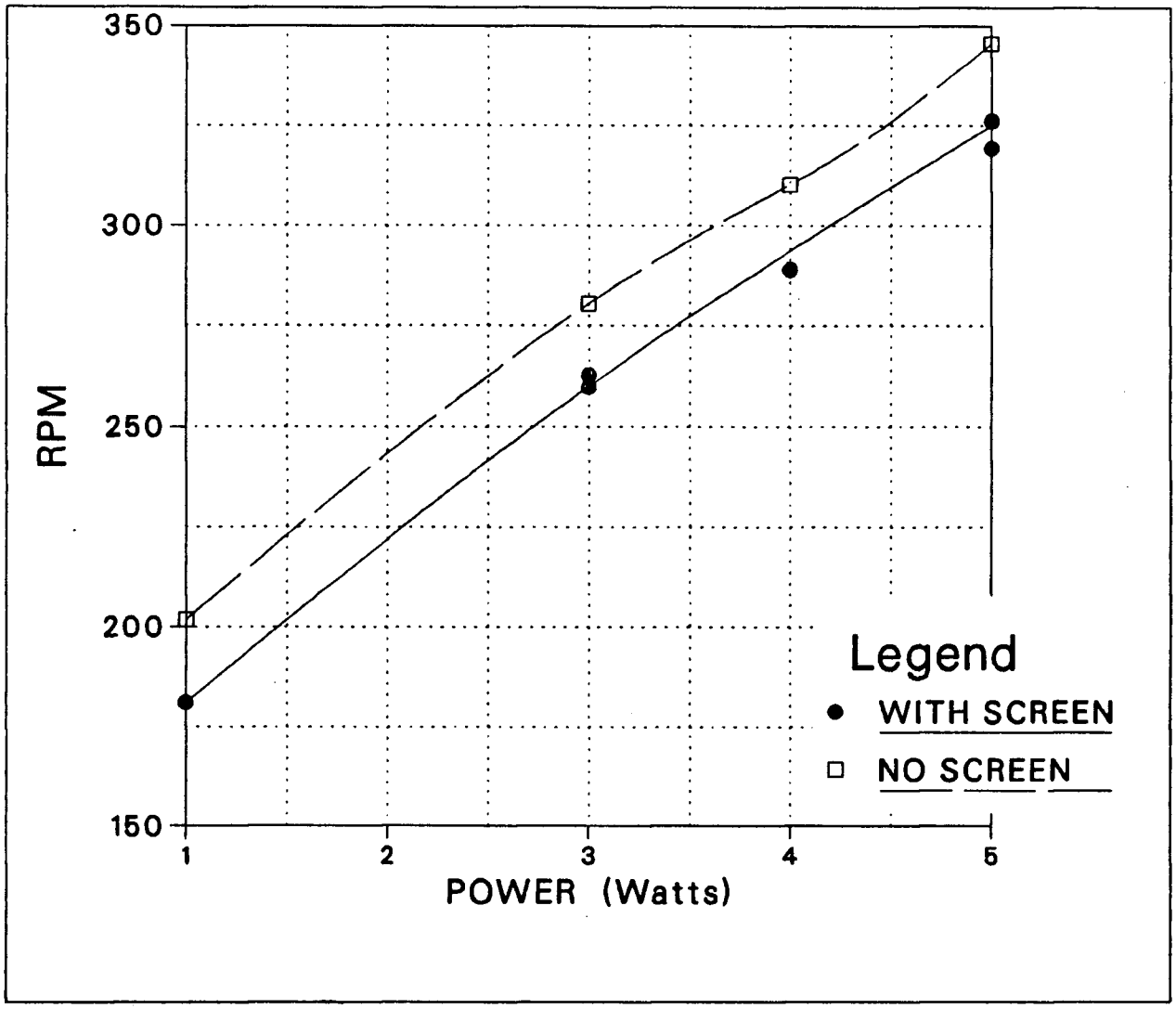

FIGURE 31–RPM vs. Power: Thick Nylon Disk, with and without Screen

---

4.0 W without the cylinder. We conclude that at most streaming accounts for about 13% of the torque on the disk, although as explained above, this figure is certainly too high.

This experiment showed that acoustic streaming is not an important factor in the operation of our meter. The next experiment was done to investigate the role of reflection in causing radiation pressure, and to see whether or not reflection of the sound beam can play a part in causing torque on the disk in the meter.

6.4 Acoustic Forces Due to Reflection

This second experiment was designed to show that a sound beam exerts a force when it is reflected, but no torque results when it is reflected from the edge of a circular disk because the resulting force is directed through the axis of the disk. This situation is shown in Figure 7 and discussed in section 2.7. To test this theory, we compared the behaviour of two disks which were identical except that one had notches milled around its edge as shown in Figure 32 while the other was left round. To avoid diffraction effects, the notches were made with dimensions larger than the acoustic wavelength in the liquid.

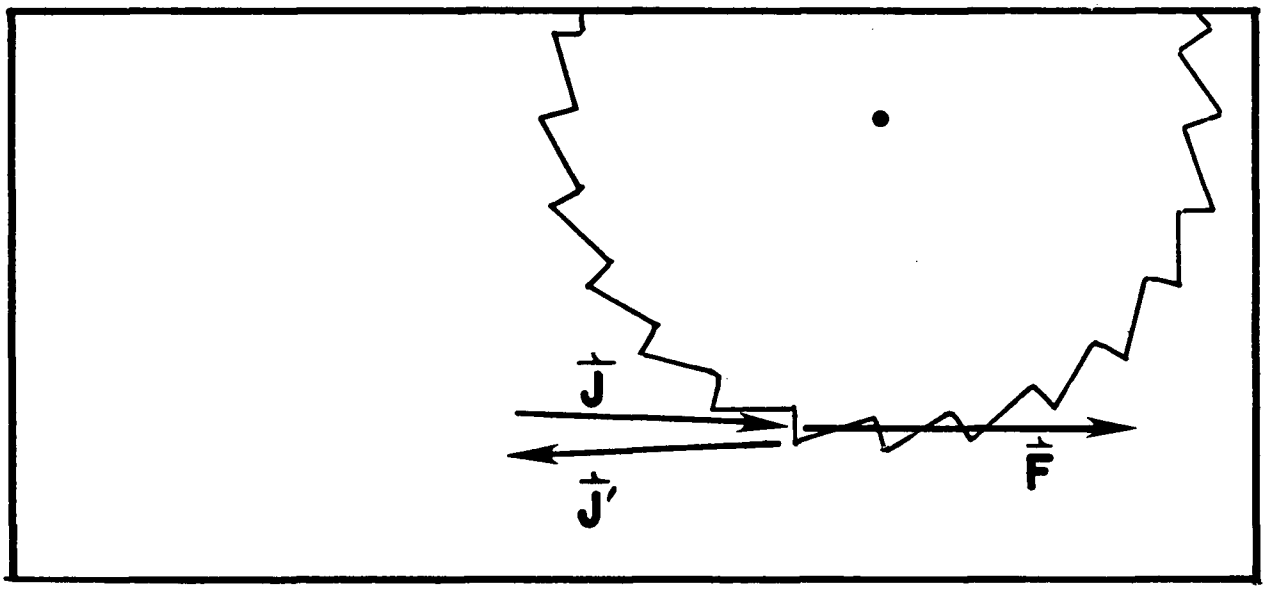

FIGURE 32–Notched Disk in an Acoustic Beam

Torque should result when sound is reflected from the teeth of a notched disk

If reflection of a sound beam yields a force, there should be a torque on the noched wheel. If this force is directed along $-d\vec{p}/dt$ as shown in Figure 7, we expect no torque on the smooth disk. The disks were made of Copper because it was readily available and, at normal incidence has a coefficient of reflection of 0.932 for acoustic waves.†

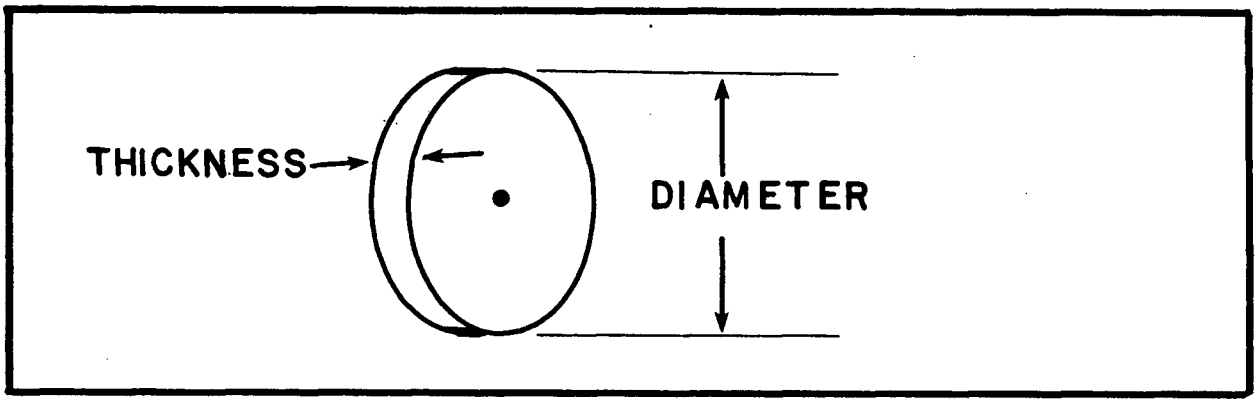

FIGURE 33–Disk Thickness and Diameter

Two copper disks 24.2 mm diameter by 3.0 mm thick were made. These dimensions are shown in Figure 33. One of these disks was left smooth while the other had teeth milled around its edge as shown in Figure 34. Both disks were mounted on one shaft as shown in Figure 35 and placed in the sound beam in succession. When the smooth disk was placed in the sound beam, the shaft did not rotate at all. When the axle was moved so that the toothed disk was in the sound beam, the shaft and both disks spun quickly. As the toothed wheel rotated, the voltage at the input to the transducer fluctuated indicating that power was periodically being reflected back into the transducer.

---

† The coefficient of reflection at normal incidence is given by: $R = VV^*$, $V_{norm} = (\rho_{Cu}c_{Cu} - \rho_{H_2O}c_{H_2O})/(\rho_{Cu}c_{Cu} + \rho_{H_2O}c_{H_2O})$ The density and speed of sound in Copper are: $\rho_{Cu} = 8.93\,\mathrm{g/cm^3}$, and $c_{Cu} = 4760\,\mathrm{m/s}$ respectively [CRC Press 1976, p.E-47].

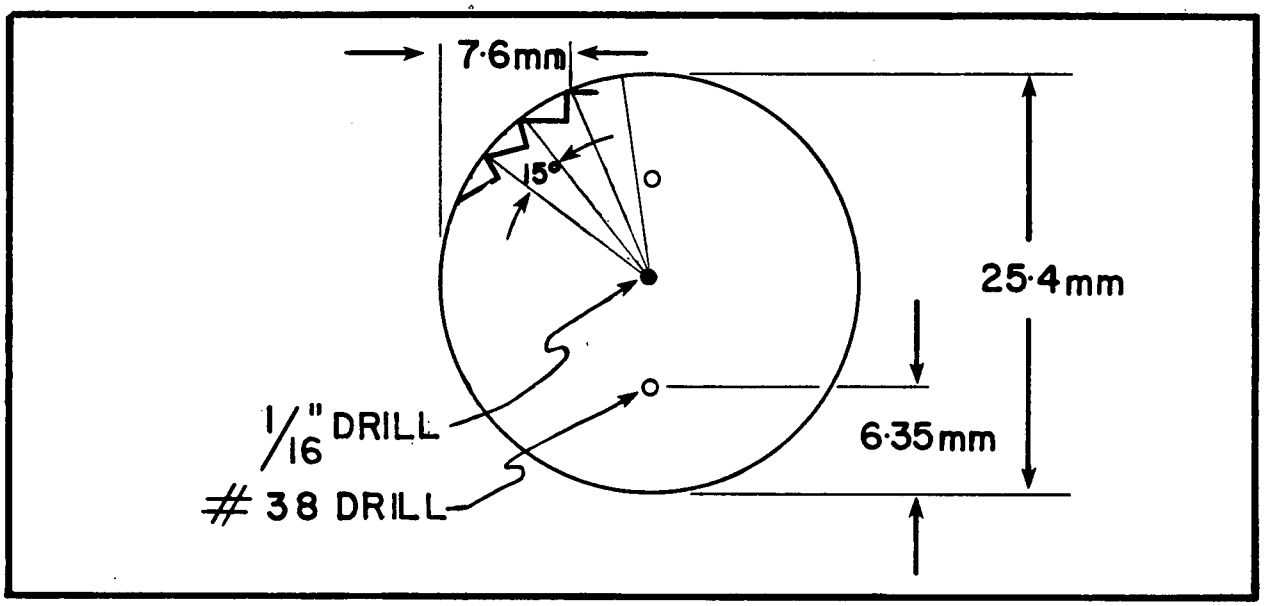

FIGURE 34–The Notched Disk

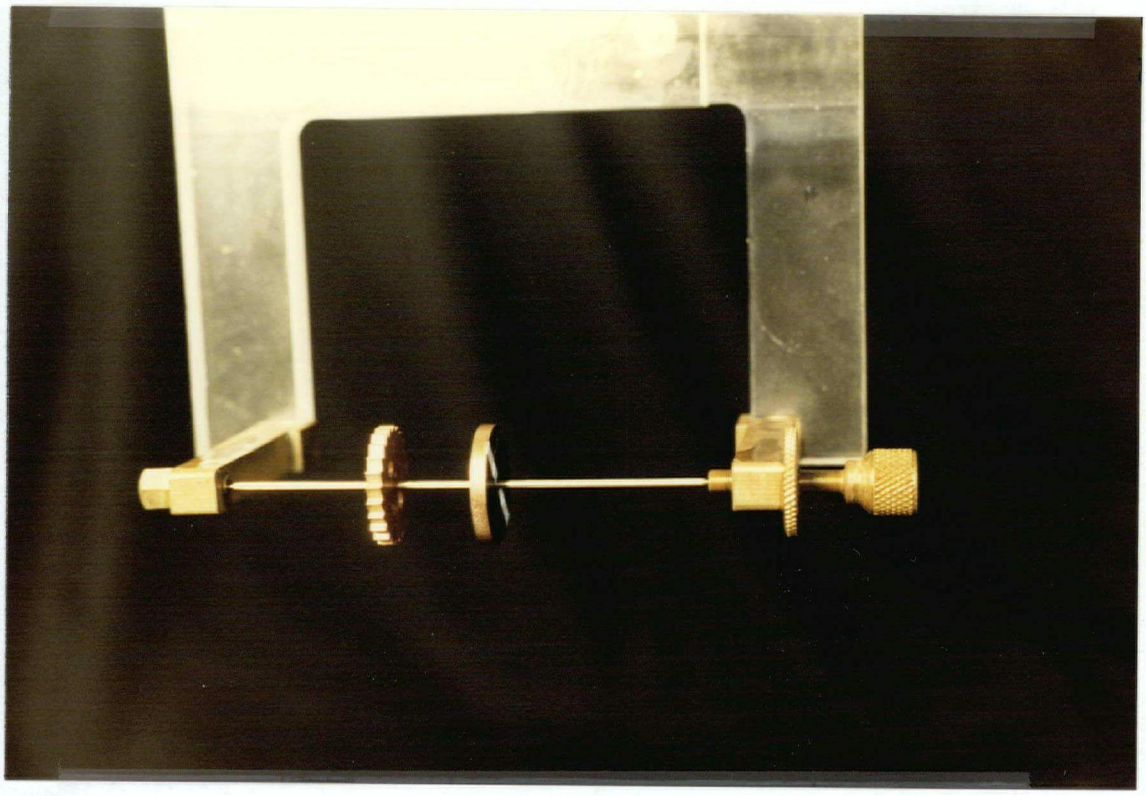

FIGURE 35–Copper Disks Mounted in Tandem

6.5 Linearity of Torque vs. Power Input

The third experiment was designed to show that the torque on the rotating disk in our meter is directly proportional to the intensity of the acoustic beam as predicted in section 2.7. A 28.0 mm diameter by 3.9 mm thick nylon disk was mounted 1.0 cm from the end of a shaft as shown in Figure 36. This disk was positioned in the sound beam at its experimentally determined optimum position and driven with a 35.8 V_{p-p} input to the transducer. With this input power, it rotated at 202 RPM. The water temperature was 20.3 C . Smaller 2.2 mm diameter by 3.2 mm thick disks were then successively added at positions A, B, C, and D as shown in Figure 36. The power needed to maintain 202 RPM was noted for each case. The results are shown in Figure 37. Since the viscous drag is proportional to the number of disks on the shaft, this graph shows that the torque caused by the acoustic beam increases linearly with the input power.

The rest of the experiments reported in this thesis were done to study the scaling laws associated with this meter, and to optimize its geometry so that the disk rotates as quickly as possible for a given acoustic power input. These experiments measure:

1.) The optimum position for one particular disk, and the variation in the rotation rate as the disk is moved away from this position.

2.) The optimum disk thickness for this lens, and the variation in optimum position with disk thickness.

3.) The optimum disk diameter and the variation of optimum position with disk diameter.

4.) The rotation rate vs. acoustic intensity for some typical disks.

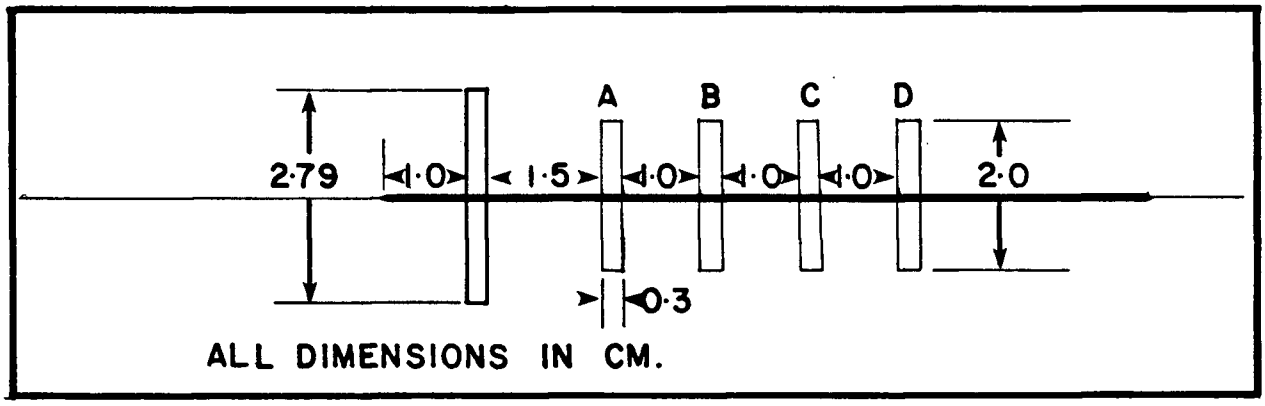

FIGURE 36–Setup for the Third Experiment

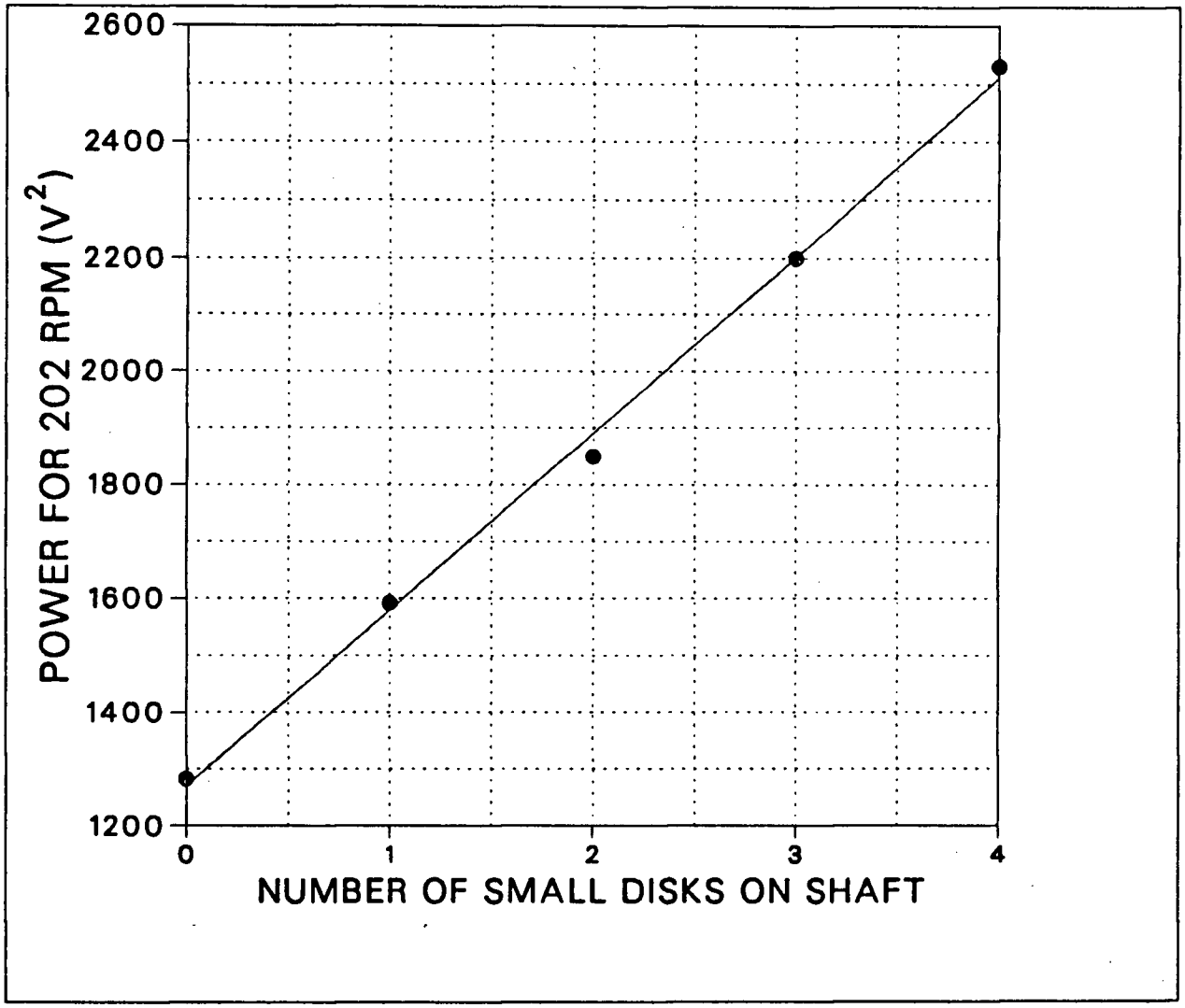

FIGURE 37–Power Needed to Maintain 202 RPM vs. Number of Small Disks on the Shaft

6.6 Optimizing Position

This fourth experiment was done to confirm that there is only one position in the acoustic field of the lens where the rotation rate of the disk is maximized. To do this, we found the optimum position for one disk by trial and error and measured its rotation rate as it was moved away from this position along each of the three axes in turn (refer to Figure 17). The rotation rate is quite sensitive to adjustment of the vertical position of the disk, and the vertical scale on our apparatus is quite coarse, with a resolution of $\pm.25$ mm so we wanted to use a disk with a diameter large enough that these increments were comparatively small. We also wanted the disk to have a diameter small enough that its rotation rate would be high and thus easy to measure quickly and accurately with our apparatus. In view of these requirements, a nylon disk of 33 mm diameter, and 3.9 mm thickness was used. The data shown in Figure 38, Figure 39, and Figure 40 shows how the rotation rate varied as the disk was moved vertically, laterally in the beam, and along the beam.

At the optimum position, the axis of the disk was 9.35 cm from the transducer face, and 1.45 cm above the center of the transducer as shown in Figure 41. To make sure that the optimum height was not strongly dependent on the position of the disk along the beam, the disk height was adjusted to maximize the rotation rate at several distances from the transducer. The optimum height for the disk is plotted versus distance from the transducer in Figure 42.

It is reasonable to expect that the optimum position of the disk laterally in the beam is independent of the distance to the transducer because the beam is cylindrically symmetric. To check this, the wheel rotation rate was measured as a function of position

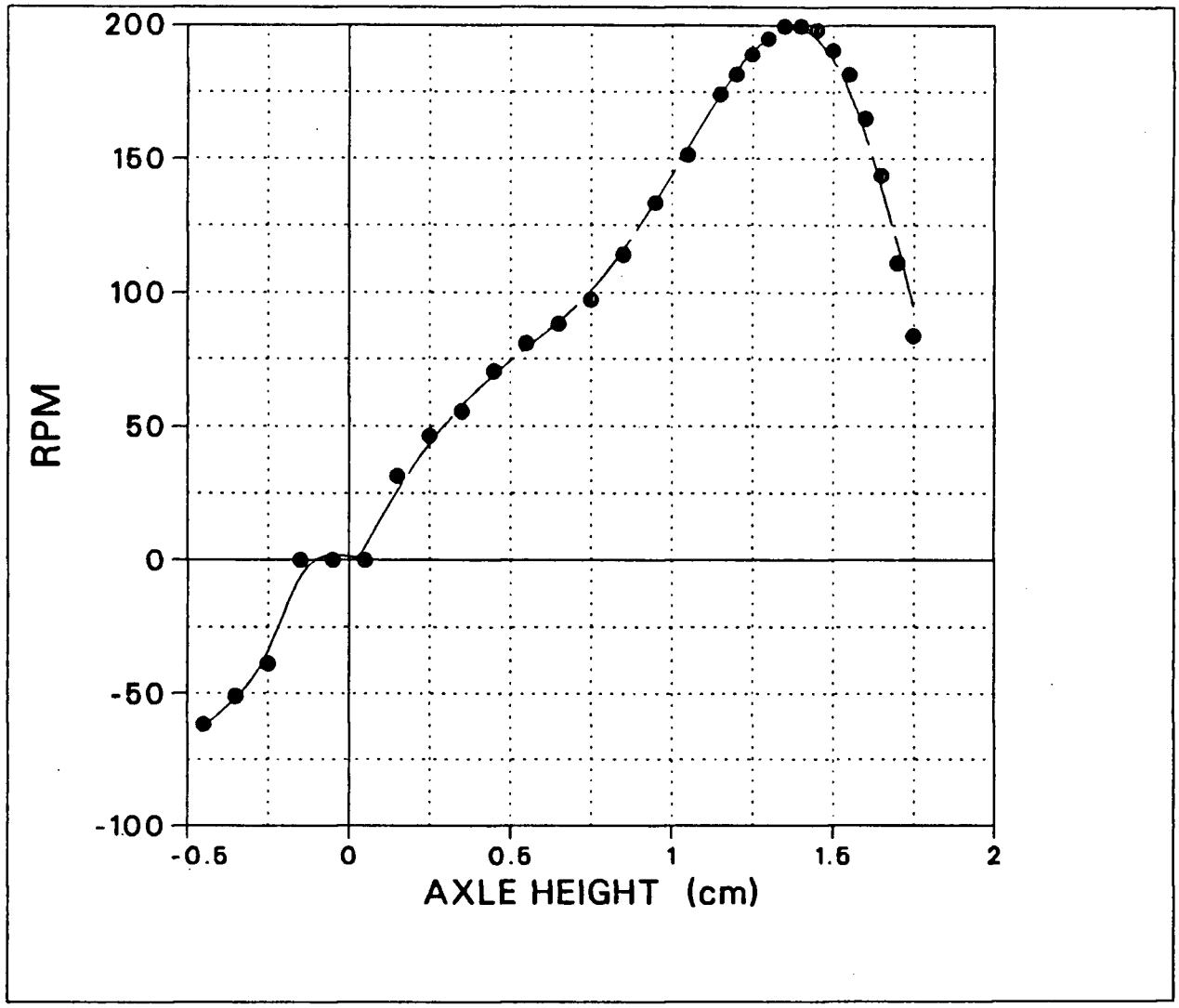

FIGURE 38–RPM vs. Disk Height

---

across the beam at four different distances from the transducer. To maximize the resolution, a thinner, 2.0 mm thick by 2.5 cm diameter disk was used for these measurements. The results are shown in Figure 43.

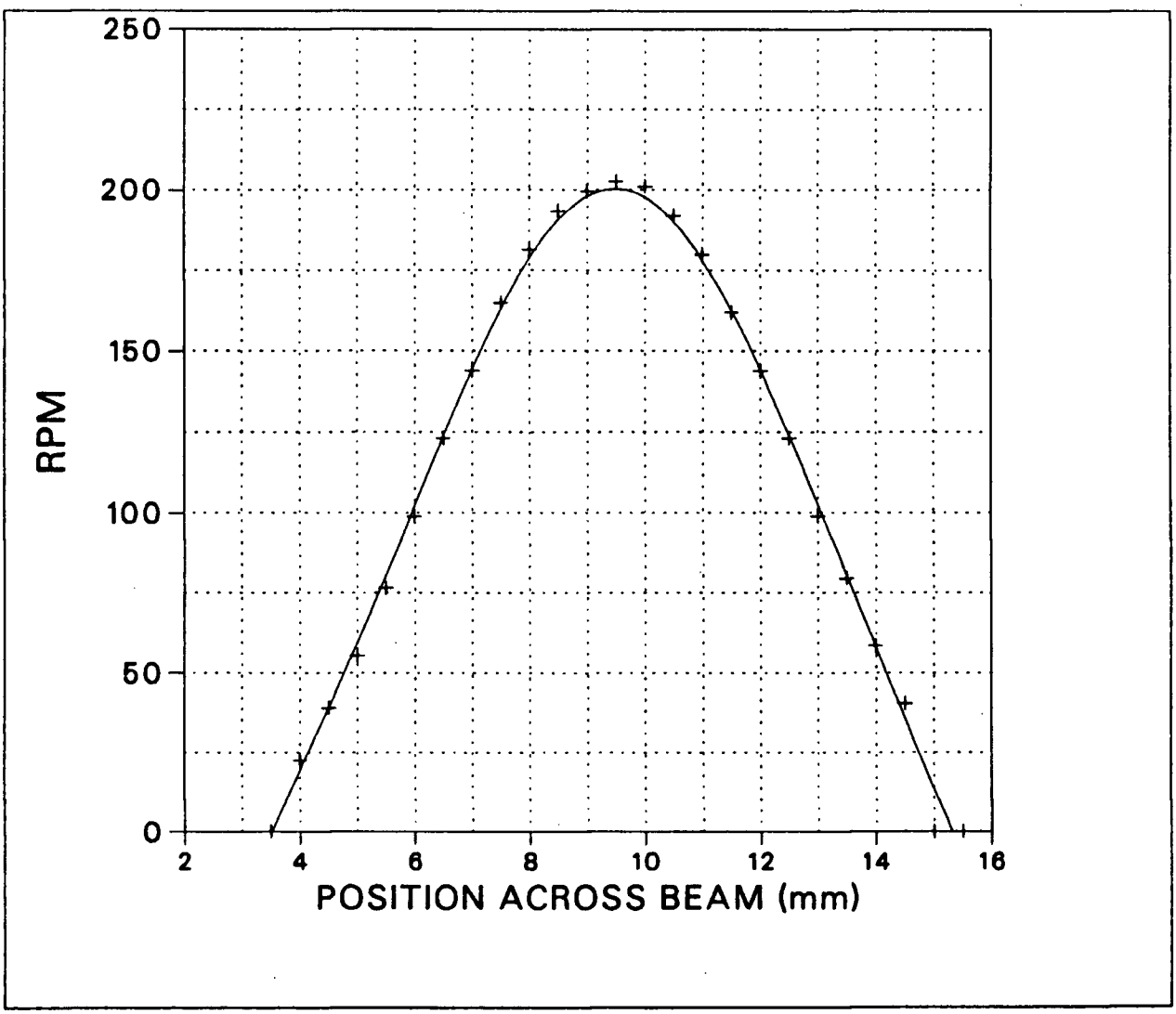

FIGURE 39–RPM vs. Lateral Position in Sound Beam

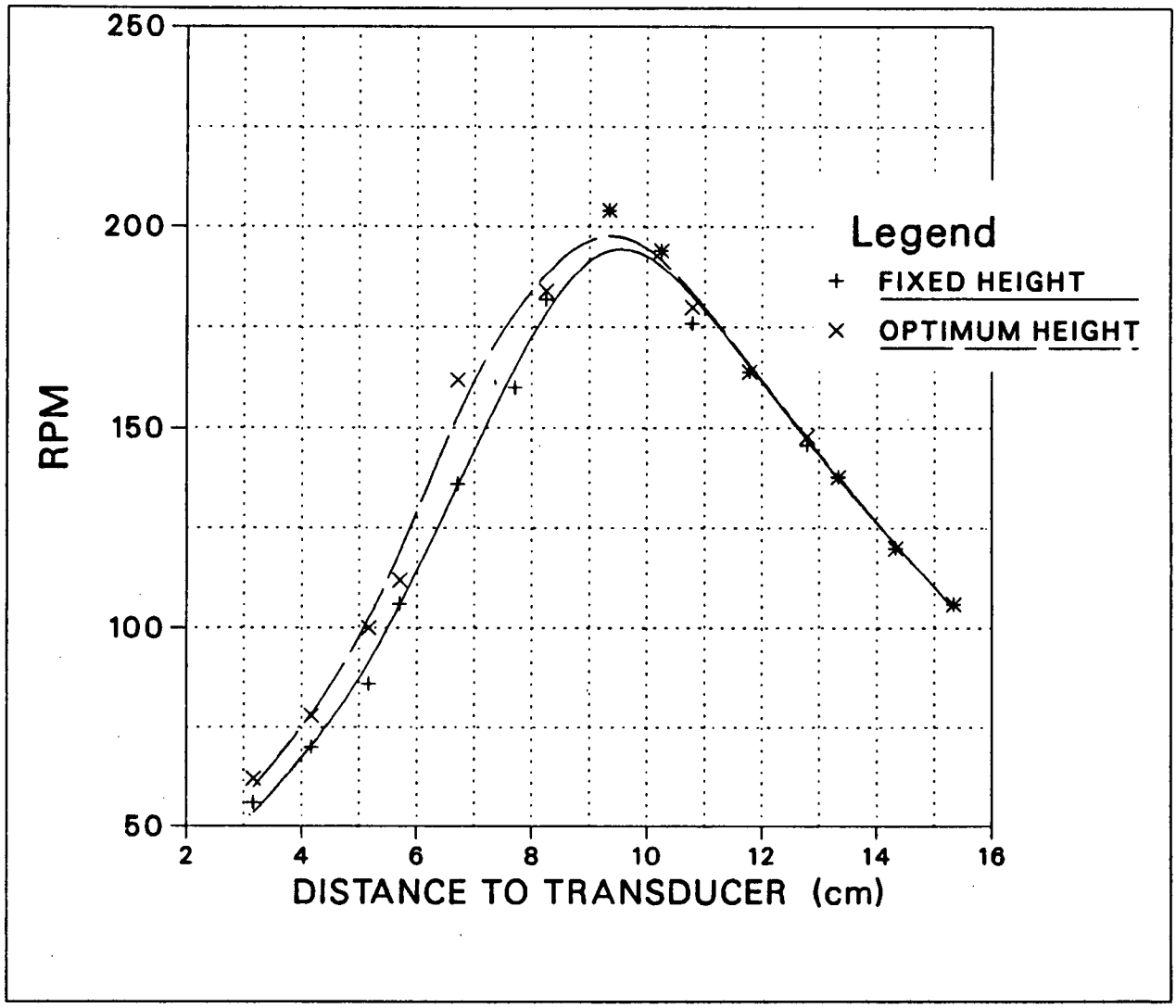

FIGURE 40–RPM vs. Distance to Transducer Face

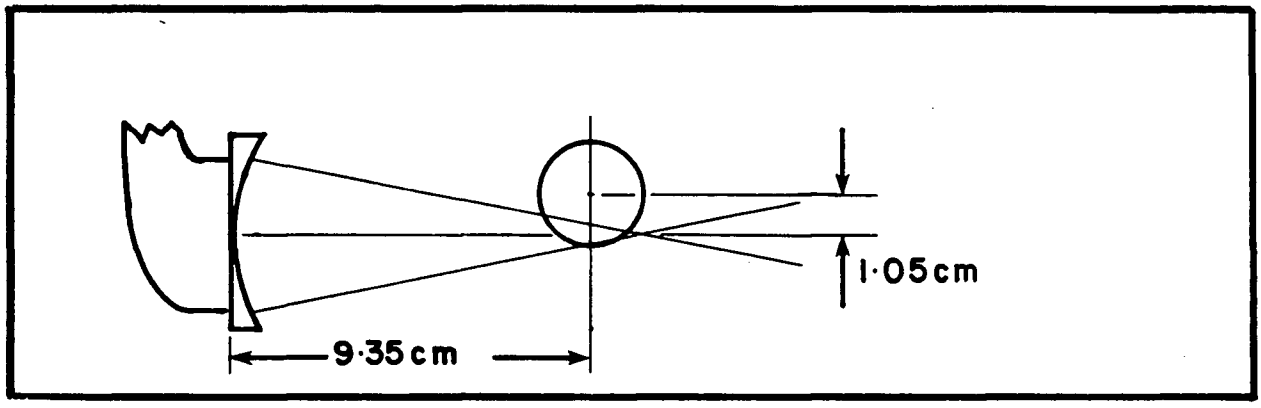

FIGURE 41–Optimum Position for a 2.5 cm Diameter Nylon Disk

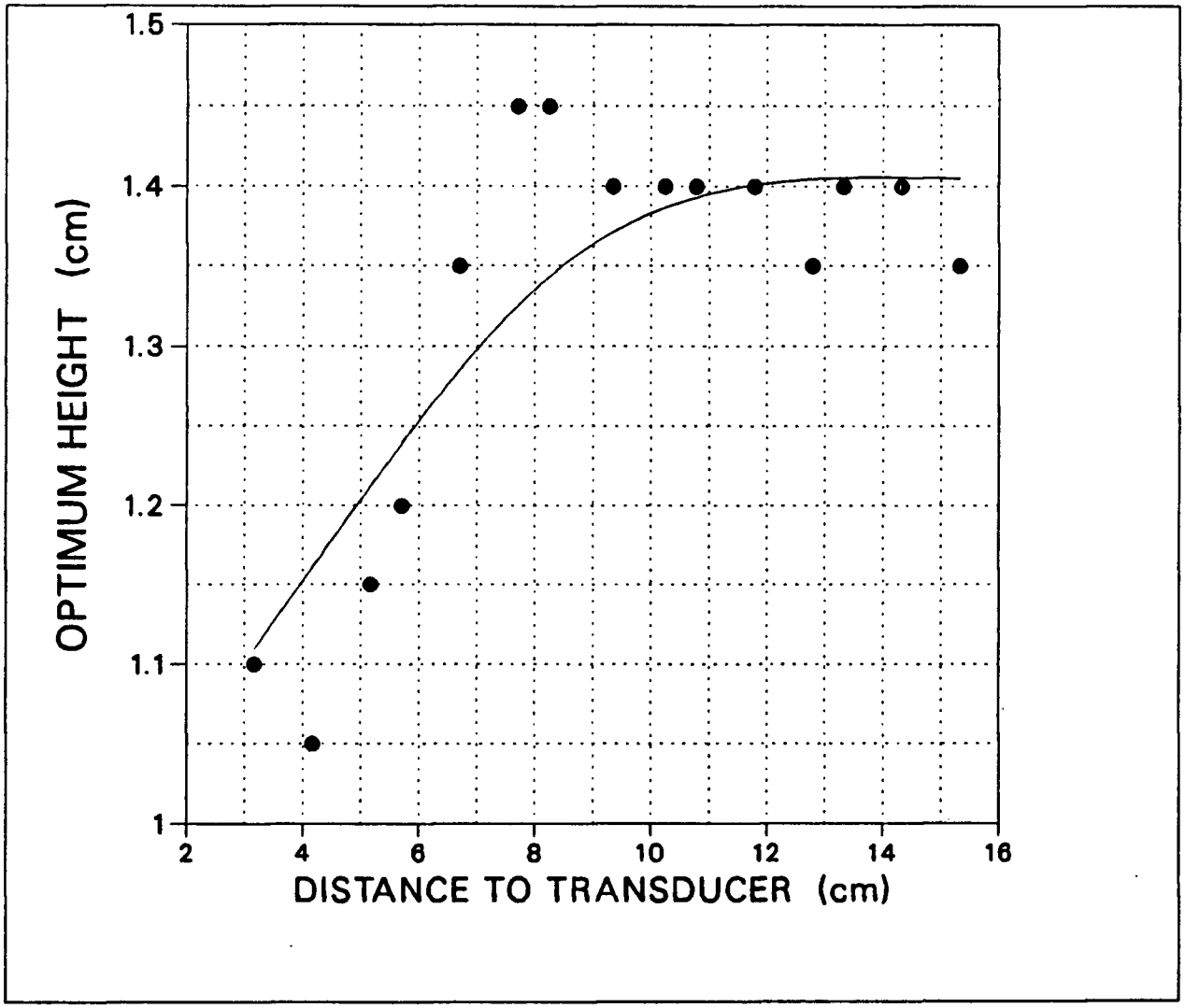

FIGURE 42–Optimum Height vs. Distance to Transducer Face

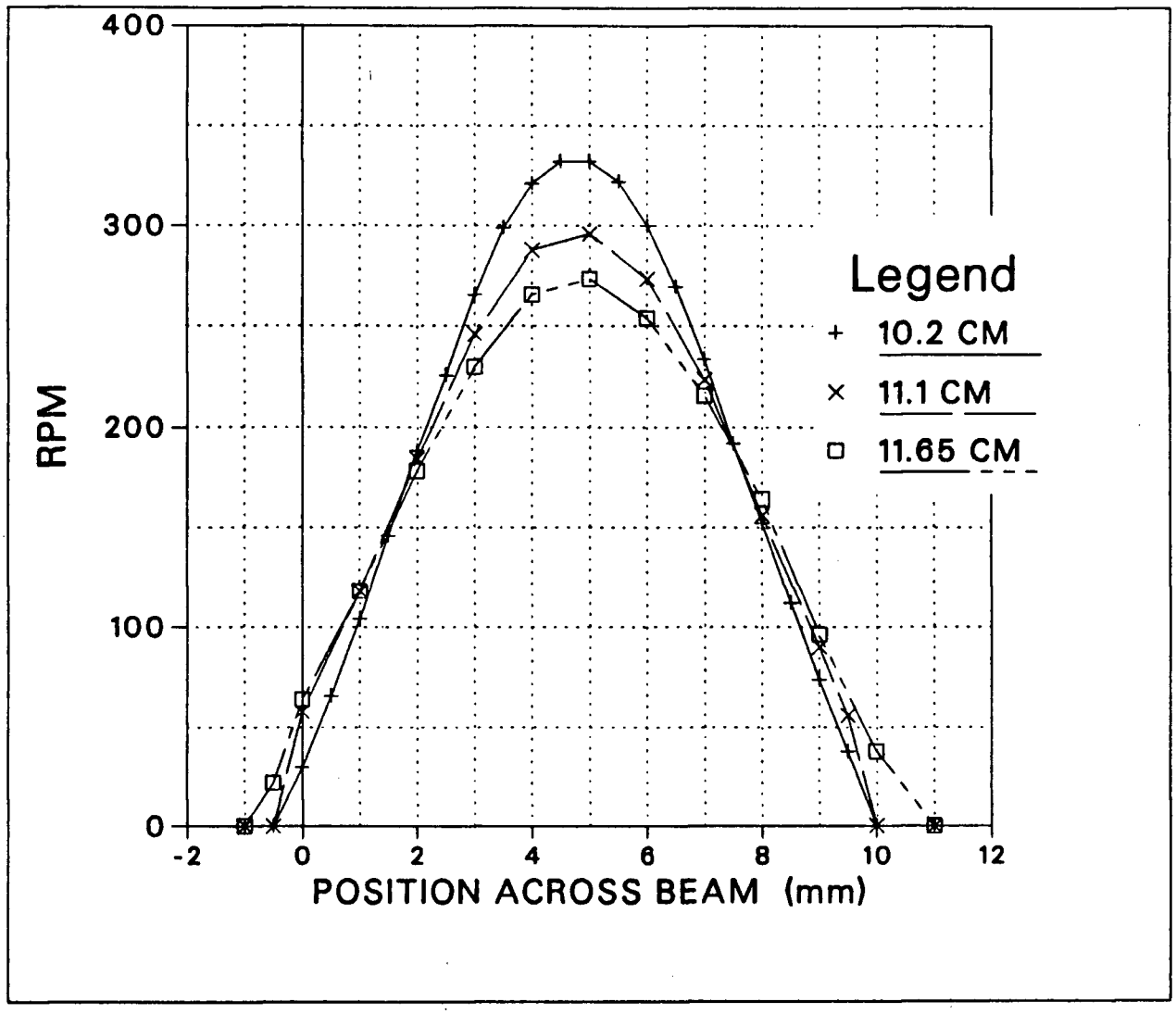

FIGURE 43–RPM vs. Lateral Position at Various Distances From the Transducer

6.7 Optimum Disk Thickness

The fifth experiment was designed to find the best disk thickness. The ultrasonic beam has a finite cross sectional area, so that up to a point, the thicker the disk, the more of the beam it will intercept, and the faster it will rotate. The drag on the disk also increases with the disk thickness. This tends to make thicker disks rotate more slowly. There should be some intermediate thickness where at a given distance from the transducer the rotation rate is maximized.

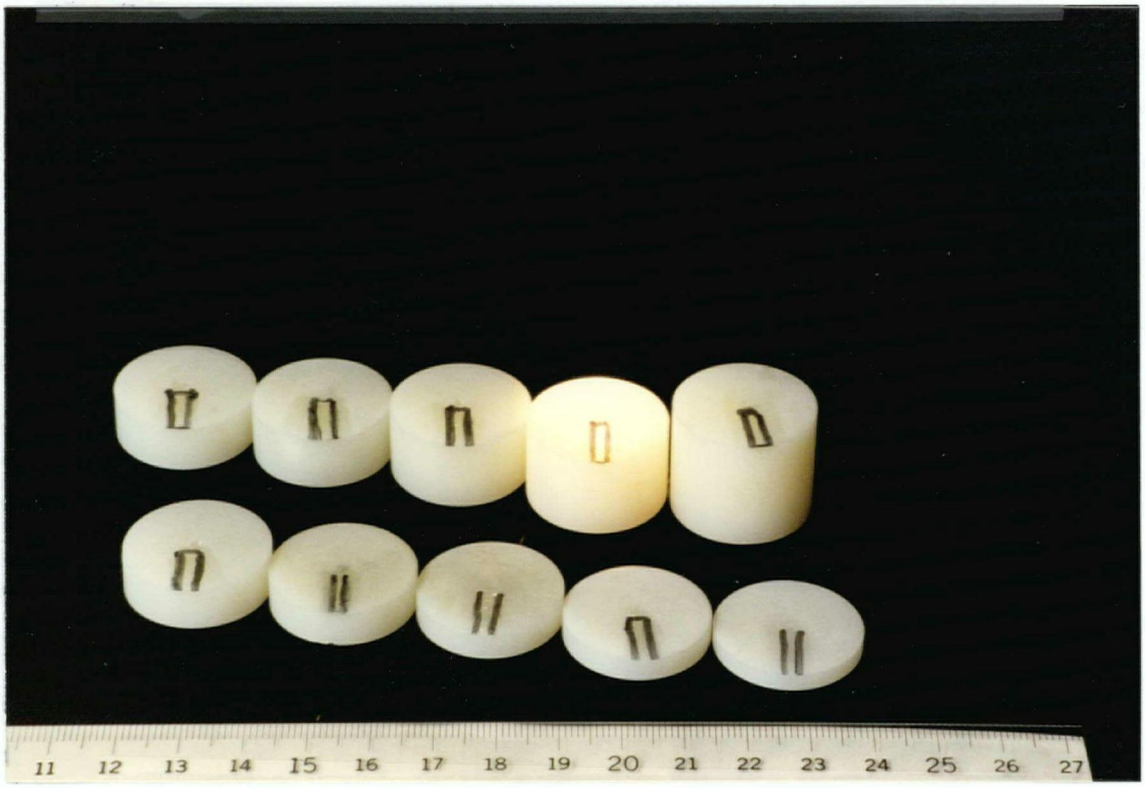

FIGURE 44–Some Disks of Various Thicknesses

Thirteen nylon disks were prepared with a nominal diameter of 25 mm and thicknesses between 2.0 mm and 20.4 mm as shown in Figure 44. The exact dimensions of these disks are given in Table I. All of these disks were turned on a lathe from Nylon rod. Their flat surfaces were sanded smooth with 400 grit sandpaper under water. Each disk had a small strip of mylar film glued to it with RTV Silicone for measuring the speed of rotation.

TABLE I.–Exact Dimensions of Disks of Varying Thickness

DISK NUMBER	DIAMETER ±0.013 mm	THICKNESS ±0.013 mm
T1	24.92	2.032
T2	24.88	2.578
T3	24.90	3.200
T4	24.96	3.315
T5	24.90	4.254
T6	24.87	5.093
T7	24.88	6.452
T8	24.88	7.722
T9	24.89	8.750
T10	24.83	10.236
T11	24.84	12.763
T12	24.83	15.227
T13	24.96	20.390

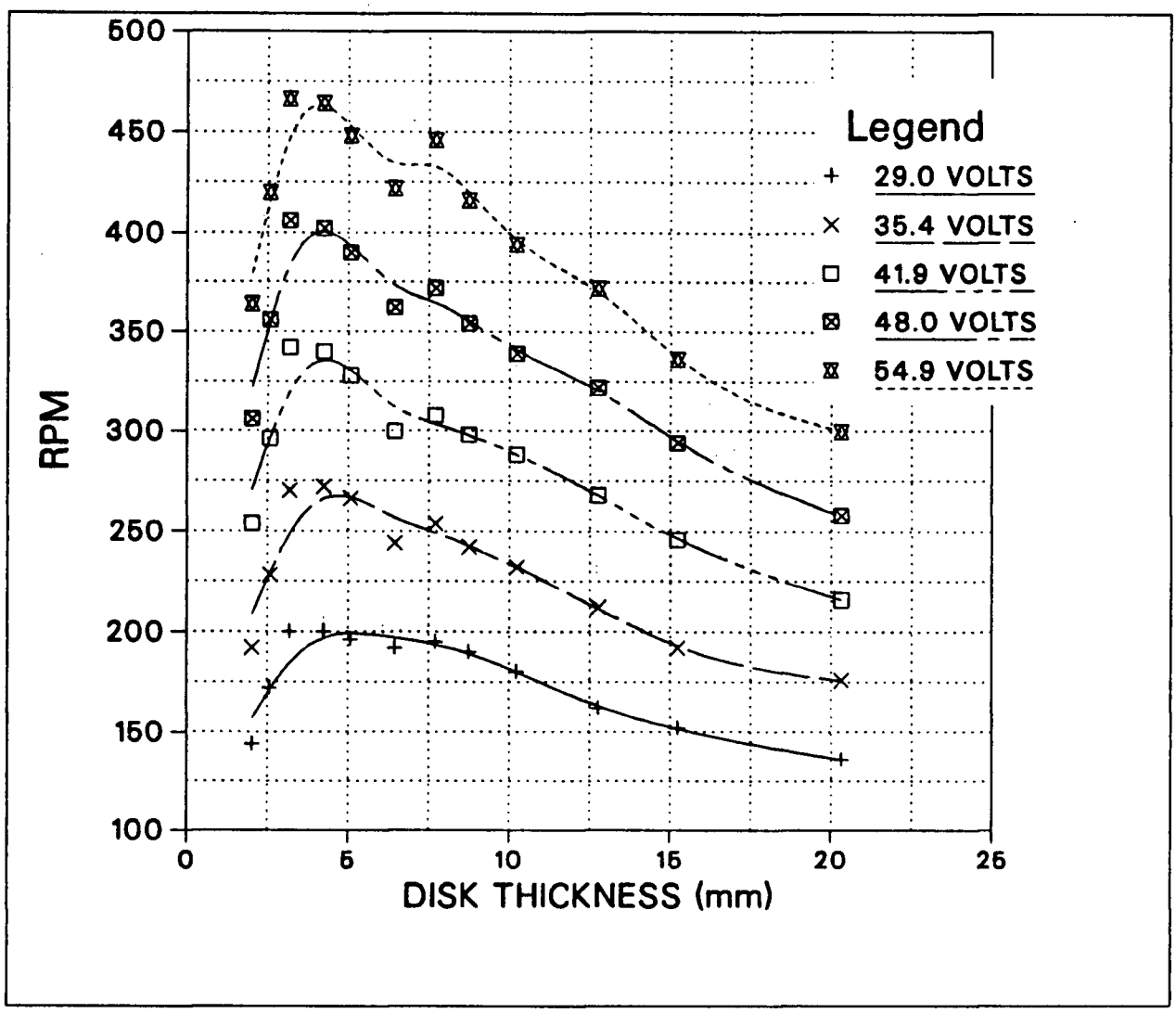

FIGURE 45–RPM vs. Disk Thickness at Various Power Levels

First the optimum position for a 2.5 cm diameter disk was found and the shaft moved to that position. Next, the thinnest disk was placed on the shaft and moved laterally in the beam until it was centered, and its rotation rate was maximized. The speed of rotation was then measured at transducer input voltages of: 29.0, 35.4, 41.9, 48.0, and 54.9 V_{p-p}. This set of measurements was repeated with each of the other disks. Each disk was placed with its center at the same point on the shaft. Water temperature was 20.7 C. Results of

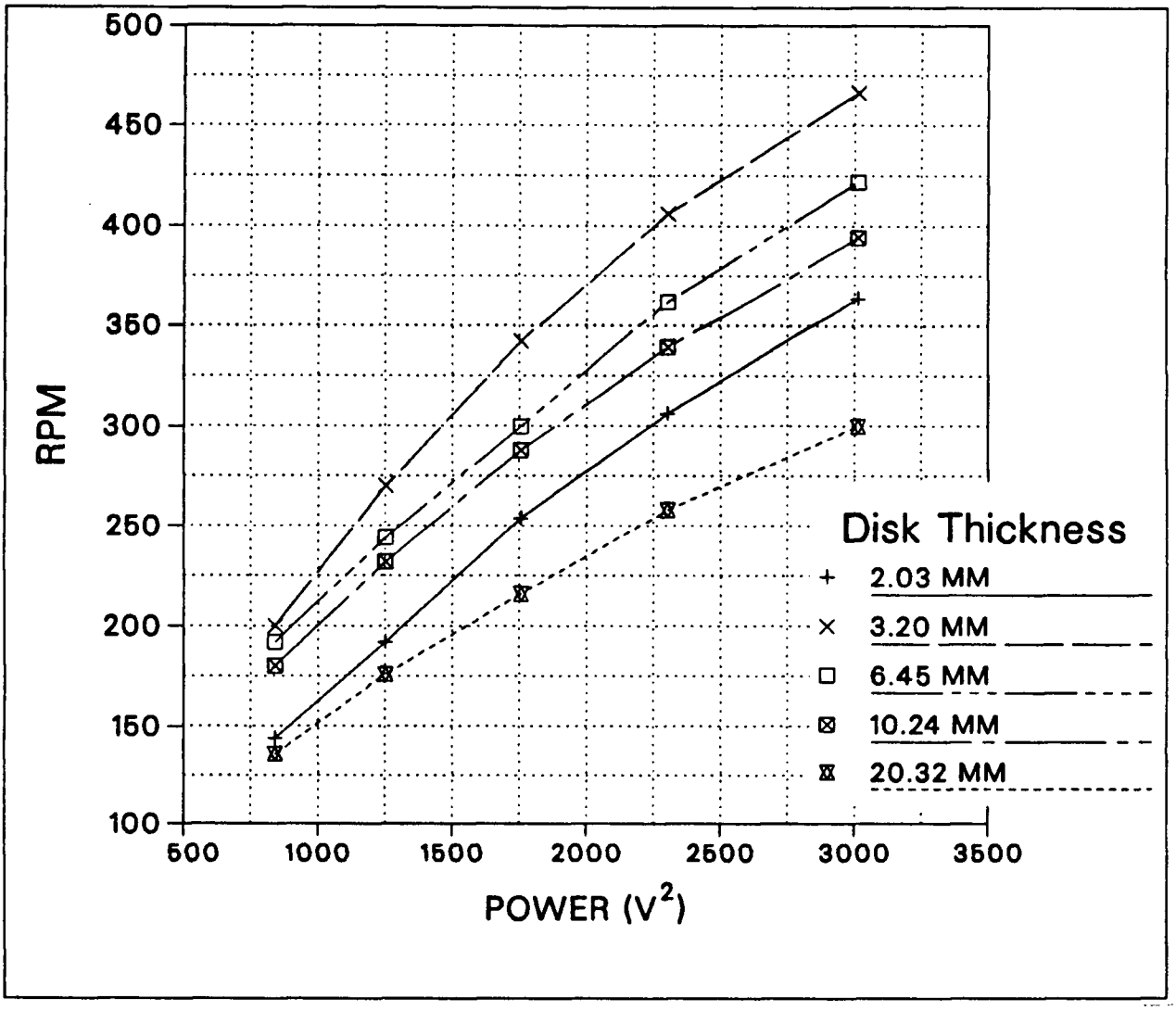

FIGURE 46–RPM vs. Power for Various Disk Thicknesses

---

these experiments are shown in Figure 45 and Figure 46. From these results, it seems that a disk thickness of about 3.9 mm yields the fastest rotation rate for any input power.

It seemed likely that the optimum distance to the transducer might be a function of disk thickness. To check this, the rotation rate of a thicker disk was measured as the distance to the transducer was varied. The driving voltage to the transducer was kept fixed at 41.5 V_{p-p}, and the disk height, and lateral position were not altered. The results from

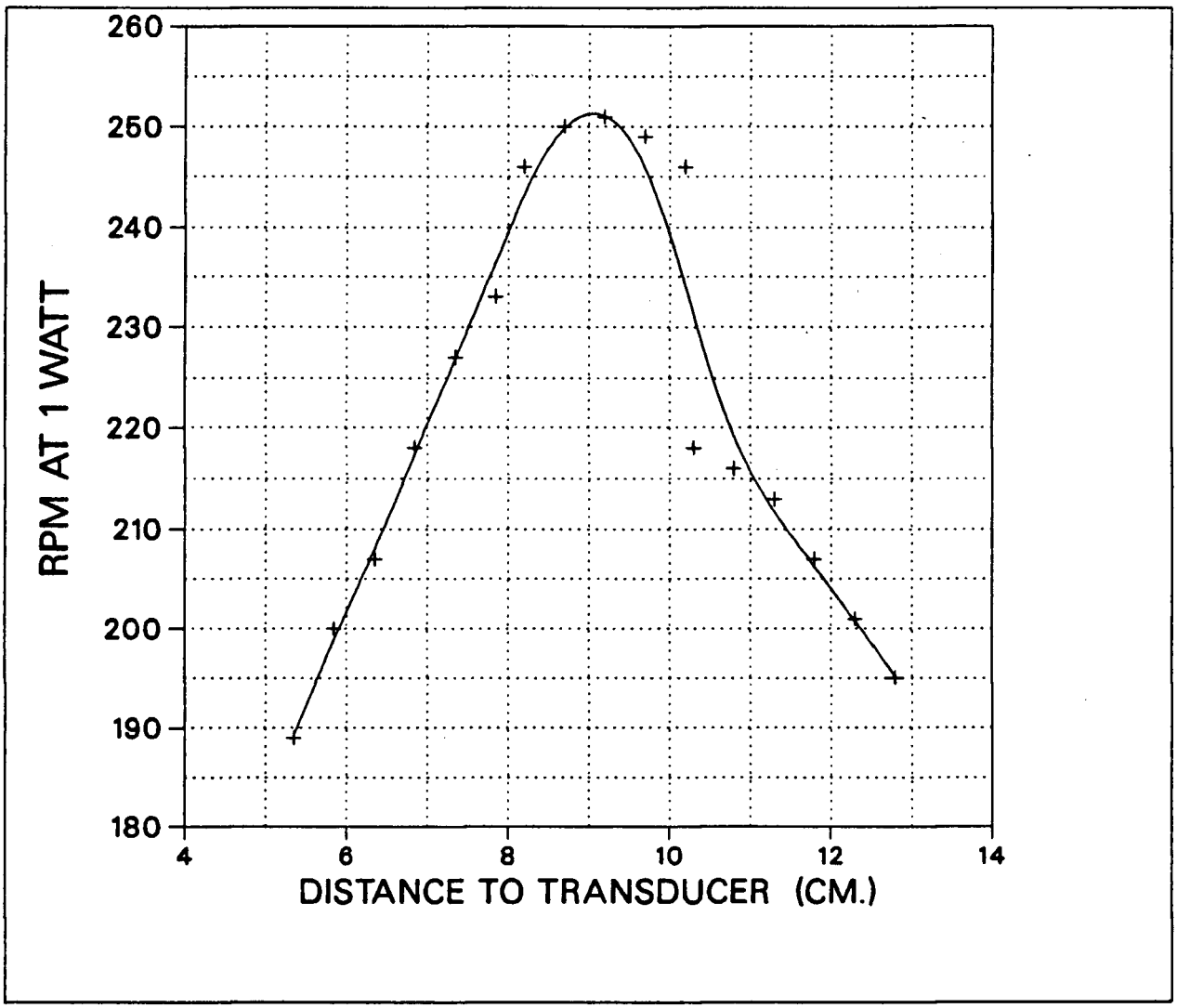

FIGURE 47–RPM vs. Distance to the Transducer for a Thick Disk

---

this experiment are shown in Figure 47. Comparing these results with those of Figure 40 shows that the optimum distance to the transducer does not vary significantly with disk thickness.

6.8 Scaling of Rotation Rate with Disk Diameter

The sixth set of experiments was done to investigate the scaling of the rotation rate with the disk diameter. The optimum height of the shaft above center of the beam varies with the disk diameter so two sets of measurements were made. One with the bottom of the disk in the same position relative to the beam, and another with each disk at its optimum height. A third set of measurements was made to see if the rotation rate versus diameter at constant torque agrees with the theory presented in section 4.1. For these measurements, fifteen disks were prepared with diameters ranging between 12.5 mm, and 63.5 mm as shown in Figure 48. All of the disks had a nominal thickness of 3.8 mm, their exact dimensions are given in Table II.

FIGURE 48–Some Disks of Various Diameters

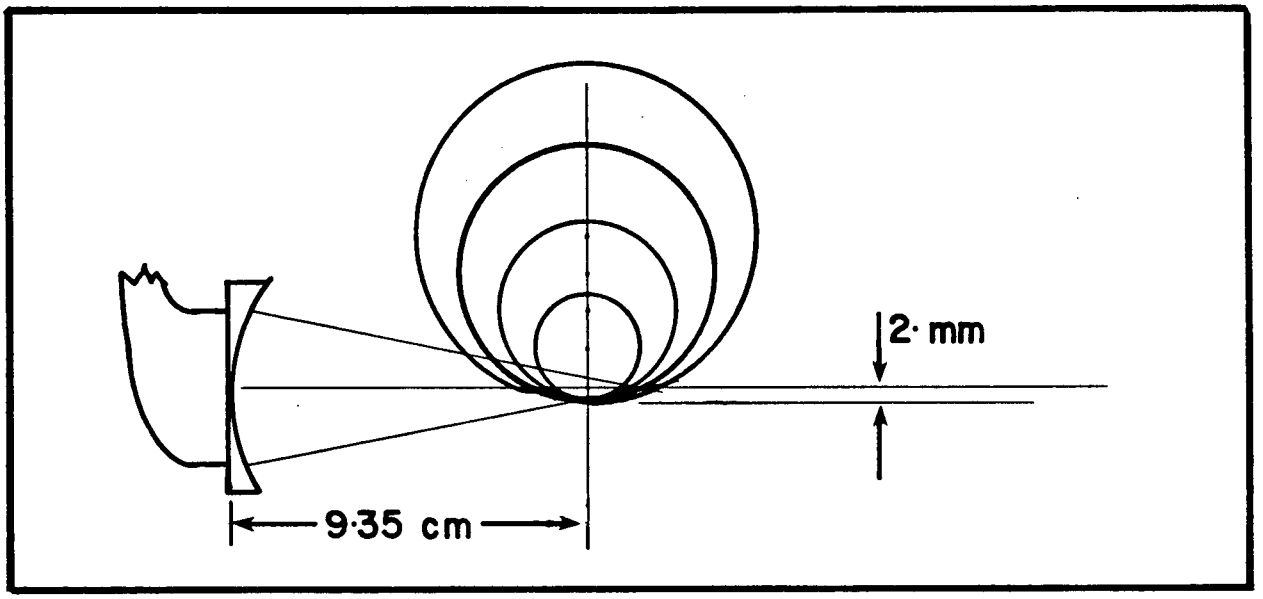

FIGURE 49–Disks Mounted With Their Bottoms at the Same Point in the Sound Beam

---

In the first of these experiments, the optimum position was found for the 25 mm diameter disk (D6). The distance from the shaft to the transducer was then fixed at this distance of 9.45 cm. Each disk was installed on the shaft in turn, and the height of the shaft was adjusted to keep the bottom of each disk at the same point as the bottom of the 25mm disk as shown in Figure 49. The rotation rate was then measured for each disk for six transducer input voltages, 32.6, 35.7, 42.3, 49.8, 55.3, and 64.4 V_{p-p}. Water temperature was 20.9 C. The results are shown in Figures 50, and 51. Great care had to be taken to prevent bubbles from adhering to the disks. The rotation rate of the small disks especially was greatly reduced by the presence of bubbles.

TABLE II. Dimensions of Disks of Various Diameters

DISK NUMBER	DIAMETER ±0.0013 mm	THICKNESS ±0.0013 mm
D1	12.713	3.801
D2	15.189	3.823
D3	17.856	3.785
D4	20.422	3.797
D5	22.936	3.861
D6	25.311	3.848
D7	27.940	3.912
D8	30.505	3.645
D9	33.058	3.797
D10	35.598	3.683
D11	37.986	3.607
D12	44.412	3.835
D13	50.813	3.747
D14	57.061	3.861
D15	63.017	3.645

As shown in Figure 52, over the range of disk diameters used, there is a power law relationship between the rotation rate of a disk and its radius. For this case:

$$\text{RPM} \sim R^{-1.4} \tag{76}$$

In the second experiment of this set, rotation rate was measured as a function of disk diameter with each disk in its own optimum position. The distance from axle to

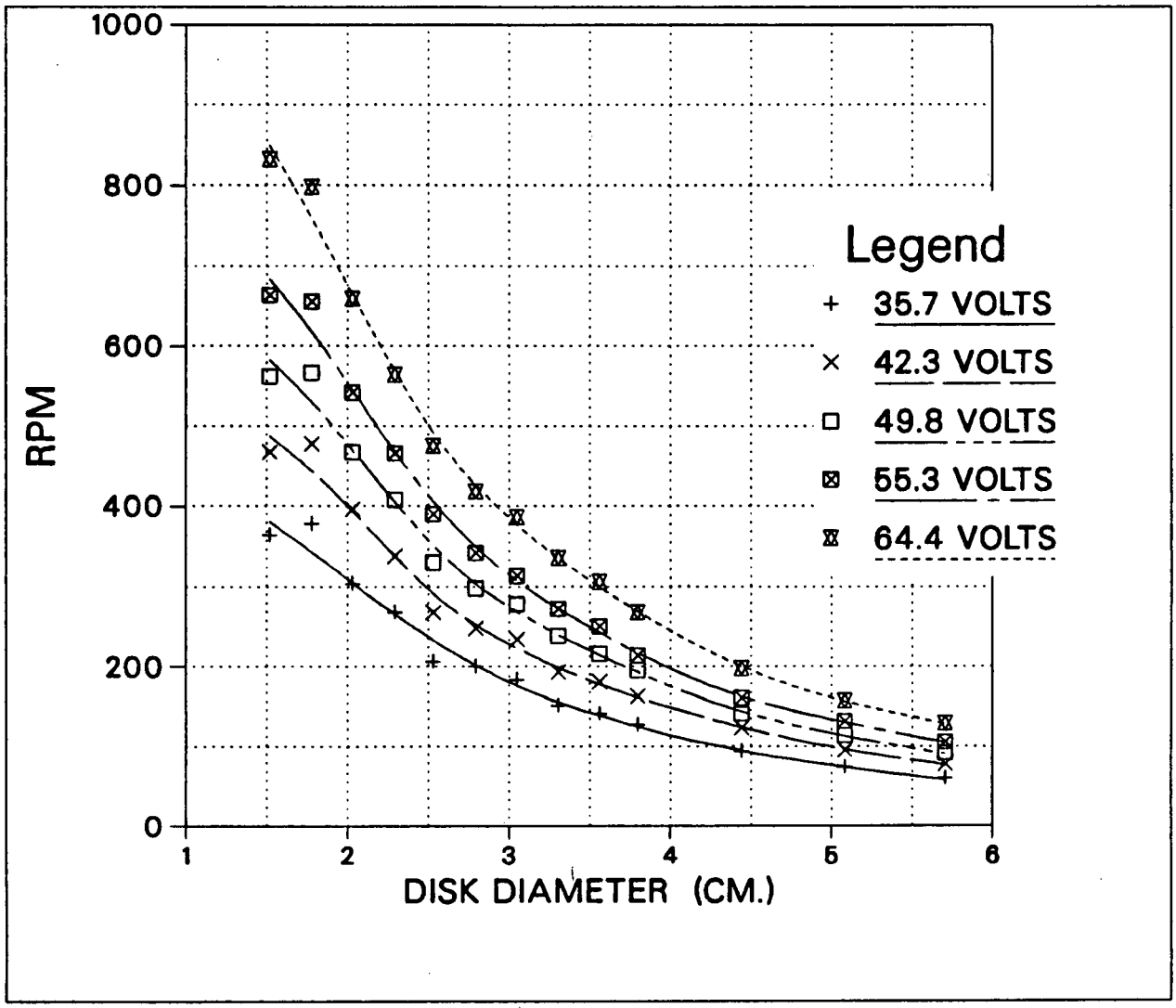

FIGURE 50–RPM vs. Disk Diameter at various Power Levels
Disks are mounted with their bottoms at the same point in the sound beam.

---

transducer, and the axle height were both varied to maximize the rotation rate for each disk. Table III shows the optimum position for each of the disks used.

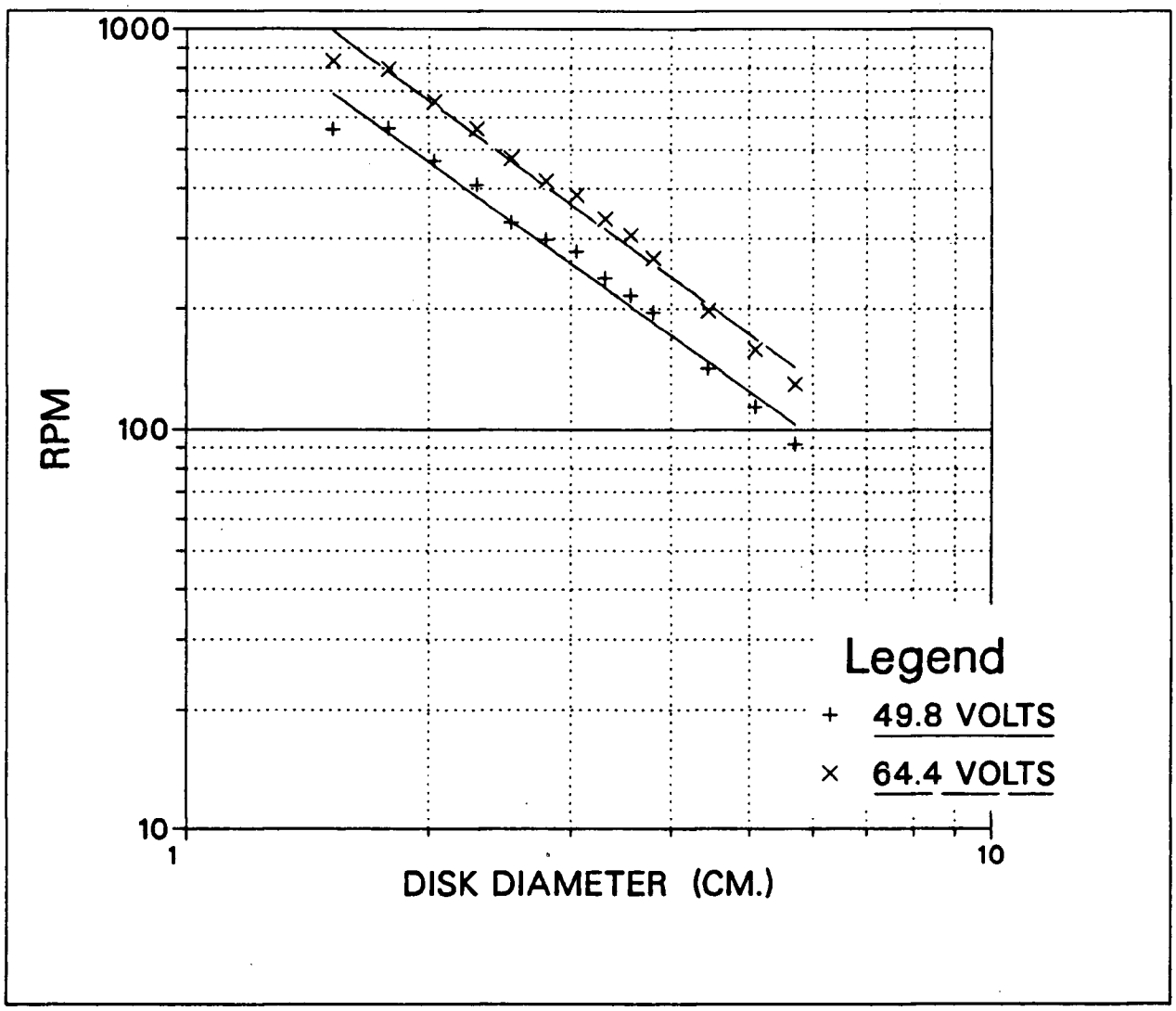

FIGURE 51–RPM vs. Disk Diameter at 2W and 5W
Disks are mounted with their bottoms at the same point in the sound beam.

The uncertainty quoted in Table III for the optimum distance to the transducer is the range over which no significant change was observed in the rotation rate as the shaft was moved. The optimum axle height is plotted versus the disk diameter in Figure 52.

When the optimum position was found for each disk, its rotation rate was measured with 41.2 V_{p-p} applied to the transducer. The results are shown in Figure 53 From this

TABLE III Optimum Position for Disks of Different Diameters

DISK NUMBER	DISTANCE TO TRANSDUCER cm	HEIGHT OF AXLE ABOVE BEAM CENTER ± 0.05 cm
D5	9.35 ± 0.2	1.0
D6	9.45 ± 0.2	1.1
D7	9.5 ± 0.55	1.2
D8	9.3 ± 0.55	1.35
D9	9.35 ± 0.6	1.45
D10	9.5 ± 0.45	1.6
D11	9.35 ± 0.6	1.65
D12	9.6 ± 0.85	2.0
D13	9.85 ± 0.75	2.25
D14	9.85	2.55
D15	9.85	2.85

figure, it is seen that:

$$\text{RPM} \sim R^{-1.78} \tag{77}$$

In the final experiment of this set, we wanted to test the theoretical relationship of RPM to diameter at constant torque as expressed in equation 71 of Chapter 4. To do this, we needed to find a way to apply the same amount of torque to each of our disks. I decided to use the torque acting on disk D5, in its optimum position, with a transducer input voltage of $53.1\,V_{p-p}$ as a standard. One at a time, each of the remaining disks was mounted on a shaft in tandem with this disk as shown in Figure 54. First, disk D5

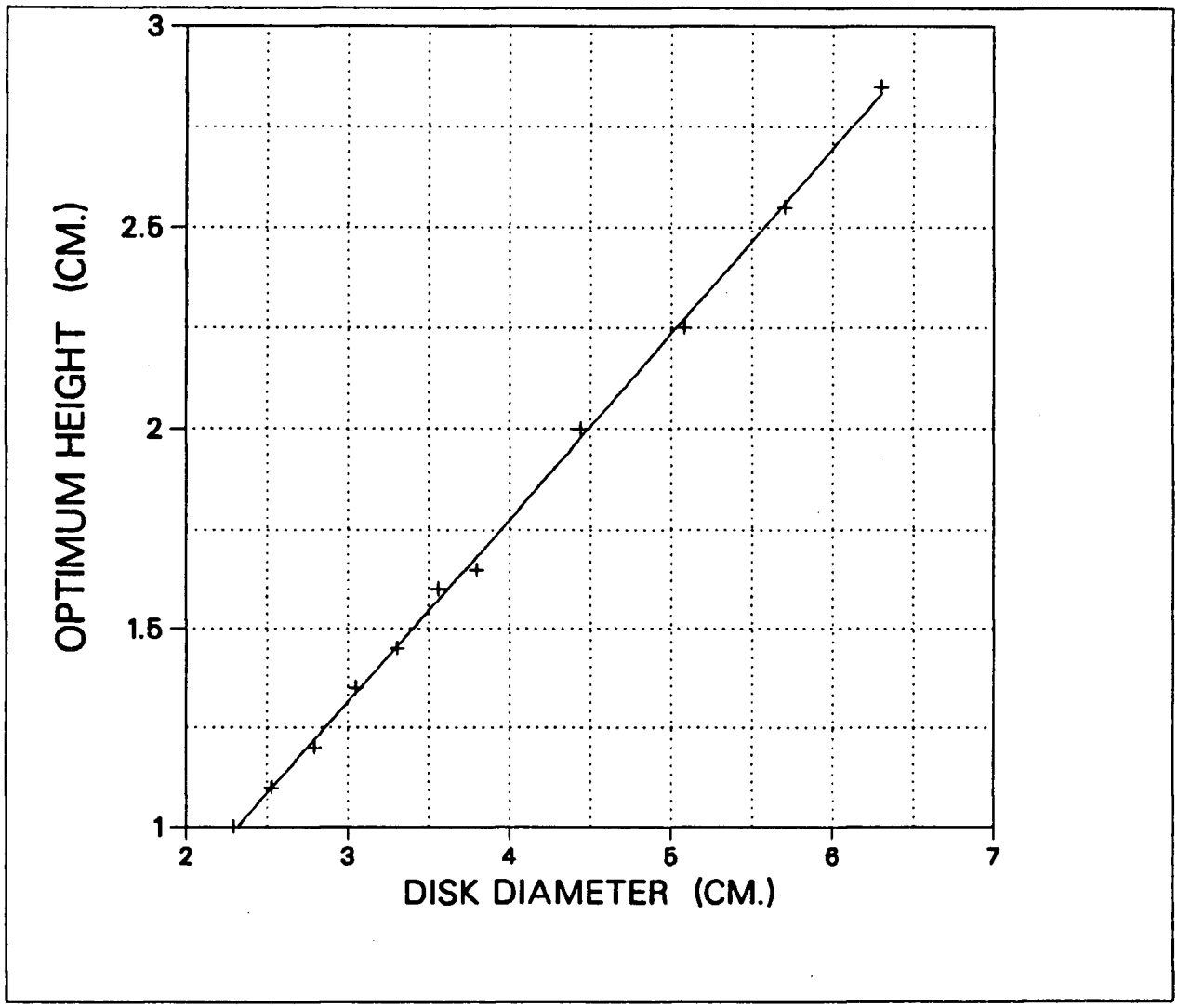

FIGURE 52–Optimum Axle Height vs. Disk Diameter

---

was driven by the sound beam, and the rotation rate of the axle with its two disks was measured. Then the axle was flipped over so that the other disk was driven by the beam. The beam power was adjusted to obtain the same rotation rate as when disk D5 was being driven. In this way, the amount of beam power needed to provide the standard torque on each disk was found. The results are shown in Table IV.

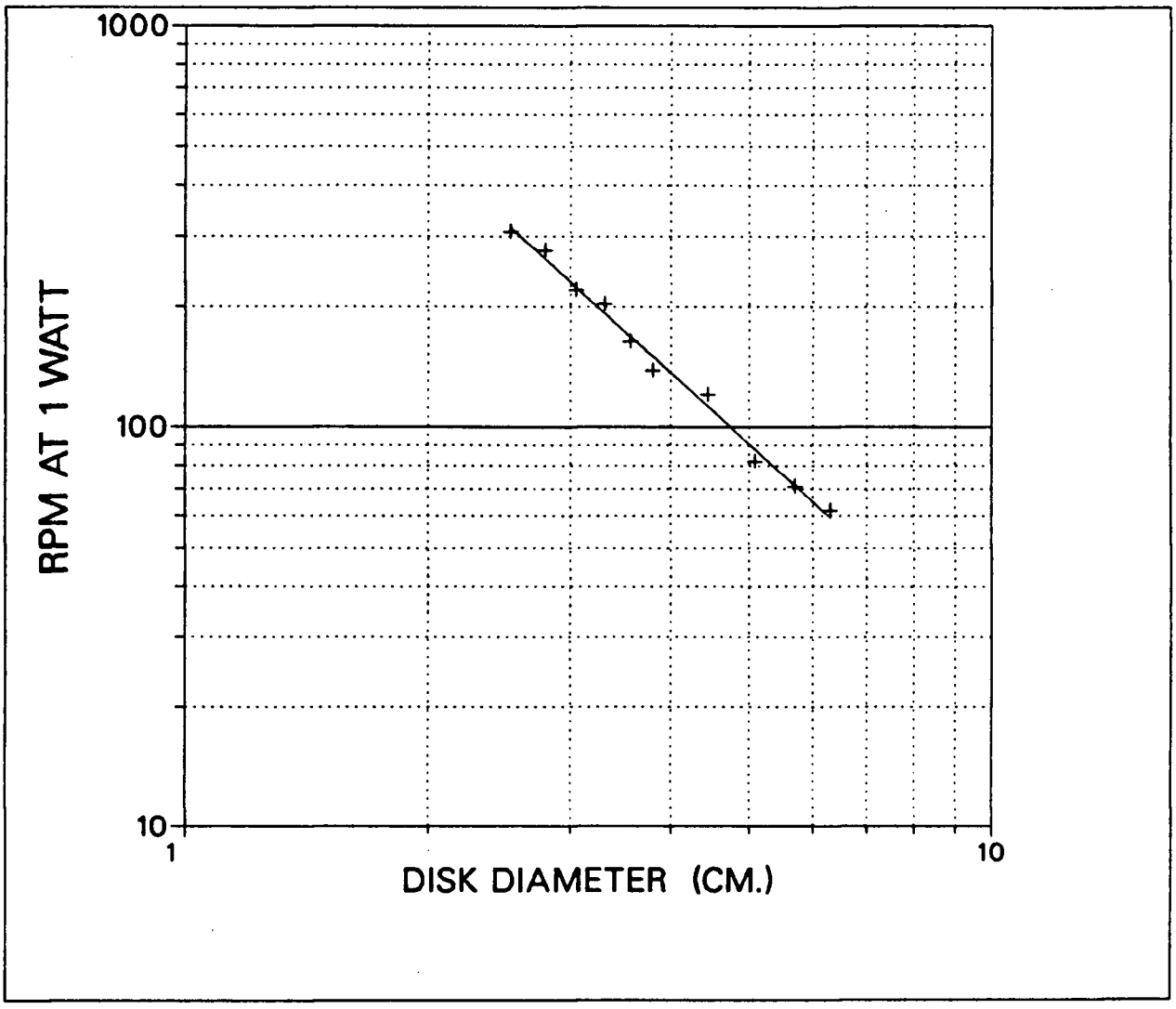

FIGURE 53–RPM vs. Disk Diameter with Disks in Optimum Position

---

The temperature was 21.9 ± 0.2 C for these measurements. This method assumes that the acoustic torque on disk D5 does not vary significantly with the rotation rate which varied from 35 RPM when it was paired with disk D15 to 175 RPM when it was paired with disk D4. Finally, each of the disks was mounted on a shaft by itself, centered in the sound beam, and driven by an acoustic beam with a power level corresponding to the appropriate

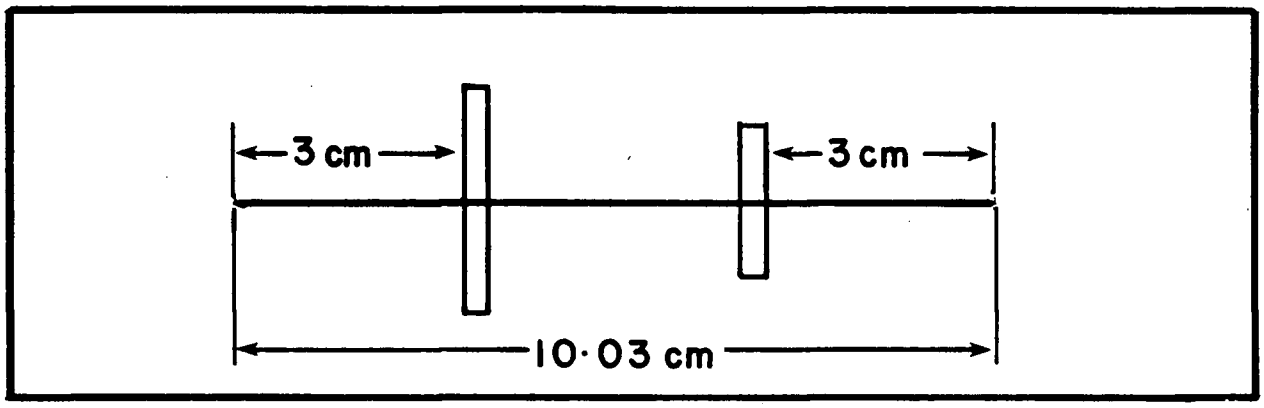

FIGURE 54–Two Disks Mounted in Tandem

---

voltage from Table IV. The results are plotted as Figure 55. From this plot, we see that the speed of rotation at constant torque is related to the disk radius by:

$$\text{RPM} \sim R^{-2.54} \tag{78}$$

TABLE IV. Transducer Input Voltages for Standard Torque

DISK NUMBER	VOLTAGE FOR STANDARD TORQUE V_{p-p}
D4	58.2
D5	53.1
D6	49.5
D7	50.3
D8	50.6
D9	53.8
D10	54.9
D11	54.0
D12	58.2
D13	55.0
D14	57.5
D15	50.7

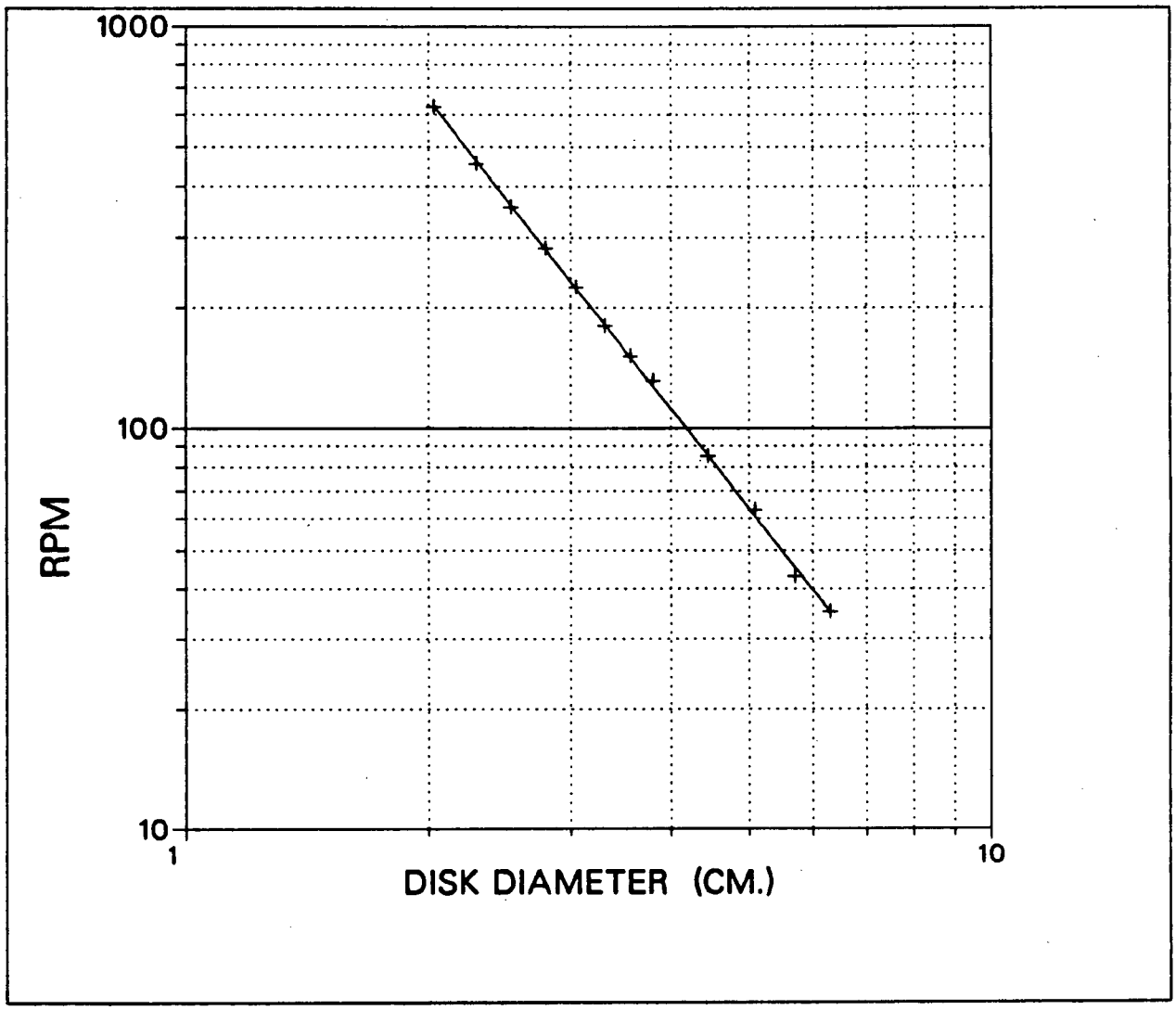

FIGURE 55–RPM vs. Disk Diameter at Constant Torque

6.9 Rotation Rate versus Acoustic Power Input

To use this device as an intensity meter, it is important to find out how its output, the rotation rate of the disk, varies with the acoustic power input. In this final experiment, RPM was measured as a function of input power for two disks of diameter 2.5 cm ($D6$) and 3.3 cm ($D9$). Each disk was placed in its optimum position from Table III and RPM was measured for transducer input voltages between 15.7 V_{p-p} and 133.4 V_{p-p}. Water temperatures were 25.5 C and 23.5 C for the experiment on disks D6 and D9 respectively. The results of this experiment are shown in Figures 56, 57 and 58.

Figures 57 and 58 show that at sufficiently high power levels, the rotation rate is related to the input power by a power law:

$$\text{RPM} \sim I^{\chi} \tag{79}$$

Here I, is the intensity of the beam, with $\chi = 0.65$ for D6, and $\chi = 0.682$ for D9. These curves deviate from this power law at transducer input voltages below about 30 V_{p-p} for D6, and about 24 V_{p-p} for D9.

Now that we have reported the results of our experiments, we can make some conclusions about how this meter operates.

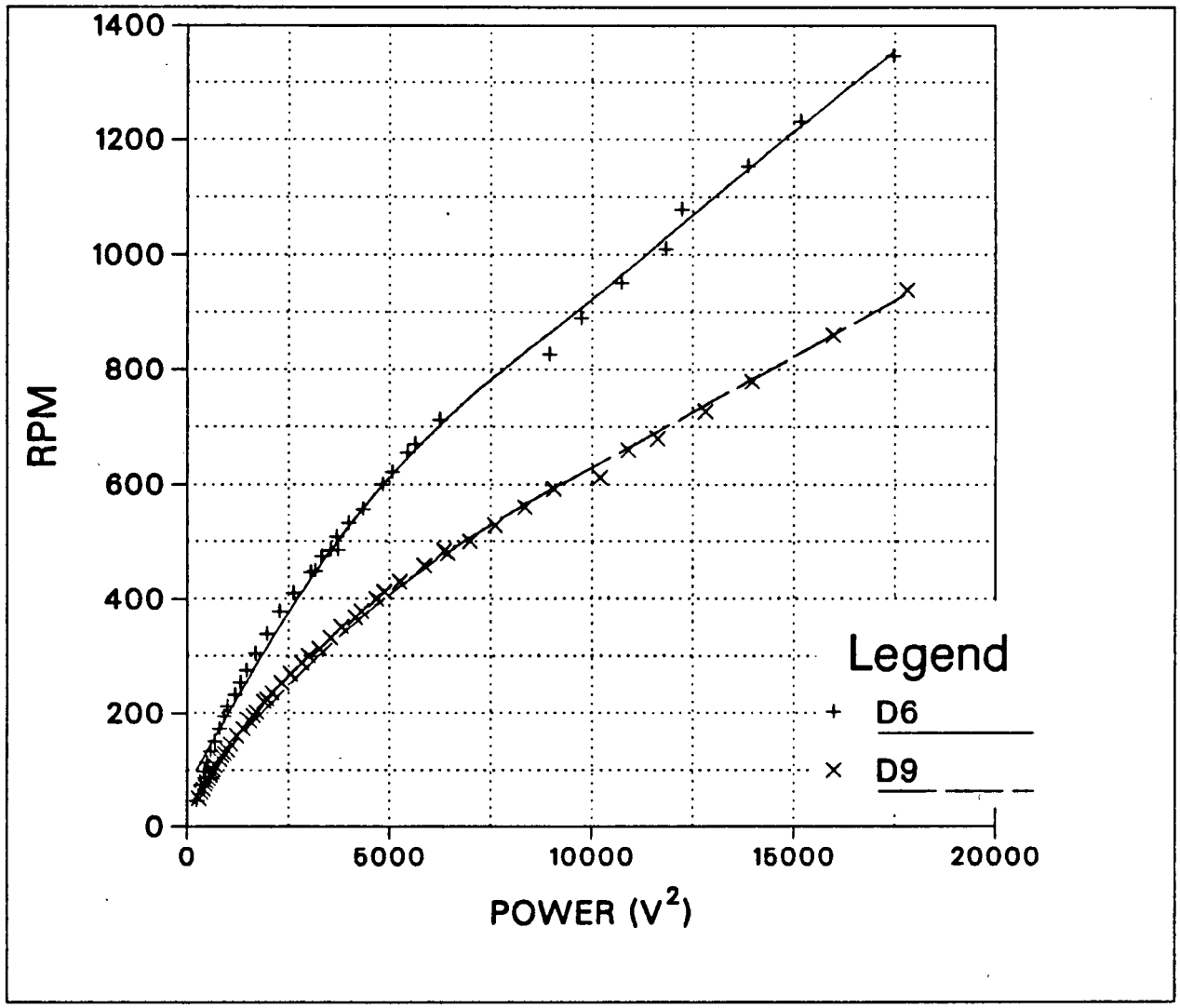

FIGURE 56–RPM vs. Power for Disks D6 and D9
Each disk was in its optimum position for these measurements.

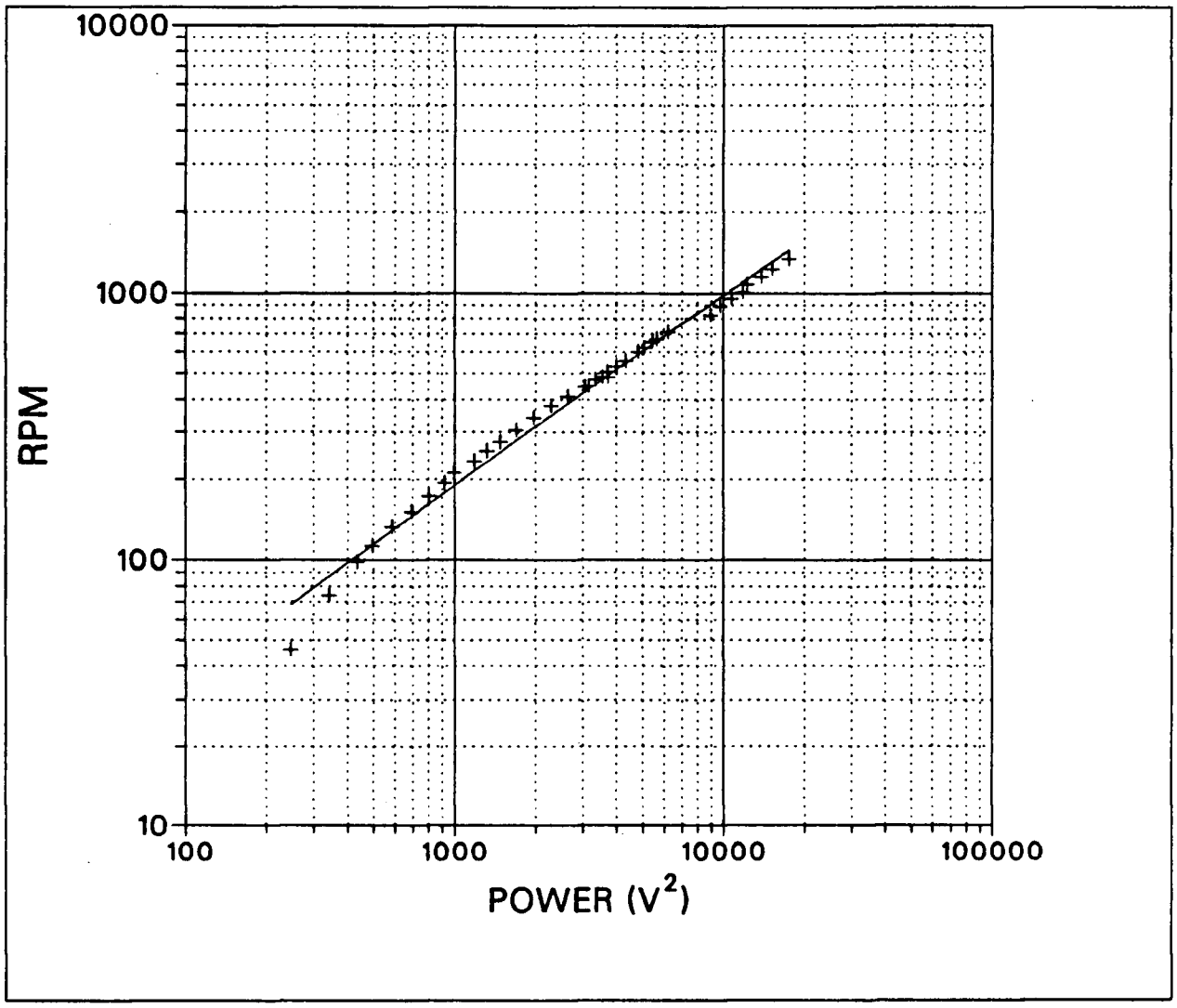

FIGURE 57–RPM vs. Power for Disk D6
(at optimum position)

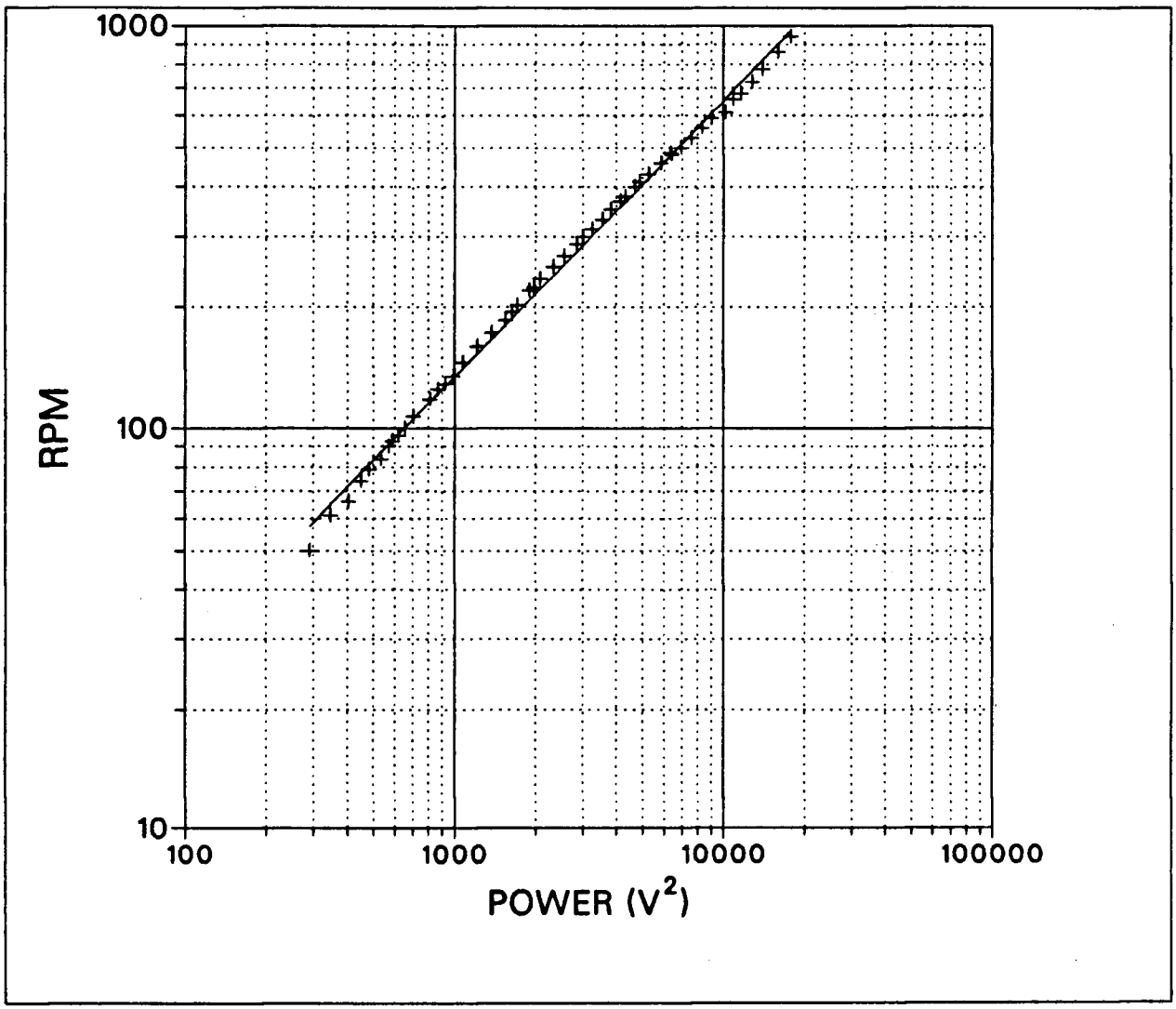

FIGURE 58–RPM vs. Power for Disk D9
(at optimum position)

CHAPTER 7–Discussion and Conclusions

In this thesis, we have reported the results of some investigations into the behaviour of a simple new meter for measuring the intensity of an ultrasonic beam. We have studied the mechanism by which it works and made some measurements to determine the scaling laws which will be important to its optimization.

7.1 Radiation Pressure Causes the Disk to Rotate

In the first set of experiments we showed that radiation pressure, and not streaming, is responsible for most of the driving torque on the disk. At most, streaming accounts for 13% of the driving torque on a 2.5 cm diameter by 1.5 cm thick Nylon disk driven by a 1.0 MHz ultrasonic beam in distilled water. Streaming could be more important if more of the sound beam were absorbed in the fluid surrounding the disk. This would be the case if the frequency of the sound beam were increased, or if the fluid was changed from water to a different liquid with a higher coefficient of absorption.

In the second experiment, we investigated the forces that act on an object when it reflects a sound beam. The results agree quite well with the theory presented in section 2.7 which predicts that there will be such a force, and that when sound is reflected from a circular disk, this force will be directed through the axis of the disk and will not cause the

disk to rotate. The dramatic difference between the rotation rate of the toothed wheel, which spun quickly, to that of the smooth wheel which did not rotate at all also helps to confirm that streaming is not important in causing the disks to rotate. If the torque on the disks was due to streaming, one would not expect it to depend so dramatically on the presence or absence of teeth on the disk. Streaming could be made relatively more important if the torque due to radiation pressure were reduced. This would be the case if the disks were made of a material that reflected more of the sound incident on it (e.g. Copper).

The results of the third experiment can be interpreted in either of two different but compatible ways. The theory presented in section 2.7 predicts that the torque on an absorbing disk due to radiation pressure should be directly proportional to the intensity of the incident sound field. If we assume that the intensity of the sound beam emanating from our transducer is proportional to the square of the transducer input voltage, and we assume that for each small disk added to the shaft, the torque required to drive the shaft at a fixed rotation rate is increased by the same amount, then the linear curve of Figure 37 confirms this theory. We could also begin by assuming that the theory is correct, and the torque on a disk is indeed directly proportional to the intensity of the sound beam. In this case, the results of this experiment show that the intensity of the sound beam is in proportion to the square of the transducer input voltage. Probably both of these interpretations are true. It seems unlikely that a nonlinearity in the response of the transducer is exactly balanced by a nonlinearity in the action of radiation pressure on the disk. This could be checked by measuring the beam intensity directly with a calibrated hydrophone.

The results of these first three experiments show that radiation pressure causes the forces which make this meter work, and that these forces are consistent with the theory presented in Chapter 2. The rest of the experiments were concerned with optimizing the meter.

7.2 Optimization Experiments

The first step in optimizing this meter is to find the best position in the sound beam to place a given disk so that its rotation rate is maximized.This is complicated because this optimum position depends on the diameter of the disk and we are also interested in optimizing the dimensions of the disk. There are some general rules. For any disk, the maximum rotation rate corresponds with the disk being centered laterally in the sound beam. The optimum distance from the axle to the transducer face is about 9.4 cm as shown in Figure 41 and Table III. This places the axis of the disk about 1.5 cm in front of the focal point of the lens as shown in Figure 23. The optimum height of the axle above the center of the beam is 0.91 times the radius of the disk as shown in Figure 52. The best height and lateral position in the beam appear to vary little with the distance to the transducer as shown in Figures 42 and 43. The best distance from the axle to the transducer does not appear to vary much with disk diameter or thickness as shown in Table III.

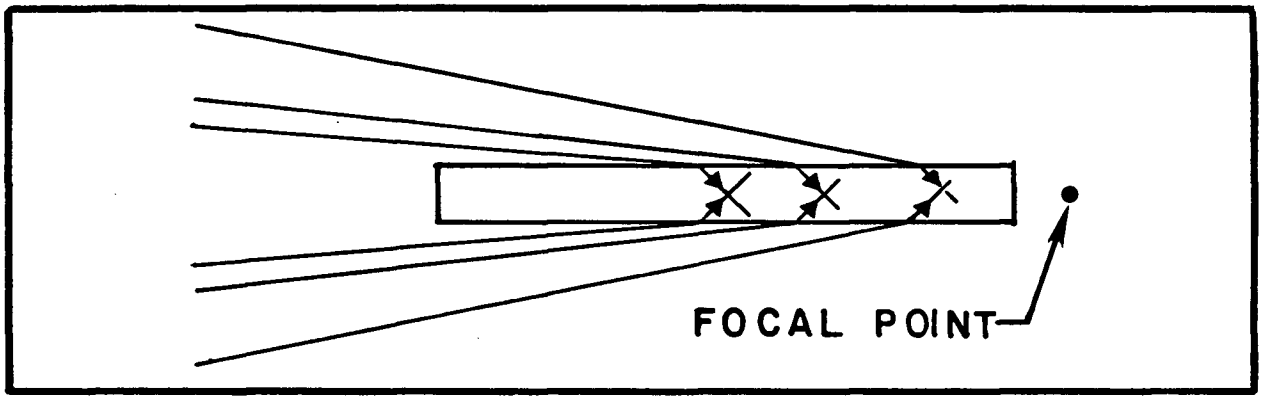

FIGURE 59–Sound Capture by a Disk

Let us discuss these results. It is not surprising that the maximum rotation rate is always obtained with the disk centered in the sound beam regardless of any other factors. It is, however curious that the optimum position for the disk is with its axle in front of the focal point. This could be because the fraction of the sound beam that hits the sides of the disk is refracted and directed inside the disk as shown in Figure 59. This optimum position could also be affected by the absorption of sound in the water. The flux of acoustic energy should be higher closer to the transducer than it is farther away yielding a higher radiation pressure. Sound absorption cannot play a great part though, because at 1 MHz, the coefficient of sound absorption in water is only $25 \times 10^{-5}\,\mathrm{cm}^{-1}$ [Barnes and Beyer 1964].

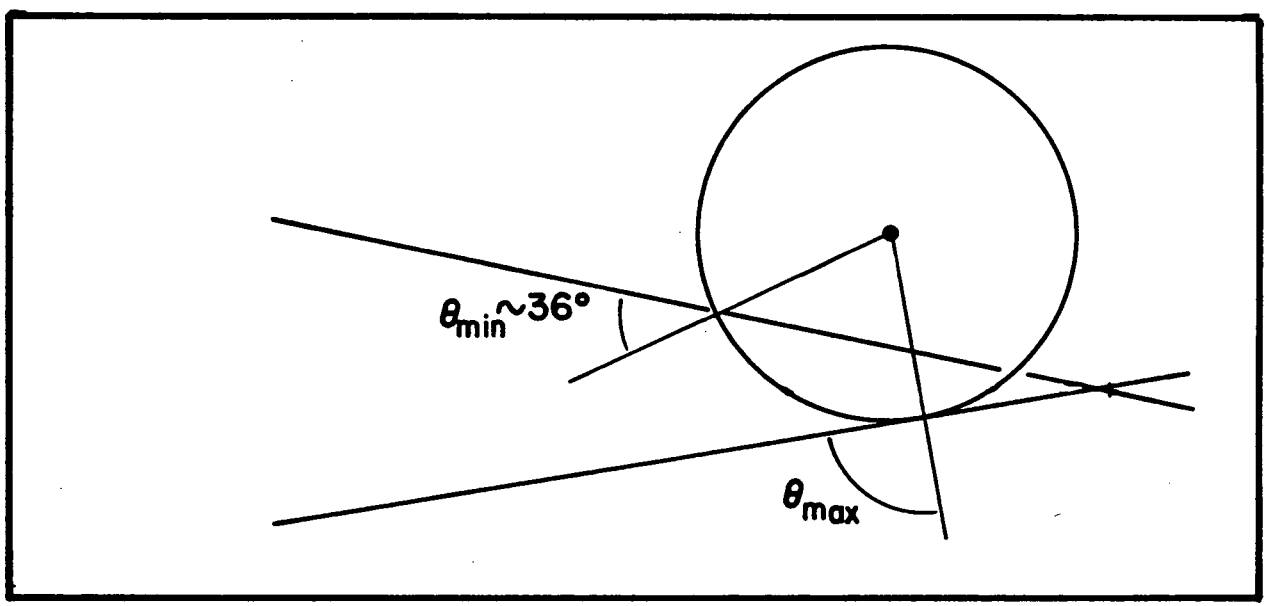

FIGURE 60–Angles of Incidence for a 2.5 cm Diameter Disk in Optimum Position

---

The optimum height of the disk tells us that the sound waves propagating inside the disk are almost all transverse. Figure 60 shows a 2.5 cm Diameter disk in its optimum position in the converging sound beam from our lens. As shown, the angle of incidence of

the sound beam varies between approximately 36° and 90° on the curved surface of the disk. With a velocity of 2620 m/s in nylon, [CRC Press 1976, p.E-47], the critical angle for longitudinal waves at a water–nylon interface is 35°. For angles of incidence greater than this, longitudinal waves can not penetrate the disk except where they are converted to transverse waves at the interface. This analysis is only strictly true for plane waves impinging at an angle on a plane surface, but it should be roughly true here because the wavelength of the sound in the water is 1.5 mm much smaller than either the focal length of the lens or the radius of curvature of the disk.

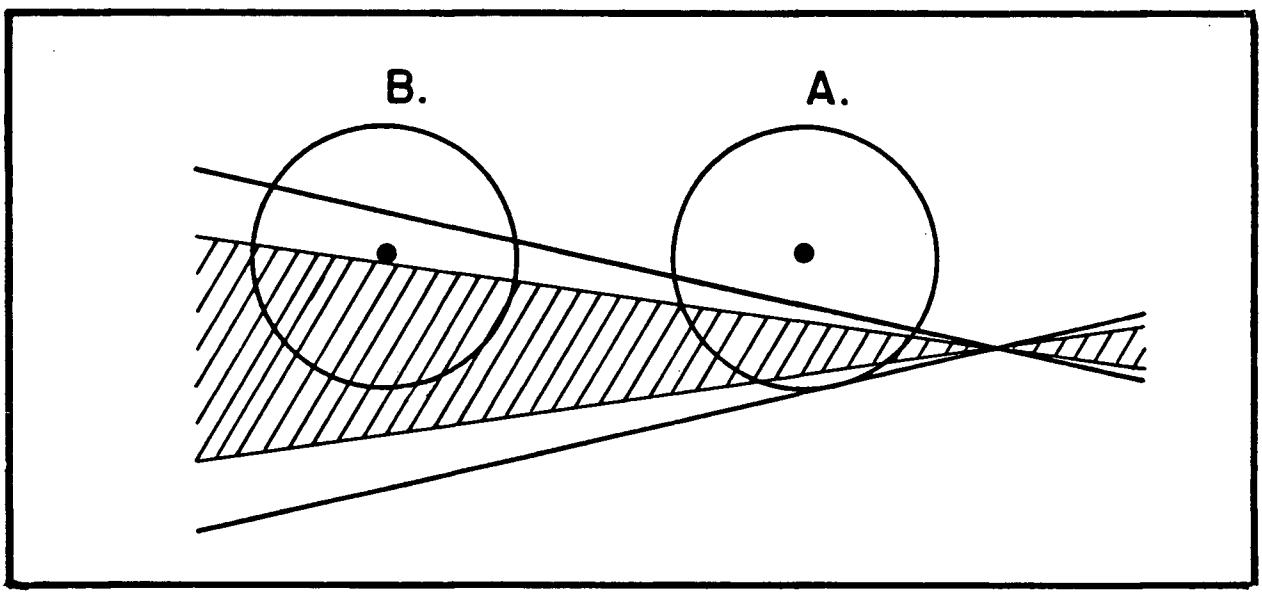

FIGURE 61–Disk in a Non–Uniform Acoustic Beam

In position A, the disk intercepts all of the more intense central area of the beam. When the disk is moved horizontally to position B, it must be lowered to intercept all of the intense part of the beam.

The slight drop in optimum height that occurs when the disk is moved closer to the transducer could be explained if the beam is more intense near its center as shown in Figure 61. As the disk is moved closer to the transducer, it must be lowered to intercept most of the intense part of the beam. This type of beam profile could arise because of the

mode of excitation of the transducer or because the outside edges of the beam must pass through a thicker part of the lens where more of the sound is absorbed. The beam profile could be measured by scanning a small hydrophone across the beam.

Figures 38, 39, and 40 show that the optimum position for a disk can be found by moving it to its best position along each of the three axes in turn and then fine tuning. There are no positions where the rotation rate is just locally maximized.

Now that we have established the best position for our disk, we can settle on its optimum dimensions. Figure 45 shows that a disk 3.9 mm thick represents the best compromise between increasing the driving torque by intercepting more of the beam and increasing drag by increasing the surface area of the disk.

It is more difficult to settle on an optimum disk diameter than an optimum disk thickness. During the experiments, we noted that smaller disks (less than about 2.3 cm in diameter) were especially vulnerable to disturbance by small bubbles and bits of dust sticking to their surfaces and reducing their rotation rates erratically. One could use a larger disk, however the larger the disk, the more slowly it rotates for a given beam intensity. As we found in section 6.8:

$$\text{RPM} \sim R^{-1.78} \tag{77}$$

This makes it more difficult to measure the rotation rate of a large disk quickly and accurately. The best compromise is probably a disk about 2 cm in diameter, unless the fluid surrounding the disk is exceptionally clean, and acoustic intensities are low enough that cavitation is not a factor in creating bubbles, in which case a smaller disk could be used.

Figure 55 shows results that confirm the theory presented in Chapter 4 for the drag on a rotating disk. This theory predicts in equation (71) that at constant torque:

$$\text{RPM} \sim R^{-x}$$

where R is the radius of the disk, and $x = 8/3$. We can measure x to be 2.58 from the data in Figure 55 in good agreement with the theory.

For any meter to be useful, its output must be related to its input by some well defined, preferably simple, function over a large range of input values. Here the output is the rate of disk rotation, and the input is the intensity of the incident ultrasonic beam. The results of the sixth experiment, as presented in Figures 57 and 58, show that the rotation rate of the disk is related to the input intensity by:

$$\text{RPM} = I^{\chi} \tag{80}$$

where χ is 0.65 for the 2.5 cm diameter disk (D6), and 0.68 for the 3.3 cm diameter disk (D9). Here, we are assuming that the intensity of the ultrasonic beam was directly proportional to the square of the transducer input voltage. This assumption is probably very good at the moderate power levels that were used. We can see from equation (71) that for a perfect disk rotating in an ideal, infinite, fluid that χ should be 2/3, in very good agreement with the experimental results. Figures 57 and 58 show that (80) is valid for input voltages above about 30.2 V_{p-p} for the 2.5 cm diameter disk, and 24 V_{p-p} for the 3.3 cm diameter disk.The maximum input voltage used in either case was about 130 V_{p-p} so (80) holds true as the intensity of the incident beam changes by a factor of 30, and possibly more. One possible reason that (80) no longer holds at lower power levels is that the theory presented in section 4.1 for the drag on a rotating disk assumes that the fluid

near the disk flows as if the disk were of infinite diameter. As pointed out there, the theory should break down at rotation rates below about 150 RPM for a 2.5 cm diameter disk where the assumption that the boundary layer on the disk is much smaller than the radius of the disk is no longer true. A similar calculation predicts that for a 3.3 cm diameter disk, we can expect deviations from this theory to occur when the rotation rate is less than about 60 RPM. Figures 57 and 58 show that the experimental data deviates from the theoretical line at a rotation rate of 200 RPM for the 2.5 cm diameter disk, and 90 RPM for the 3.3 cm diameter disk in rough agreement with this qualitative part of the theory. Figure 62 shows the curves of Figures 57 and 58 replotted in terms of the dimensionless parameter δ/R it is clear that deviation from power law behaviour begins in both cases when δ/R increases to about $1/40$.

We would like our meter to obey (80) over as large a range as possible. This advances a new criterion for choosing the diameter of our disk, and the fluid surrounding it. From equations 71 and 72 we have:

$$\frac{\delta}{R} \approx \frac{\sqrt{\nu/\omega}}{R} \sim R^{-0.1}\sqrt{\nu} \tag{81}$$

We want to keep δ/R as small as possible and see from (81) that we should choose a disk as large in diameter as possible. More importantly, to extend the range of power law behaviour, we should choose a fluid with a viscosity as small as possible.

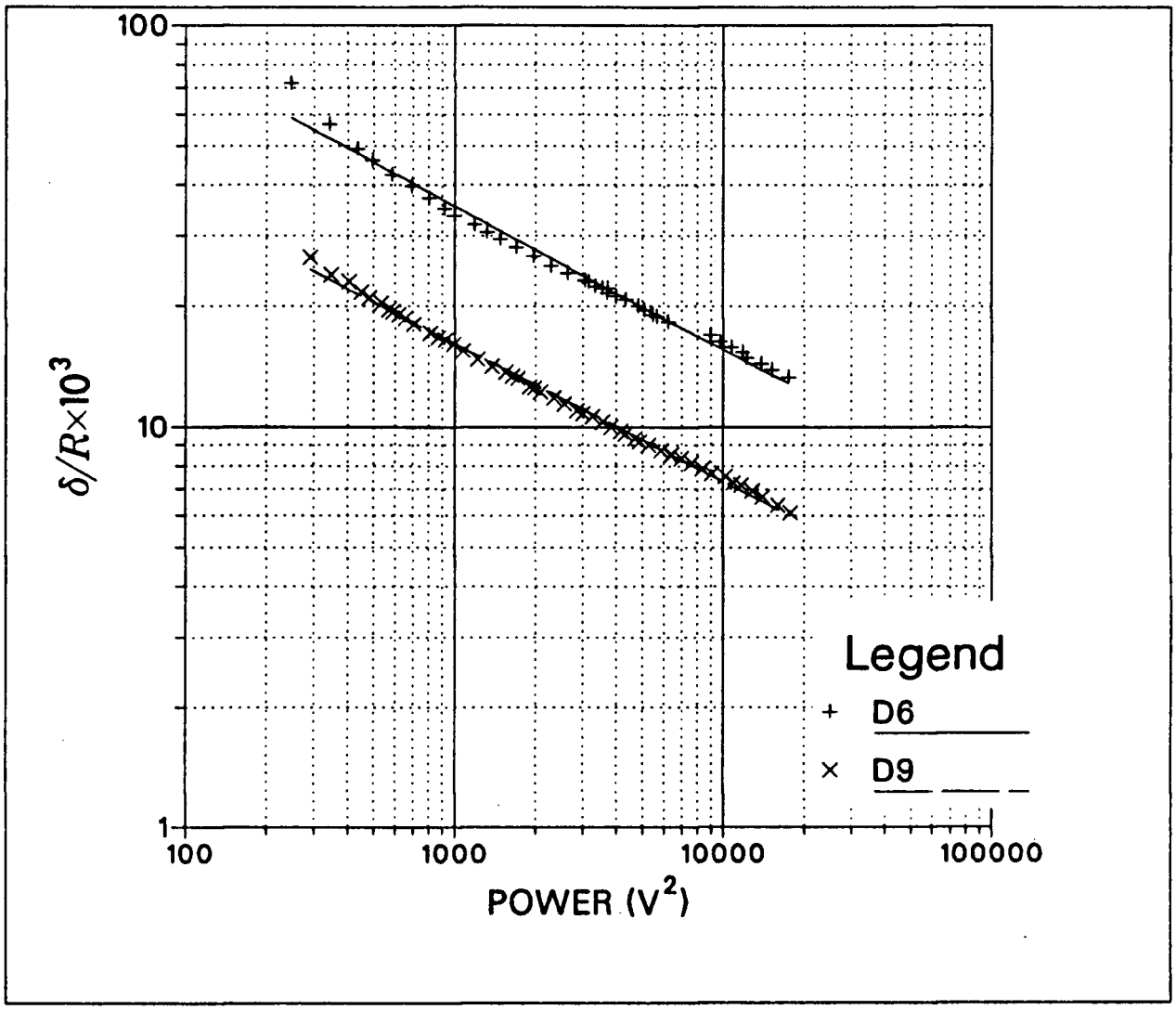

FIGURE 62–δ/R vs. Power for Disks D6 and D9
The values of δ/R for D6 have been doubled to separate the curves

---

7.3 Summary

In this thesis, I report new results which clarify the mode of operation, and will be useful for optimizing the design of the rotating disk sound intensity meter shown in Figure 1. I have shown that:

- Acoustic streaming plays a very small part in causing the disk to rotate. It provides less than 13% of the driving torque on a typical disk. Radiation pressure provides almost all of the torque on the disk. (cf section 6.3)

- With the 10.8 cm focal length lens used in these experiments, the optimum dimensions for a Nylon disk are about 3.8 mm thick by 2.3 cm in diameter. (cf section 7.2)
- A disk of radius R rotates most quickly when it is centered laterally in the beam, its axis is $0.91R$ above the center of the acoustic beam, and 1.5 cm in front of the focal point of the lens as shown in Figure 41.
- At sufficiently high intensities, the rotation rate (ω) of the disk is related to the intensity (I) of the acoustic beam by the power law $\omega \sim I^{2/3}$. Both this power law, and the departure from it at low rotation rates are consistent with the theory presented in Chapters two and four. (cf section 7.2)

7.4 What Remains to be Done?

We have studied several of the factors that will be important in optimizing this meter but there are at least two important areas that were not investigated. Firstly, the geometry of the sound field is dependent on the lens used to focus the collimated sound beam from the transducer. In this experiment we used only one lens of focal length 10.8 cm. A lens of different design or focal length might improve the performance of this device. The second area that deserves full investigation is the effect of changing the disk material. Nylon was used here because it was conveniently available. An ideal material would be light in weight, absorb sound very well, and have an acoustic impedance closely matched to the fluid it is to be used in. Chances are that the optimum placement of the disk will be found to depend strongly on the type of lens used, and on the material that the disk is made of.

Two final areas where the performance of this meter could be fine tuned are the texture of the disk surface, and the viscosity of the fluid surrounding the disk. One texture that may be worth trying is the array of fine grooves that has proved useful for reducing the drag on racing sailboats. As mentioned above, changing from water to a liquid of lower viscosity may extend the range over which rotation rate is related to acoustic intensity by a power law to lower intensities. Of course, changing the fluid will also affect the optimum lens design, disk dimensions, disk material, and disk position.

We have seen that this meter has a well defined calibration curve which is obeyed over a significant range of intensities. It has the advantages of simplicity, robustness, and, because its output is a train of pulses, it has the potential to operate well in very noisy electrical environments where it would be difficult to use analog transducers. Much work still can be done to optimize its characteristics, but this meter should find application in the future.

Bibliography

Apfel, R.E. 1970. The Role of Impurities in Cavitation Threshold Determination. *J.Acoust.Soc.Am. 48(5):1179.*

Aris, R. 1962. *Vectors, Tensors, and the Basic Equations of Fluid Mechanics*. Prentice-Hall, London.

Barnes, R.P.Jr., and R.T. Beyer 1964. Ultrasonic Absorption in Water at Finite Amplitudes. *J.Acoust.Soc.Am. 36(7):1371.*

Beissner, K. 1982. On the Plane Wave Approximation of Acoustic Intensity. *J.Acoust.Soc.Am. 71(6):1406.*

Beyer, R.T. 1960. Parameter of Nonlinearity in Fluids. *J.Acoust.Soc.Am. 32(6):719.*

Beyer, R.T. 1974. *Nonlinear Acoustics*. U.S. Govt. Printing Office, Washington D.C. *# 1975-0-596-215.*

Beyer, R.T. 1978. Radiation Pressure–The History of a Mislabeled Tensor. *J.Acoust.Soc.Am. 63(4):1025.*

Blackstock, D.T. 1962. Propagation of Plane Sound Waves of Finite Amplitude in Nondissipative Fluids. *J.Acoust.Soc.Am. 34(1):9.*

Brekhovskikh, L.M. 1980. *Waves in Layered Media* 2nded.. Academic Press, N.Y..

Chu, Boa-Teh and R.E. Apfel 1982. Acoustic Radiation Pressure Produced by a Beam of Sound. *J.Acoust.Soc.Am. 72(6):1673.*

Coppens, A.B., R.T. Beyer, M.B. Seiden, J. Donohue, F. Guepin, R.H. Hodson, C. Townsend 1965. Parameter of Nonlinearity in Fluids II. *J.Acoust.Soc.Am. 38:797.*

CRC Press 1976 (R.C. Weast ed.). *CRC Handbook of Chemistry and Physics* 57th ed.. CRC Press, Cleveland .

Erdmann-Jesnitzer, F. and H. Louis 1973. Shock Waves Generated by Imploding Cavitation Bubbles and Their Influence on Materials. in *Finite Amplitude Wave Effects in Fluids, Proceedings of the 1973 Symposium: Copenhagen*, L.Bjørno ed., IPC Science and Technology Press, Guildford, Surrey, U.K...

Flynn, H.G. 1964. Physics of Acoustic Cavitation in Liquids. Chapter 9 of:*Physical Acoustics*,Vol. 1B, W.P.Mason ed., Academic Press, N.Y..

Goldstein, S. 1965. *Developments in Fluid Mechanics Vol.1.* Dover Publications, N.Y..

Hagelberg, M.P., G. Holton,and S. Kao 1967. Calculation of B/A for Water From Measurements of Ultrasonic Velocity vs. Temperature and Pressure to $10,000\,kg/cm^2$. *J.Acoust.Soc.Am. 41(3):564.*

Hamitt, F.G. 1980. *Cavitation and Multiphase Flow Phenomena.* McGraw–Hill, U.S.A..

Hueter, T.F. and R.H. Bolt 1955. *Sonics.* John Wiley and Sons, N.Y..

Ingard, K.U. and D.C. Pridmore–Brown 1956. Scattering of Sound by Sound. *J.Acoust.Soc.Am. 28(3):367.*

Koblanski, J. 1983. U.S. Patent #4,408,494 Oct 11, 1983. .

Koblanski, J. 1986. Canada Patent #1,209,240 1986. .

Lighthill, M.J. 1979. *Waves in Fluids* (paperback ed.). Cambridge University Press, Cambridge.

Morse, P.M. and K.U. Ingard 1968. *Theoretical Acoustics* (paperback ed.). Princeton University Press, Princeton, N.J..

Neppiras, E.A. 1980. Acoustic Cavitation. *Phys.Rep. 61(3):159–251.*

Nyborg, W.L. 1965. Acoustic Streaming. in *Physical Acoustics Vol.IIb*(W.P.Mason ed.) Academic Press, N.Y..

Randall, R.H. 1951. *Introduction to Acoustics.* Adison–Wesley.

Schlichting, H. 1955. *Boundary Layer Theory* 1st English ed.. McGraw Hill.

Stapper, M. 1978. A Simplified Approach to the Mechanics of Acoustical Wave Propagation Applicable to the Problems of Radiation Pressure. Part II. The Application to Rayleigh and Langevin Radiation Pressure. *Acustica 39:111.*

Temkin, S. 1981. *Elements of Acoustics.* Wiley and Sons, N.Y..

Tjøtta, S. 1958. On Some Non–Linear Effects in a Sound Field With Special Emphasis on the Generation of Vorticity and the Formation of Streaming Patterns II. Streaming Caused by a Sound Beam. *Arch.Math.Naturvid. 55:37.*

Zieniuk, J. and R.C. Chivers 1976. Measurement of Ultrasonic Exposure With Radiation Force and Thermal Methods. *Ultrasonics (July) p.161.*

APPENDIX I.

Lagrangian and Eulerian Coordinate Systems

Eulerian, or spatial coordinates are the ones we use every day. In this system, the coordinate, x, refers to a fixed point in space. It is sometimes more convenient when dealing with problems in fluid mechanics to use the "material" or Lagrangian coordinate system. In this system, the coordinate, a, refers to the point in space currently occupied by the particle of fluid which started out at the Eulerian coordinate $x = a$ when the fluid was at equilibrium. As the particles of fluid are generally in motion, the point in space referred to by the Lagrangian coordinate "a" changes with time. It is common practise for authors to use the same symbol for both types of coordinate, and to let the reader figure out what system is being used from the context. In this appendix, I follow the example of Beyer [Beyer 1974] and call Eulerian coordinates "x", and Lagrangian coordinates "a". Functions are superscripted with either an "E", or an "L", depending on the type of argument.

We can establish a transformation between these two coordinate systems by considering the displacements of fluid particles from their equilibrium positions. The position in space described by "a" is:

$$x = a + \xi^{\mathrm{L}}(a, t) \tag{A1}$$

where ξ^L is the displacement from equilibrium of the particle which was situated at $x = a$ when the fluid was in equilibrium. This relationship can be inverted to give:

$$a = x - \xi^E(x,t) \qquad (A2)$$

where ξ^E is the displacement of the particle instantaneously found at position x at time t from its equilibrium position. ξ^E, and ξ^L are shown in Figure 63.

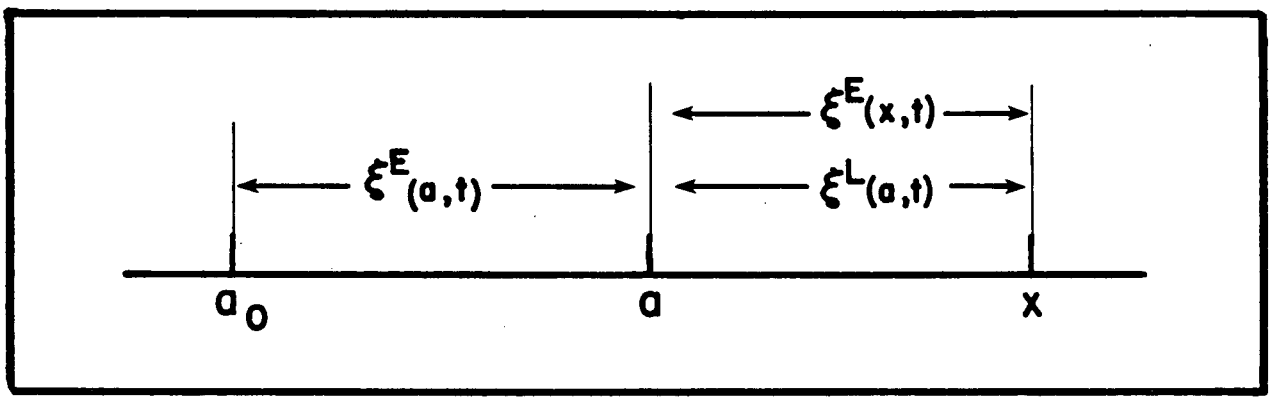

FIGURE 63–The Relationship Between Eulerian and Lagrangian Coordinates
This figure shows a fluid at time t. A sound beam has distorted the fluid so that the fluid particle which was at a_0 when the fluid was at equilibrium has been displaced to position a. The fluid particle which was at position a has been displaced to position x.

If Q is some function of the state of the fluid such as pressure or density, it can be expressed in terms of either coordinate system. If we know $Q^E(x,t)$, a function of Eulerian coordinates, we can write:

$$Q^L(a,t) = Q^E(a + \xi^L(a,t),t) \qquad (A3)$$

since we know Q^E completely, the RHS of (A3) can be expanded in a Taylor series about $x = a$ to give:

$$Q^L(a,t) = Q^E(a,t) + \frac{\partial Q^E}{\partial x}|_{x=a}\xi^{\mathrm{E}}(x,t) + \frac{1}{2!}\frac{\partial^2 Q^E}{\partial x^2}|_{x=a}\xi^{\mathrm{E}}(x,t)^2 + , \cdots \qquad (A4)$$

At this point, some authors make a mistake and write $\xi^{\mathrm{E}}(a,t)$ instead of $\xi^{\mathrm{E}}(x,t)$ [Blackstock 1962]. This is clearly wrong, and in general $\xi^{\mathrm{E}}(a,t) \neq \xi^{\mathrm{E}}(x,t)$ as shown in Figure 63. It is fortunate that the error introduced by this mistake only affects terms higher than the second order in this transformation. The displacements of fluid particles from their equilibria are often small in problems of acoustics so that terms of third order and higher in ξ^{E} or ξ^{L} can be neglected. The transformation can be correctly written:

$$Q^L(a,t) = Q^E(x,t)|_{x=a} + \frac{\partial Q^E}{\partial x}|_{x=a}\left\{\xi^{\mathrm{E}}(a,t) + \frac{\partial \xi^{\mathrm{E}}}{\partial x}|_{x=a}(\xi^{\mathrm{E}}(a,t) + \frac{\partial \xi^{\mathrm{E}}}{\partial x}|_{x=a}\xi + \cdots)\right\} + \frac{1}{2!}\frac{\partial^2 Q^E}{\partial x^2}\{\cdots\} + \cdots \qquad (A5)$$

To second order in ξ, we have:

$$Q^L(a,t) = Q^E(x,t)|_{x=a} + \frac{\partial Q^E}{\partial x}|_{x=a}\xi^{\mathrm{E}}(a,t) \qquad (A6)$$

The inverse transformation can be similarly computed to be:

$$Q^E(x,t) = Q^L(a,t)|_{a=x} - \xi^{\mathrm{L}}(a,t)\frac{\partial Q^L}{\partial a}|_{a=x} \qquad (A7)$$

APPENDIX II.

Exact Calculations of Eulerian Radiation Pressure

We begin with the one-dimensional equations of motion in Eulerian coordinates, the force equation:

$$\rho\frac{\partial \mathbf{U}}{\partial t} + \rho\mathbf{U}\frac{\partial \mathbf{U}}{\partial x} = -\frac{\partial \mathbf{P}}{\partial x} \tag{A8}$$

the equation of state:

$$\frac{\mathrm{D}}{\mathrm{Dt}}\left(\mathbf{P}\rho^{\gamma}\right) = 0 \tag{A9}$$

and the continuity equation:

$$\frac{\partial \rho}{\partial t} + \frac{\partial \rho\mathbf{U}}{\partial x} = 0 \tag{A10}$$

we let:

$$\rho = \rho_0 + \epsilon\rho_1 + \epsilon^2\rho_2 + \cdots \tag{A11}$$

$$\mathbf{P} = \mathbf{P}_0 + \epsilon\mathbf{P}_1 + \epsilon^2\mathbf{P}_2 + \cdots \tag{A12}$$

$$\mathbf{U} = 0 + \epsilon\mathbf{U}_1 + \epsilon^2\mathbf{U}_2 + \cdots \tag{A13}$$

(A8) becomes with these substitutions:

$$(\rho_0 + \epsilon\rho_1 + \epsilon^2\rho_2 + \cdots)(\epsilon\frac{\partial \mathbf{U}_1}{\partial t} + \epsilon^2\frac{\partial \mathbf{U}_2}{\partial t} + \cdots) + (\epsilon\mathbf{U}_1 + \epsilon^2\mathbf{U}_2 + \cdots)(\epsilon\frac{\partial \mathbf{U}_1}{\partial x} + \epsilon^2\frac{\partial \mathbf{U}_2}{\partial x} + \cdots) = -\epsilon\frac{\partial \mathbf{P}_1}{\partial x} + -\epsilon^2\frac{\partial \mathbf{P}_2}{\partial x} + \cdots \tag{A14}$$

Collecting the terms that are first order in ϵ gives:

$$\epsilon\left[\rho_0\frac{\partial \mathbf{U}_1}{\partial t} + \frac{\partial \mathbf{P}_1}{\partial x}\right] = 0 \tag{A15}$$

The second order terms give:

$$\epsilon^2\left[\rho_0\frac{\partial \mathbf{U}_2}{\partial t} + \rho_1\frac{\partial \mathbf{U}_1}{\partial t} + \rho_0\mathbf{U}_1\frac{\partial \mathbf{U}_1}{\partial x} + \frac{\partial \mathbf{P}_2}{\partial x}\right] = 0 \tag{A16}$$

Putting (A11), (A12), and (A13) into (A9) gives:

$$\frac{\mathrm{D}}{\mathrm{Dt}}\{(\rho_0 + \epsilon\rho_1 + \epsilon^2\rho_2 + \cdots)^{-\gamma}(\mathbf{P}_0 + \epsilon\mathbf{P}_1 + \epsilon^2\mathbf{P}_2 + \cdots)\} = 0 \tag{A17}$$

We can expand the first part of the LHS of (A17) to give:

$$(\rho_0 + \epsilon\rho_1 + \epsilon^2\rho_2 + \cdots)^{-\gamma} = 1 - \gamma(\frac{\epsilon\rho_1}{\rho_0} + \frac{\epsilon^2\rho_2}{\rho_0} + \cdots) + \frac{\gamma(\gamma+1)}{2!}(\frac{\epsilon\rho_1}{\rho_0} + \frac{\epsilon^2\rho_2}{\rho_0} + \cdots) + \cdots \tag{A18}$$

The zeroth order terms from (A17) give:

$$\frac{\partial}{\partial t}(\mathbf{P}_0{\rho_0}^{-\gamma}) = 0 \tag{A19}$$

which is trivial since both $\mathbf{P}_0$, and ρ_0, are constant. The first order terms are:

$$\epsilon \frac{\partial}{\partial t} \left\{ \frac{\mathbf{P}_1}{\mathbf{P}_0} - \frac{\gamma \rho_1}{\rho_0} \right\} = 0 \qquad (A20)$$

The second order terms are:

$$\epsilon^2 \frac{\partial}{\partial t} \left\{ \frac{\mathbf{P}_2}{\mathbf{P}_0} - \frac{\gamma \rho_2}{\rho_0} + \frac{\gamma(\gamma+1)}{2} \frac{{\rho_1}^2}{{\rho_0}^2} - \frac{\gamma \mathbf{P}_1 \rho_1}{\mathbf{P}_0 \rho_0} \right\} + \epsilon^2 \frac{\partial}{\partial x} \left\{ \frac{\mathbf{P}_1}{\mathbf{P}_0} - \frac{\gamma \rho_1}{\rho_0} \right\} = 0 \qquad (A21)$$

Finally, we substitute (A11), (A12), and (A13) into (A10) and collect terms of equal order. The first order terms give the equation:

$$\epsilon \left\{ \frac{\partial \rho_1}{\partial t} + \frac{\partial \rho_0 \mathbf{U}_1}{\partial x} \right\} = 0 \qquad (A22)$$

The second order terms yield:

$$\epsilon^2 \left\{ \frac{\partial \rho_2}{\partial t} + \frac{\partial \rho_0 \mathbf{U}_2}{\partial x} + \frac{\partial \rho_1 \mathbf{U}_1}{\partial x} \right\} = 0 \qquad (A23)$$

Now, we take our three first order equations (A15), (A20) and (A22) and combine them. We substitute (A22) into (A20) and get:

$$\frac{\partial}{\partial t} \frac{\mathbf{P}_1}{\mathbf{P}_0} + \gamma \frac{\partial \mathbf{U}_1}{\partial x} = 0 \qquad (A24)$$

We differentiate this result with respect to time:

$$\partial_{tt} \frac{\mathbf{P}_1}{\mathbf{P}_0} + \gamma \partial_{xt} \mathbf{U}_1 = 0 \qquad (A25)$$

and differentiate (A15) with respect to space:

$$\rho_0 \partial_{tx} \mathbf{U}_1 + \partial_{xx} \mathbf{P}_1 = 0 \qquad (A26)$$

Now (A25) and (A26) are combined to give a wave equation for $\mathbf{P}_1$:

$$\frac{\rho_0}{\gamma \mathbf{P}_0} \partial_{tt} \mathbf{P}_1 = -\rho_0 \partial_{xt} \mathbf{U}_1 = \partial_{xx} \mathbf{P}_1 \tag{A27}$$

We define:

$$c_0^2 \equiv \frac{\gamma \mathbf{P}_0}{\rho_0} \tag{A28}$$

so that:

$$\frac{1}{c_0^2} \partial_{tt} \mathbf{P}_1 = \partial_{xx} \mathbf{P}_1 \tag{A29}$$

The solution set for this equation includes all functions for which:

$$\mathbf{P}_1(x,t) = \mathbf{P}_1(x - c_0 t) \tag{A30}$$

From (A20) we have that:

$$\frac{\mathbf{P}_1}{\mathbf{P}_0} = \frac{\gamma \rho_1}{\rho_0} + constant \tag{A31}$$

The constant in (A31) must be zero because when the fluid is in equilibrium, its pressure and density will be at their equilibrium values $\mathbf{P}_0$, and ρ_0, so that $\mathbf{P}_1 = 0$ and $\rho_1 = 0$.

We are considering an acoustic wave passing through the fluid and this gives us our first order boundary condition. The wave is initially harmonic so we have:

$$\mathbf{U}_1|_{x=0} = X_0 \omega \sin(\omega t) \tag{A32}$$

Here X_0 represents the maximum excursion from equilibrium of the pistonlike transducer which is oscillating and causing the wave. We have assumed in (A32) that this

excursion is much less than one wavelength of the sound in the fluid so that to first order, the face of the piston can be considered to lie at $x = 0$. We now define ϵ to be:

$$\epsilon \equiv \frac{X_0 \omega}{c_0} \tag{A33}$$

so that ϵ goes to zero with X_0. We now know all of the first order variables:

$$\begin{aligned} \epsilon \mathbf{U}_1 &= X_0 \omega \sin(\omega t - kx) \\ \epsilon \mathbf{P}_1 &= \rho_0 c_0 X_0 \omega \sin(\omega t - kx) \\ \epsilon \rho_1 &= \frac{\rho_0 X_0 \omega}{c_0} \sin(\omega t - kx) \end{aligned} \tag{A34}$$

We continue to the second order equations, combining (A16), (A21) and (A23) in exactly the same way that we combined the first order terms to yield:

$$\frac{1}{c_0^2} \partial_{tt} \mathbf{P}_2 - \partial_{xx} \mathbf{P}_2 = 2\rho_0 \partial_x \mathbf{U}_1 \partial_x \mathbf{U}_1 + \partial_{tt} \left\{ \frac{\mathbf{P}_1 \rho_1}{\mathbf{P}_0} - \frac{(\gamma + 1)}{2} \frac{{\rho_1}^2}{\rho_0} \right\} \tag{A35}$$

The RHS of (A35) can be simplified by substitution from (A34) to give:

$$\frac{1}{c_0^2} \partial_{tt} \mathbf{P}_2 - \partial_{xx} \mathbf{P}_2 = \rho_0 \epsilon^2 \omega^2 (\gamma + 1) \cos 2(\omega t - kx) \tag{A36}$$

A particular solution to (A36) is:

$$\mathbf{P}_2 = \frac{(\gamma + 1)}{4} \rho_0 c_0 \omega \epsilon^2 x \sin 2(\omega t - kx) = \mathbf{A} x \sin 2(\omega t - kx) \tag{A37}$$

We can construct a general solution to (A36) by setting its RHS to zero, and adding a complete set of solutions to the resulting homogeneous equation to the particular solution of (A37). Here, we can omit terms involving $\sin(\omega t - kx)$ and $\cos(\omega t - kx)$ because

we do not expect any odd harmonics to enter the second order solution. The resulting solution is:

$$\mathbf{P}_2 = \mathbf{A}x\sin 2(\omega t - kx) + \mathbf{B}\sin 2(\omega t - kx) + \mathbf{D}\cos 2(\omega t - kx) + \mathbf{E} \qquad (A38)$$

The other second order equation, (A16) can also be simplified by substituting the known values of its first order terms from (A34) This gives:

$$\rho_0 \frac{\partial \mathbf{U}_2}{\partial t} + \frac{\partial \mathbf{P}_2}{\partial x} = 0 \qquad (A39)$$

Differentiating (A38) with respect to x gives:

$$\frac{\partial \mathbf{P}_2}{\partial x} = \mathbf{A}\sin 2(\omega t - kx) - 2k\mathbf{A}x\cos 2(\omega t - kx) - 2k\mathbf{B}\cos 2(\omega t - kx) + 2k\mathbf{D}\sin 2(\omega t - kx) \qquad (A40)$$

Integrating (A39) with respect to t then gives:

$$\mathbf{U}_2 = \frac{\mathbf{A}}{2\omega\rho_0}\sin 2(\omega t - kx) + \frac{k\mathbf{A}x}{\omega\rho_0}\sin 2(\omega t - kx) + \frac{k\mathbf{B}}{\omega\rho_0}\sin 2(\omega t - kx) + \frac{k\mathbf{D}}{\omega\rho_0}\cos 2(\omega t - kx) + \mathbf{E} \qquad (A41)$$

Now we can make use of the boundary condition:

$$\mathbf{U}(-X_0\cos\omega t\,,\, t) = X_0\omega\sin\omega t \qquad (A42)$$

Here we have not neglected the motion of the transducer face as we did in (A32). $\mathbf{U}$ is given by the series expression of (A13), and we have already found solutions for $\mathbf{U}_1$, and

$\mathbf{U_2}$ in equations (A34), and (A41). We substitute these expressions into (A42) so that we can solve for the undetermined constants in (A41) . We get:

$$\begin{aligned} X_0\omega\sin(\omega t) = X_0\omega\sin(\omega t + kX_0\cos(\omega t)) + \frac{\mathbf{B}}{c_0\rho_0}\sin 2(\omega t + kX_0\cos(\omega t)) \\ -\frac{\mathbf{A}X_0\omega}{c_0\rho_0}\cos(\omega t)\sin 2(\omega t + kX_0\cos(\omega t)) \\ +\frac{\mathbf{A}}{2\omega\rho_0}\cos 2(\omega t - kX_0\cos(\omega t)) \\ +\frac{\mathbf{D}}{c_0\rho_0}\cos 2(\omega t - kX_0\cos(\omega t)) + \mathbf{E} \end{aligned} \tag{A43}$$

The trigonometric functions of (A43) can be Taylor expanded to give:

$$\begin{aligned} \sin(\omega t + kX_0\cos(\omega t)) &= \sin(\omega t) + kX_0\cos^2(\omega t) + O\epsilon^2 \\ \sin 2(\omega t + kX_0\cos(\omega t)) &= \sin(2\omega t) + 2kX_0\cos(\omega t)\cos(2\omega t) + O\epsilon^2 \\ \cos(\omega t + kX_0\cos(\omega t)) &= \cos(\omega t) - kX_0\cos(\omega t)\sin(\omega t) + O\epsilon^2 \\ \cos 2(\omega t + kX_0\cos(\omega t)) &= \cos(2\omega t) - 2kX_0\cos(\omega t)\sin(2\omega t) + O\epsilon^2 \end{aligned} \tag{A44}$$

These values can be substituted into (A43) to give:

$$\begin{aligned} \epsilon^2 c_0\cos^2(\omega t) + \left\{\frac{\mathbf{A}}{2\omega\rho_0} + \frac{k\mathbf{D}}{\omega\rho_0}\right\}\cos(2\omega t) - \frac{2k\epsilon\mathbf{D}}{\omega\rho_0}\cos(\omega t)\sin(2\omega t) \\ +\frac{\epsilon^2\mathbf{A}}{\omega\rho_0}\cos^2(\omega t)\sin(2\omega t) + \mathbf{E} + O\epsilon^3 = 0 \end{aligned} \tag{A45}$$

Where we have recognized that $\epsilon = kX_0$ and cancelled some terms. Finally we can solve for the undetermined constants in (A41). We obtain an expression for the fluid velocity correct to second order. It is:

$$\begin{aligned} \mathbf{U} \approx \epsilon\mathbf{U_1} + \epsilon^2\mathbf{U_2} = X_0\omega\sin(\omega t - kx) + \frac{\mathbf{A} + k\mathbf{D}}{2\omega\rho_0}\cos(2\omega t - kx) \\ +\frac{k\mathbf{A}x}{\omega\rho_0}\sin 2(\omega t - kx) - \frac{\epsilon^2 c_0}{2} \end{aligned} \tag{A46}$$

With:

$$\mathbf{A} = \epsilon^2 \rho_0 c_0 \omega \frac{(\gamma+1)}{4}$$

$$\mathbf{D} = -\epsilon^2 \rho_0 c_o^2 \frac{(\gamma+5)}{8} \qquad (A47)$$

$$\mathbf{E} = -\frac{\epsilon^2 c_0}{2}$$

There is a relationship between fluid pressure and velocity. It is:[Blackstock 1962,eq.[11′] and [13]]

$$\mathbf{P} = \mathbf{P}_0 \left\{ 1 + \frac{\gamma - 1}{2} \frac{\mathbf{U}}{c_0} \right\}^{\frac{2\gamma}{\gamma-1}} \qquad (A48)$$

This can be expanded to give:

$$\mathbf{P} = \mathbf{P}_0 + \rho_0 c_0 \mathbf{U} \left(1 + \frac{\gamma+1}{4} \frac{\mathbf{U}}{c_0} + \cdots \right) \qquad (A49)$$

Substituting (A47) into (A49) and keeping only the constant terms gets us, at long last to an expression for the average Eulerian pressure in a sound beam:

$$\langle \mathbf{P} \rangle = \mathbf{P}_0 + \frac{\gamma - 3}{8} \rho_0 c_0^2 \epsilon^2 \qquad (A50)$$

APPENDIX III.

List of Symbols

A ..... Amplitude of sound beam ..... (sec. 3.4)

b ..... Bulk Viscosity ..... (sec. 3.2)

b_1 ..... Speed of transverse waves in solid ..... (sec. 2.8)

B/A ..... Parameter of nonlinearity ..... (sec. 2.2)

c_0 ..... Speed of sound in fluid ..... (sec. 2.3)

c_1 ..... Speed of longitudinal waves in solid ..... (sec. 2.8)

C_p ..... Specific heat, constant pressure ..... (sec. 2.2)

C_v ..... Specific heat, constant volume ..... (sec. 2.2)

C_0 ..... Saturation concentration of dissolved gas ..... (sec. 5.8)

C_∞ ..... Concentration of dissolved gas at infinity ..... (sec. 5.8)

d ..... "Impact parameter" (fig. 10) ..... (sec. 2.8)

D/Dt ..... Total derivative ..... (sec. 2.2)

$\langle \mathbf{E} \rangle$ ..... Acoustic energy density ..... (sec. 2.5)

$\vec{\mathbf{F}}$ ..... Force on a fluid element ..... (sec. 2.2)

$\vec{\mathbf{F}}$ ..... Driving force for streaming ..... (sec. 3.4)

I ..... Sound Intensity ..... (sec. 3.4)

$\vec{\mathbf{J}}$ ..... Momentum density in sound beam ..... (sec. 2.6)

$\vec{\mathbf{J}}'$ ..... Momentum density in reflected beam ..... (sec. 2.7)

k ..... Sound wave number ..... (sec. 2.6)

$\vec{k}$ ..... Sound wave vector ..... (sec. 2.6)

L ..... Scale length ..... (sec. 3.4)

M ..... Torque ..... (sec. 4.1)

$\vec{p}$ ..... Momentum ..... (sec. 2.6)

$\mathbf{P}$ ..... Hydrostatic pressure ..... (sec. 2.2)

$\langle \mathbf{P} \rangle$ ..... Average Eulerian pressure ..... (sec. 2.1)

$\langle \mathbf{P}^L \rangle$ ..... Average Lagrangian pressure ..... (sec. 2.5)

$\mathbf{P}^{Lan}$ ..... Langevin radiation pressure ..... (sec. 2.5)

$\mathbf{P}^{\mathbf{Ra}}$ ..... Rayleigh radiation pressure ..... (sec. 2.5)

$\mathbf{P}_{\mathbf{AC}}^{Blake}$ ..... Blake cavitation threshold ..... (sec. 5.3)

$\mathbf{P}_{\mathbf{AC}}^{R.D.}$ ..... Threshold for rectified diffusion ..... (sec. 5.3)

$\mathbf{P}_v$ ..... Vapour pressure of liquid ..... (sec. 5.3)

$\mathbf{P}_0$ ..... Equilibrium hydrostatic pressure ..... (sec. 2.1)

$\mathbf{P}'_0$ ..... Effective hydrostatic pressure, unconfined sound beam ..... (sec. 2.5)

$\mathbf{P}_0, \mathbf{P}_1, \mathbf{P}_2$. First terms in a series expansion of $\mathbf{P}$ ..... (sec. 2.3)

R ..... Disk Radius ..... (sec. 2.8)

$\mathbf{R}$ ..... Reflected intensity ..... (sec. 2.8)

Re ..... Reynolds number ..... (sec. 3.4)

$\mathbf{Re}$ ..... Reynolds number for a rotating disk ..... (sec. 4.1)

R_0 ..... Equilibrium bubble radius ..... (sec. 5.3)

$R(\omega)$ ..... Frequency dependent term, viscous fluid eqn. of state ..... (sec. 3.2)

S ..... Entropy of fluid ..... (sec. 2.2)

$\mathbf{T}$ ..... Transmitted beam intensity ..... (sec. 2.8)

U ..... Scale velocity ..... (sec. 3.4)

$\vec{\mathbf{U}}$ ..... Fluid velocity ..... (sec. 2.2)

$\mathbf{U}_{max}$ ..... Maximum fluid velocity in a harmonic wave ..... (sec. 2.3)

$\mathbf{U}_0, \mathbf{U}_1, \mathbf{U}_2$. First terms in a series expansion of $\mathbf{U}$ ..... (sec. 2.3)

V ..... Amplitude reflection coefficient for ultrasound ..... (sec. 2.8)

V^* ..... Complex conjugate of V ..... (sec. 2.8)

$\overleftrightarrow{\mathbf{V}}$ ..... Rate of deformation tensor ..... (sec. 3.2)

$\mathbf{X_{SF}}$ ..... Shock formation distance ..... (sec. 2.4)

Z, Z_l, Z_t .... Acoustic impedances defined in eqn. (43) ..... (sec. 2.8)

α ..... Sound absorption coefficient ..... (sec. 3.3)

γ ..... Ratio of specific heats C_p/C_v ..... (sec. 2.2)

γ_1 ..... Angle of refraction, transverse waves ..... (sec. 2.8)

δ ..... Boundary layer thickness ..... (sec. 4.1)

ϵ ..... Expansion parameter, method of successive approximations ..... (sec. 2.3)

θ ..... Angle of incidence ..... (sec. 2.8)

θ_c ..... Critical angle for refraction ..... (sec. 2.8)

θ_1 ..... Angle of refraction, longitudinal waves in solid ..... (sec. 2.8)

κ ..... Thermal conductivity ..... (sec. 2.4)

μ ..... Coefficient of shear viscosity ..... (sec. 3.2)

ν ..... Kinematic viscosity ..... (sec. 4.1)

ξ ..... Displacement of fluid particle from equilibrium ..... (sec. 2.6)

ξ_0 ..... Displacement amplitude of harmonic wave ..... (sec. 2.6)

ρ ..... Fluid density ..... (sec. 2.2)

ρ_0 ..... Equilibrium fluid density ..... (sec. 2.3)

$\rho_0, \rho_1, \rho_2 \ldots$ First terms in the series expansion of ρ ..... (sec. 2.3)

σ ..... Surface tension ..... (sec. 5.3)

$\overleftrightarrow{\sigma}$ ..... Stress tensor ..... (sec. 3.2)

ω ..... Angular frequency ..... (sec. 2.3)

$\langle \cdots \rangle$ ..... Time average ..... (sec. 3.3)